



Elsevier has created a [Monkeypox Information Center](#) in response to the declared public health emergency of international concern, with free information in English on the monkeypox virus. The Monkeypox Information Center is hosted on Elsevier Connect, the company's public news and information website.

Elsevier hereby grants permission to make all its monkeypox related research that is available on the Monkeypox Information Center - including this research content - immediately available in publicly funded repositories, with rights for unrestricted research re-use and analyses in any form or by any means with acknowledgement of the original source. These permissions are granted for free by Elsevier for as long as the Monkeypox Information Center remains active.

# Journal Pre-proof

Towards hospital-on-chip supported by 2D MXenes-based 5th generation intelligent biosensors

Vishal Chaudhary, Virat Khanna, Hafiz Taimoor Ahmed Awan, Kamaljit Singh, Mohammad Khalid, Yogendra Mishra, Shekhar Bhansali, Chen-Zhong Li, Ajeet Kaushik

PII: S0956-5663(22)00887-9

DOI: <https://doi.org/10.1016/j.bios.2022.114847>

Reference: BIOS 114847

To appear in: *Biosensors and Bioelectronics*

Received Date: 2 August 2022

Revised Date: 19 September 2022

Accepted Date: 20 October 2022

Please cite this article as: Chaudhary, V., Khanna, V., Ahmed Awan, H.T., Singh, K., Khalid, M., Mishra, Y., Bhansali, S., Li, C.-Z., Kaushik, A., Towards hospital-on-chip supported by 2D MXenes-based 5th generation intelligent biosensors, *Biosensors and Bioelectronics* (2022), doi: <https://doi.org/10.1016/j.bios.2022.114847>.

This is a PDF file of an article that has undergone enhancements after acceptance, such as the addition of a cover page and metadata, and formatting for readability, but it is not yet the definitive version of record. This version will undergo additional copyediting, typesetting and review before it is published in its final form, but we are providing this version to give early visibility of the article. Please note that, during the production process, errors may be discovered which could affect the content, and all legal disclaimers that apply to the journal pertain.

© 2022 Published by Elsevier B.V.



# Towards hospital-on-chip supported by 2D MXenes-based 5<sup>th</sup> generation intelligent biosensors

Vishal Chaudhary<sup>1\*</sup>, Virat Khanna<sup>2\*</sup>, Hafiz Taimoor Ahmed Awan<sup>3</sup>, Kamaljit Singh<sup>2</sup>, Mohammad Khalid<sup>3,4</sup>, Yogendra Mishra<sup>5</sup>, Shekhar Bhansali<sup>6</sup>, Chen-Zhong Li<sup>7,8\*</sup>, Ajeet Kaushik<sup>9,10\*</sup>

## AUTHOR AFFILIATION(S):

<sup>1</sup>Research Cell & Department of Physics, Bhagini Nivedita College, University of Delhi, Delhi, 110043, India

<sup>2</sup>Department of Mechanical Engineering, MAIT, Maharaja Agrasen University, HP, 174103, India

<sup>3</sup>Graphene & Advanced 2D Materials Research Group (GAMRG), School of Engineering and Technology, Sunway University, No. 5, Jalan University, Bandar Sunway, 47500 Petaling Jaya, Selangor, Malaysia

<sup>4</sup>Sunway Materials Smart Science & Engineering (SMS2E) Research Cluster, Sunway University, No. 5, Jalan Universiti, Bandar Sunway, 47500 Petaling Jaya, Selangor, Malaysia

<sup>5</sup>Mads Clausen Institute, NanoSYD, University of Southern Denmark, Alison 2, Sønderborg, 6400 Denmark

<sup>6</sup>Department of Electrical and Computing Engineering, Florida International University, Miami, FL-33174

<sup>7</sup>Center for Cellular and Molecular Diagnostics, Tulane University School of Medicine, 1430 Tulane Ave., New Orleans, LA, 70112, USA

<sup>8</sup>Department of Biochemistry and Molecular Biology, Tulane University School of Medicine, 1430 Tulane Ave., New Orleans, LA, 70112, USA

<sup>9</sup>NanoBioTech Laboratory, Health System Engineering, Department of Environmental Engineering, Florida Polytechnic University, Lakeland, FL 33805, USA

<sup>10</sup>School of Engineering, University of Petroleum and Energy Studies (UPES), Dehradun, Uttarakhand, India

---

## Corresponding Authors:

[Chaudhary00vishal@gmail.com](mailto:Chaudhary00vishal@gmail.com) (V.C.)

[akaushik@floridapoly.edu](mailto:akaushik@floridapoly.edu) (A.K.)

[chenzhongbiosensor@gmail.com](mailto:chenzhongbiosensor@gmail.com) (C-Z. L.)

\*Equal First Contributor

**Abstract**

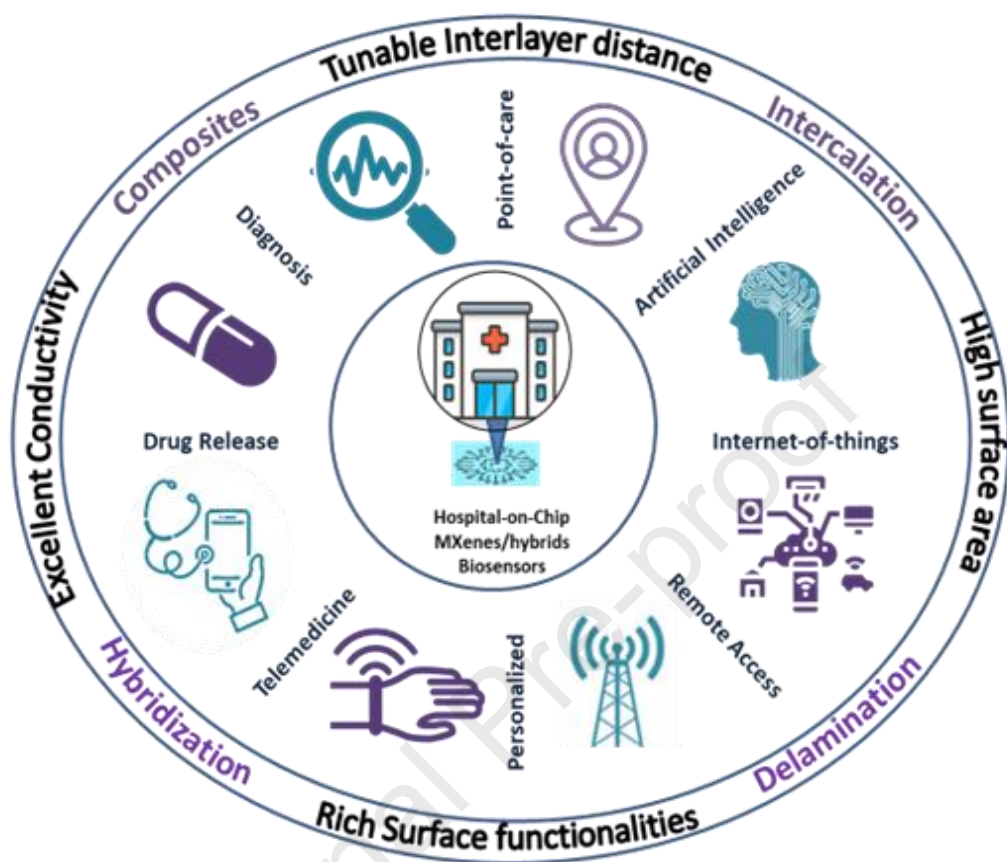
Existing public health emergencies due to fatal/infectious diseases such as coronavirus disease (COVID-19) and monkeypox have raised the paradigm of 5<sup>th</sup> generation portable and intelligent multifunctional biosensors embedded on a single chip. The state-of-the-art 5<sup>th</sup> generation biosensors are concerned with integrating advanced functional materials with controllable electronic attributes and optimal machine processability. In this direction, 2D metal carbides and nitrides (MXenes), owing to their enhanced effective surface area, tunable physicochemical attributes, and rich surface functionalities, have shown promising performances in biosensing flatlands. Moreover, their hybridization with diversified nanomaterials caters to their associated challenges for the commercialization of stability due to restacking and oxidation. MXenes and its hybrid biosensors have demonstrated intelligent and lab-on-chip prospects for determining diverse biomarkers/pathogens related to fatal and infectious diseases. Recently, on-site detection has been clubbed with solution-on-chip MXenes by interfacing biosensors with modern-age technologies, including 5G communication, internet-of-medical-things (IoMT), artificial intelligence (AI), and data clouding to progress toward hospital-on-chip (HOC) modules. This review comprehensively summarizes the state-of-the-art MXene fabrication, advancements in physicochemical properties to architect biosensors, and the progress of MXene-based lab-on-chip biosensors toward HOC solutions. Besides, it discusses sustainable aspects, practical challenges and alternative solutions associated with these modules to develop personalized and remote health solutions for every individual in the world.

**Keywords:** MXenes; 5<sup>th</sup> generation biosensor; hospital-on-chip; personalized diagnostics; Lab-on-chip

71  
72  
73  
74  
75  
76  
77  
78  
79  
80  
81  
82  
83  
84  
85  
86  
87  
88  
89  
90  
91  
92  
93  
94

95 Graphical Abstract:

96



97

98

99

100

101

102

103

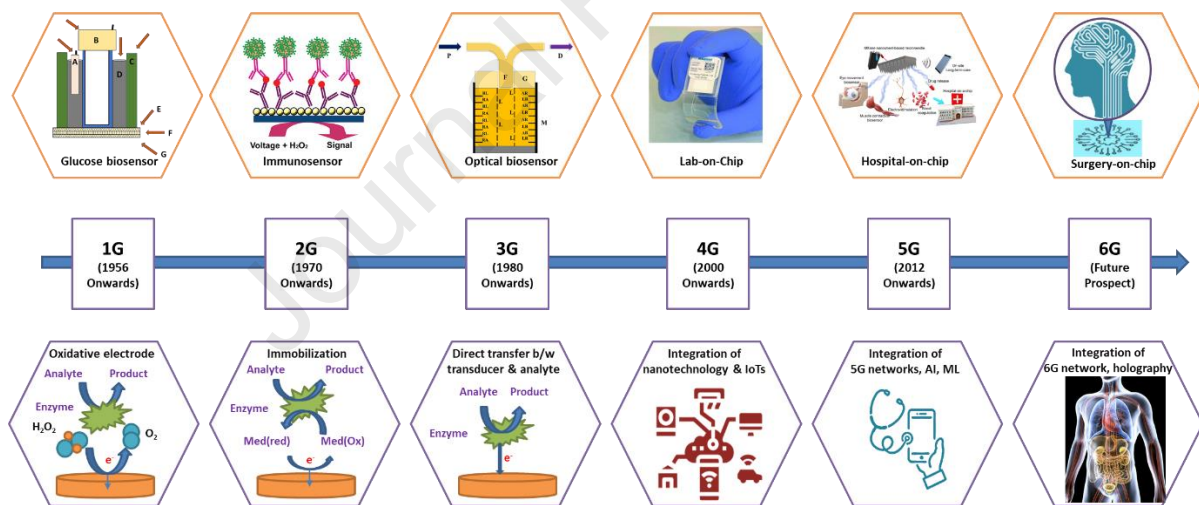
104

105

## 106 1. Emergence of 5<sup>th</sup> génération biosensing strategies

107 The latent of biosensors have been extensively explored as plausible alternatives to the  
 108 time-consuming, costly, complex and massive conventional diagnostics utilized in health  
 109 care sectors (Patel et al., 2016; Solanki et al., 2011; Verma and Bhardwaj, 2015). Biosensors  
 110 possess diversified applications, including biomedical sectors, pharmaceutical industries,  
 111 hospitals and clinical treatment, healthcare centers, and personalized healthcare  
 112 equipment. These biosensors are ideally installed for multiple disease recognition, human  
 113 health organization, prevention, patient health observation and rehabilitation. Besides,  
 114 biosensing devices are also implemented for the virus microorganisms, micro-organisms,  
 115 pathogens and bacterial exposure (Dwivedi et al., 2021; Lei et al., 2019; Novoselov et al.,  
 116 2004; Patel et al., 2016; Solanki et al., 2011).

117 Over time, applications and with temporal necessities, biosensors have evolved from  
 118 1<sup>st</sup> generation biosensors to 5<sup>th</sup> generation biosensors with the integration of developing  
 119 technologies (**Figure 1**).



120

121 **Figure 1.** Timeline for evolution of biosensors from 1<sup>st</sup> generation to 5<sup>th</sup> generation with  
 122 prospects of 6<sup>th</sup> generation modules; subparts adapted from: Glucose biosensor ((Clark and  
 123 Lyons, 2006)), Immunosensor ((Mani et al., 2009)), Optical biosensor ((Seitz, 1984)), Lab-on-  
 124 chip ((Kukhtin et al., 2019)), Hospital-on-chip ((Yang et al., 2021)).

125

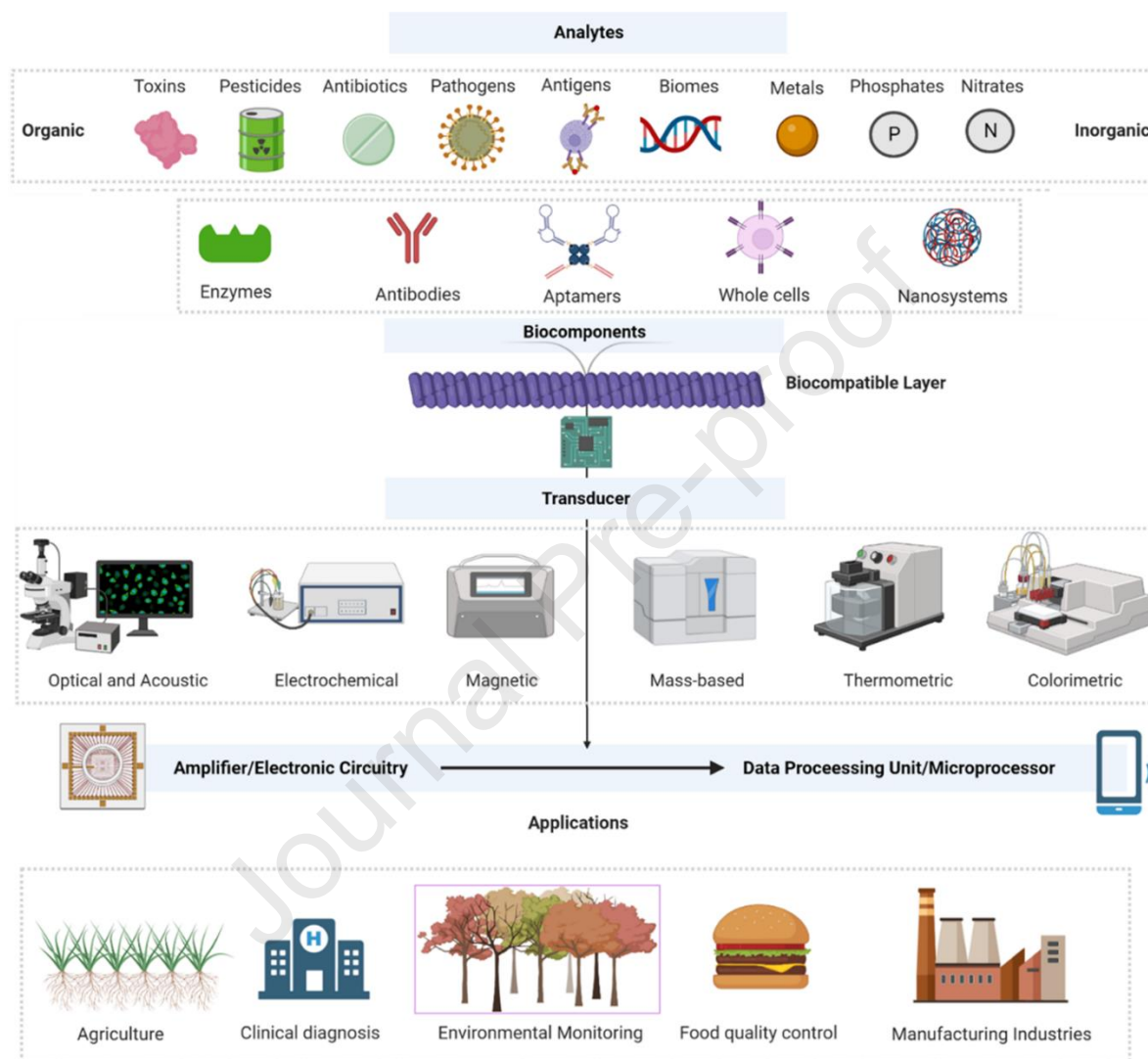
126 The fundamentals of biosensor development commenced with *in vitro* investigations  
 127 performed to mimic the sensory capabilities of living organisms. Clark and Lyons  
 128 (1962)(Clark and Lyons, 2006) reported the first biosensor to detect glucose based on

129 oxidation reaction utilizing an enzyme electrode. This pioneering work was followed by  
130 several studies based on potentiometric detection of biomolecules like urea, ushering in the  
131 era of 1<sup>st</sup> generation biosensors. However, in order to improve detection efficacy, simplify  
132 operation, and advance diagnostic quality, the 2<sup>nd</sup> generation of biosensors was introduced  
133 with a modified monitoring technique (Ansari and Malhotra, 2022; Kim et al., 2019; Xin et  
134 al., 2020). It included co-immobilization of auxiliary enzymes or/and co-reactants through  
135 analyte (like biomolecules) converting enzymes. These modifications defined the basic  
136 structure and components of a biosensor, including sensing surface, transducers and  
137 analytical circuitry (Scheller et al., 1991). For instance, the transducer attached to biosensing  
138 layers was modified with enzymes/chemicals to achieve maximal and quality detection  
139 output like ELISA (enzyme-linked immunosorbent assay) based biosensors (Scheller et al.,  
140 1991).

141 Following these developments, the International Union of Pure and Applied  
142 Chemistry (IUPAC) recognized the term "biosensor" in 1996 and defined it as "A device that  
143 uses specific biochemical reactions mediated by isolated enzymes, immune systems, tissues,  
144 organelles or whole cells to detect chemical compounds usually by electrical, thermal or  
145 optical signals." However, the immobilization of sensing electrode with mediating-enzyme  
146 raised leaching susceptibility and the indirect interaction amongst the analyte and  
147 transducer affected the biosensor efficacies. Thus, the challenges in reproducibility,  
148 selectivity and stability raised the development of 3<sup>rd</sup> generation biosensors. The  
149 fundamental of 3<sup>rd</sup> generation biosensors was based on direct communication between  
150 transducer and analyte, which enhances their monitoring output quality, stability and  
151 efficacies (Gorton et al., 1999; ZHANG and LI, 2004). It further recognized the different types  
152 of biosensors classified based on transducing mechanisms into electrochemical, optical and  
153 thermal biosensors (Kim et al., 2019; ZHANG and LI, 2004)s. The first three-generation  
154 biosensors were concerned with modifications in detection fundamentals and mechanisms  
155 to achieve high performances. However, the 4<sup>th</sup> generation onwards of biosensors is the  
156 integration of developing technologies to diversify their utilization, enhance their efficacies,  
157 and move towards everything-on-single-chip modules (Kim et al., 2019; Solanki et al., 2011).

158 These biosensor technologies are based on nanomaterials as biological sensing  
159 components integrated with IoTs and rapid data processing modules within a transducer

160 arrangement (Kaushik et al., 2018; Patel et al., 2016; Verma and Bhardwaj, 2015). It has  
 161 three fundamental components, including the sensor to detect the stimulus/biomolecules, a  
 162 transducer to adapt the stimulus to generate output signals, and processing of the sensory  
 163 signal to build the output source in representable form, as illustrated in **Figure 2**.



164

165 **Figure 2.** Schematic illustration representing the fundamental biosensor components and  
 166 detecting module for diversified applications. Created using BioRender.com.

167 With the requirements of portable, personalized, and compact healthcare  
 168 necessities, 4<sup>th</sup> generation biosensors are the integration of flexible, wearable, and nano-  
 169 micro- electronics/technology with internet-of-things (IoT). It is concerned with the  
 170 miniaturization of biosensor architect for point-of-care detection, such as lab-on-chip  
 171 modules. This has shifted the paradigm of conventional biosensors toward everything on a  
 172 single chip, termed lab-on-chip module biosensors (S.-J. Liu et al., 2022; Y. Wang et al.,  
 173 2022). The lab-on-a-chip biosensors are miniaturized devices designed with all the excellent

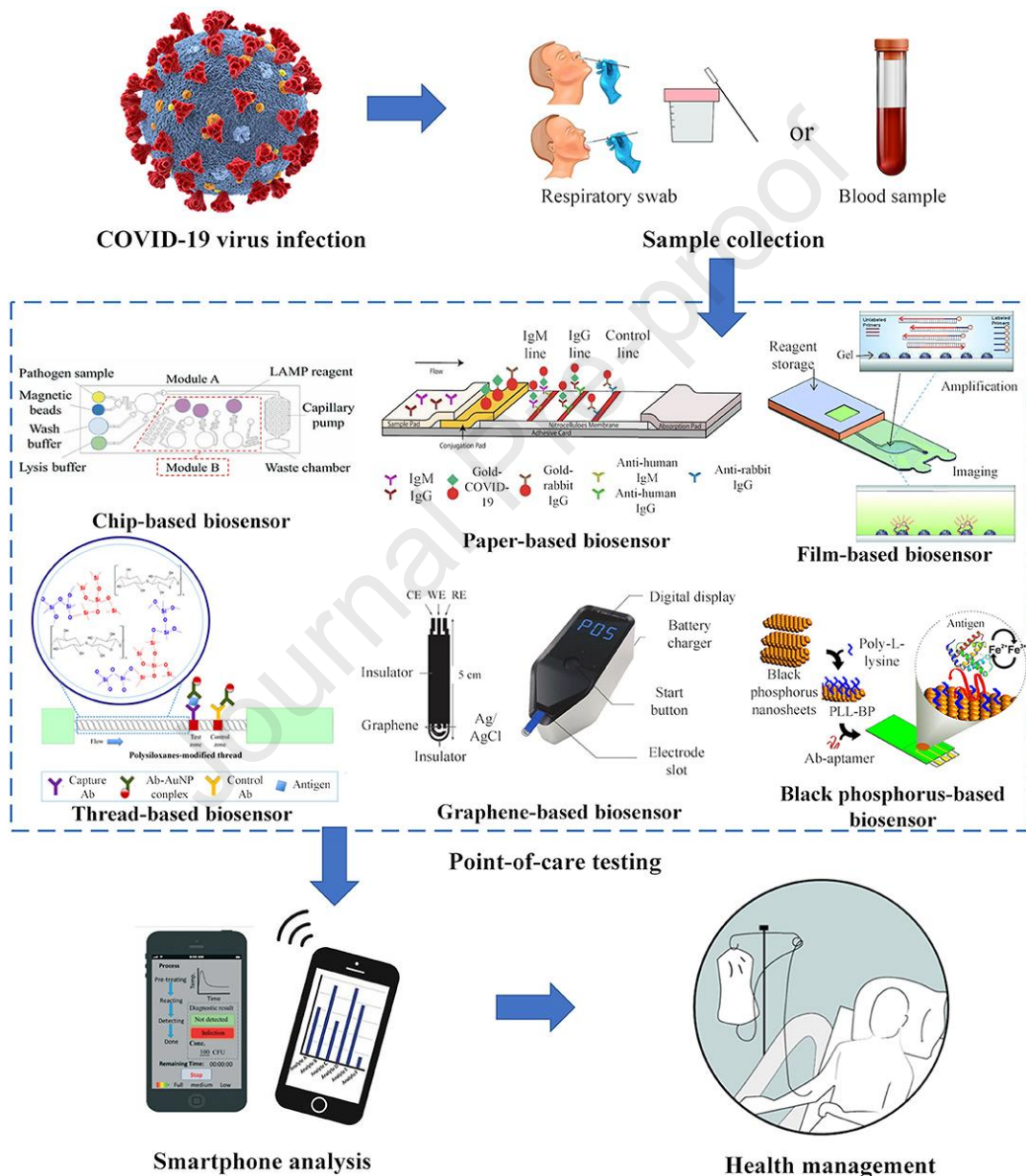


174 functionalities and parameters incorporated into one platform, from the fabrication of  
175 samples to signal delivery processing to internet-of-nano-things.

176 An ideal lab-on-a-chip device contains maximum robustness and strong-wired  
177 intelligence to employ the personal skilled free and transport the outcomes directly to the  
178 chief monitoring station (Beshar et al., 2021; Xin et al., 2020). This device also supports  
179 distinguishing the biomolecule parameters, such as RNA and DNA variations. The significant  
180 development utilized to produce lab-on-a-chip is molecular biotechnology and microfluidics  
181 systems. Most importantly, these sorts of devices are prepared through extensive  
182 microchannels enclosed with antigens, oligonucleotides, and antibodies, which permit loads  
183 of biochemical reactions produced from the lone blood drop. Usually, glass, silicone, PDMS,  
184 thermoplastic polymers and multiple paper-related schemes are applied to develop lab-on-  
185 a-chip biosensors. Paper-based and PDMS are the ones broadly used for this fabrication  
186 process owing to their cost-effectiveness and time-efficient fabrication process (Khunger et  
187 al., 2021).

188 In addition, due to their real-time diagnosis and smaller sample volumes, lab-on-a-  
189 chip biosensors have other benefits, such as rapid testing and response times, ease of  
190 handling, and sensitivity to standard analytic procedures. However, they can be applied  
191 anywhere in any environmental interface without any hurdles. In addition, lab-on-a-chip  
192 biosensors generally rely on proteomics, cell biology and microbiology applications. In  
193 proteomics, these devices exhibit the excellent potential to integrate the all-proteomics  
194 phases beginning from (1) extraction, (2) separation, (3) electrophoresis, (4) mass  
195 spectroscopy evaluation and (5) protein crystallization (Ansari and Malhotra, 2022; Verma  
196 and Bhardwaj, 2015). Similarly, cell biology copes with the vast number of cells in seconds  
197 because they can optimize all large quantity cells at the mono-level. Due to this, it can easily  
198 detect, sort out and isolate a single quantified cell when programmed. Whereas, for  
199 molecular biology, this is the quickest way of PCR detection by testing the excellent speed  $\mu$ -  
200 scale thermal shift. Due to this, DNA array can be detected more than a million times rapid  
201 genome arrangement (Chakraborty et al., 2018; Dwivedi et al., 2021; Ho et al., 2021; Lei et  
202 al., 2019; Naguib et al., 2021; Novoselov et al., 2004; Patel et al., 2016; Solanki et al., 2011;  
203 Wu et al., 2022; H. Zhang et al., 2022). However, this generation's sensors are unable to  
204 incorporate present-day intelligent technological advancements and innovations.

205 Furthermore, LOC architect possess different substrate and packaging structures,  
 206 including thread, film, paper, electronic chips, and other prominent flexible substrates, with  
 207 applications in point-of-care diagnosing diversified pathogens. For instance, Choi et al.(Choi,  
 208 2020) summarized the various point-of-care biosensors for diagnosing severe acute  
 209 respiratory syndrome coronavirus 2 (SARS-CoV-2) architected using various substrates,  
 210 nanomaterials and packaging modules (**Figure 3**).



211

212 **Figure 3.** Different types of point-of-care LOC biosensors for detecting SARS-CoV-2 (Choi,  
 213 2020).

214 Further, the emergence of artificial intelligence, bioinformatics, data clouding and  
 215 5G communications in biomedical sectors have transformed the lab-on-chip module

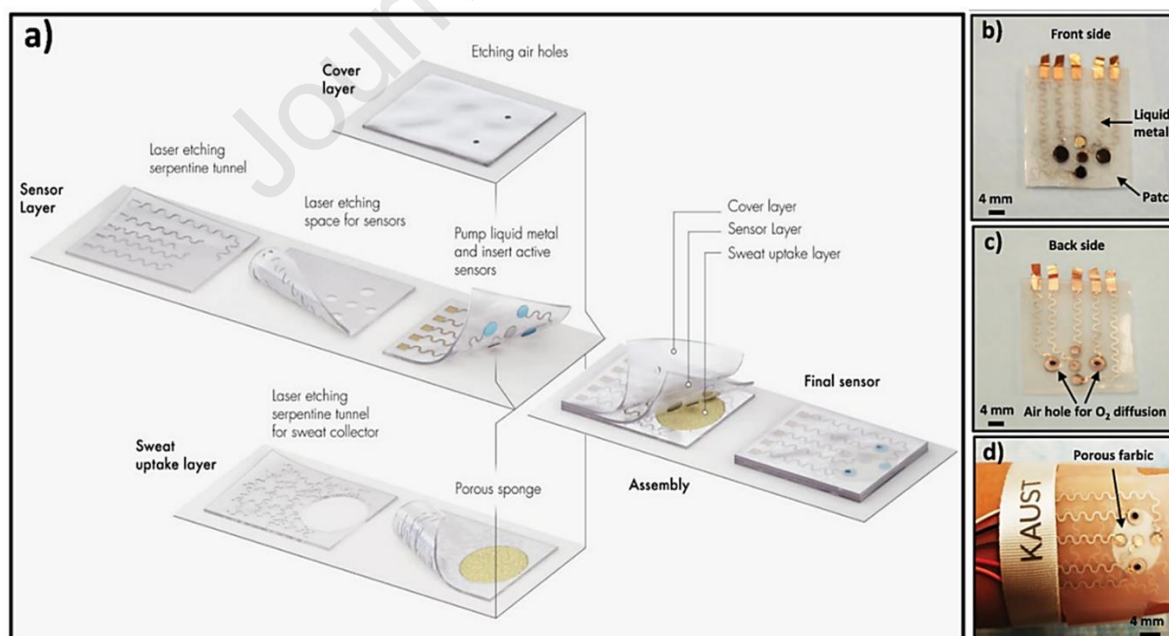
216 biosensors into 5<sup>th</sup> generation biosensors with smart, remote and intelligent prospects(Jin et  
217 al., 2020; Kim et al., 2019; Singh et al., 2021; Xin et al., 2020). Moreover, incorporating the  
218 fundamentals of triboelectricity for self-powered module biosensors and the fundamentals  
219 of green chemistry to address ecological concerns resulting in repurpose, reuse, degradable,  
220 recyclable biosensors, addressed under 5<sup>th</sup> generation of biosensors(Chaudhary et al.,  
221 2022c; Kim et al., 2020; Pathania et al., 2022). Therefore, it has raised the paradigm of  
222 intelligent, eco-friendly, and remotely accessible biosensors, whose utilization is not only  
223 limited to analyte monitoring but extended to advanced deliverables, including drug  
224 delivery, curable tactics, prevention functionality, antipathogenic activities and  
225 telemedicine. Additionally, the world is shifting towards 6G-IoT networks of ultra-reliable  
226 and low latency communications (URLLC) and enhanced mobile broadband (eMBB) at a  
227 significant pace(Nayak et al., 2020; Nguyen et al., 2022). Their integration into 5<sup>th</sup>  
228 generation modules further possesses the potential to revolutionize healthcare with real-  
229 time features like holographic communication and remote surgery. Therefore, it prompts  
230 the advancement towards 6<sup>th</sup> generation on-site biosensors. However, their development is  
231 in its infancy and requires extensive research and dedication, which has kept the current  
232 focus of research on 5<sup>th</sup> generation of biosensors.

## 233 **2. State-of-the-art 5<sup>th</sup> generation biosensors: Towards Hospital-on-chip module**

234 The state-of-the-art 5<sup>th</sup> generation biosensors are concerned with exploring advanced  
235 nanomaterials as sensing platforms, interfacing them with rapid and intelligent data  
236 processing strategies, and packing them in portable and wearable modules for diversified  
237 healthcare applications. The two major research concerns of 5<sup>th</sup> generation biosensors are  
238 dedicated to achieving utmost efficacy with stable performance and multi-functionality with  
239 the integration of other cutting-edge technologies(Chaudhary et al., 2022c).

240 The first concern related to 5<sup>th</sup> generation biosensors is catered by architecting  
241 advanced functional nanoplatfoms and engineering their physicochemical attributes.  
242 Recently, two-dimensional (2D) nanomaterials, including graphene and its derivatives, metal  
243 carbides and nitrides (MXenes), metal borides (MBenes), metal-organic framework, metal  
244 dichalcogenides and borophene, due to their high specific surface area have emerged as  
245 excellent biosensing platforms with enhanced detection and monitoring efficacies (Ahmed  
246 et al., 2020; Chakraborty et al., 2018; Chaudhary et al., 2022e, 2022a; Dwivedi et al., 2021;

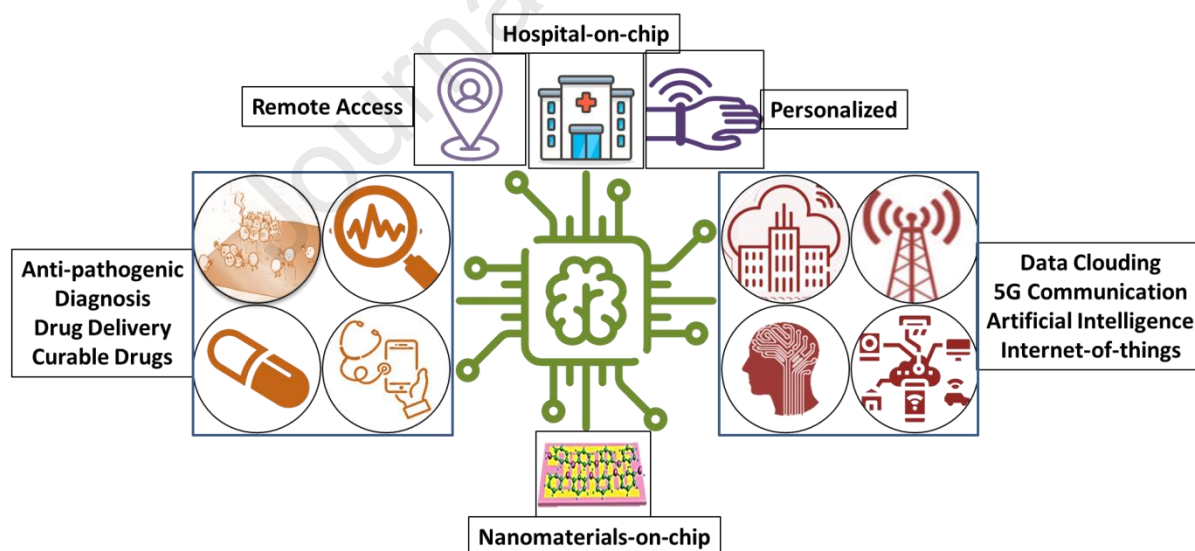
247 Ho et al., 2021; Huang et al., 2020; Jiang et al., 2020; Naguib et al., 2021; Wu et al., 2022;  
 248 Zha et al., 2019; H. Zhang et al., 2022) Amongst all, MXenes have demonstrated enormous  
 249 potential in detecting and monitoring the diversified biomolecules utilizing various  
 250 strategies, encompassing electrical, electronic, electrochemical, optical, acoustic and  
 251 plasmonic modules(Chaudhary et al., 2022a, 2022c, 2022e; Sheth et al., 2022). It is  
 252 attributed to the high effective surface area, tunable physicochemical attributes, and rich  
 253 surface functionalities of MXenes, which contribute to enhanced monitoring performances.  
 254 Moreover, their hybridization and intercalation with foreign nanomaterials cater to  
 255 difficulties associated with new MXene-based biosensors of poor stability due to oxidation  
 256 and restacking of layers. For instance, Lei et al.(Lei et al., 2019) fabricated the  
 257 electrochemical biosensors for the in-vitro perspiration investigation. Then, they applied the  
 258 multifunctional and wearable sensor prepared via MXene-composite with Prussian blue for  
 259 the sensitive, curable, and durable tracking of lactate and glucose present in sweat, as  
 260 illustrated in **Figure 4**. This further helps to enhance the linear detection and accuracy rate  
 261 to prevent personalized health issues and early-life diseases. This progress of on-site  
 262 solution based MXene biosensors has been further supported by numerous reports in the  
 263 literature, as detailed in this review.



264

265 **Figure 4.** Schematic illustration of the MXene-based biosensor system based on a lab-on-  
 266 chip module for sweat detection(Lei et al., 2019).

267 Moreover, the sudden outbreak of fatal and infectious diseases has overwhelmed  
 268 the existing global healthcare services and resulted in increased severity and mortalities,  
 269 raising a second concern related to 5<sup>th</sup> generation biosensor's architecture and packaging.  
 270 Nowadays, especially in the current coronavirus disease (COVID-19) scenario, the primary  
 271 global health concern is early diagnosis, which strengthens the treatment efficacies and  
 272 curtails the associated severity and mortality (Chaudhary et al., 2022b; Kaushik et al., 2020;  
 273 Noh et al., 2022). These consequences can be controlled through early diagnosis of  
 274 respective biomarkers/pathogens, thereby enhancing therapeutic efficiency, and developing  
 275 personalized intelligent healthcare equipment. Furthermore, it has raised the paradigm of  
 276 compact, portable, multi-functional and solution-providing biosensors with hospital-on-chip  
 277 (HOC) modules to provide healthcare access to every individual, even in the remotest part  
 278 (Kaushik et al., 2015; Tiwari et al., 2019). The importance of HOC biosensors lies in their  
 279 diversified advantages and multifunctionality of diagnosis, imaging, monitoring, sensing,  
 280 telemedicine, drug release and antipathogenic action embedded in a single chip with  
 281 prospects of remote access and personalized healthcare serving the sustainable  
 282 development goals (**Figure 5**).



283

284 **Figure 5.** Hospital-on-chip module-based 5<sup>th</sup> generation of compact, portable, and  
 285 intelligent biosensors

286 Moreover, these biosensors integrated into smart IoTs perform multifunction,  
 287 including non-invasive monitoring of various health parameters of the human body  
 288 simultaneously (Chaudhary et al., 2022c, 2022a). The research and development of

289 biosensors are dedicated to the prompt and accurate monitoring of  
290 biomarkers/biochemicals in the human body due to biological imbalances resulting from  
291 chronic diseases. Furthermore, designing compact and portable modules, especially during  
292 COVID-19, has emerged as a massive, personalized healthcare need to protect against the  
293 spread of contagion from infected to non-infected individuals(Chaudhary et al., 2022b;  
294 Pathania et al., 2022). It has raised the burden on the global wearable and personalized  
295 healthcare market due to the requirement of remote and individual access to healthcare  
296 diagnostic facilities.

297 Hence, this paradigm has recently shifted from lab-on-chip to hospital-on-chip  
298 modules due to the emergent requirements of on-site healthcare diagnostics and their  
299 solutions. Nowadays, it is becoming the scalable solution for the requirement of any family  
300 and extensively for the “doctor house call”, which made this possible virtually to every place  
301 within no time limit. Most importantly, this was necessarily thinkable because of the  
302 availability of mobile internet, broadband and other wireless technology for telemedicine  
303 and remedy decision aids (Jin et al., 2020; Verma et al., 2022). Similarly, to be thorough and  
304 effective, technologies for diagnosing and treating various household diseases must be  
305 available as soon as possible. In addition, this can be completed by healthier lifestyles, a  
306 clean environment and smart web sensors. Therefore, researchers are now implementing  
307 intelligent 5<sup>th</sup> generation biosensors to protect precious life from these dangerous diseases  
308 (Lei et al., 2019; Li et al., 2022; Novoselov et al., 2004; Pan et al., 2022; Patel et al., 2016;  
309 Solanki et al., 2011; Verma and Bhardwaj, 2015).

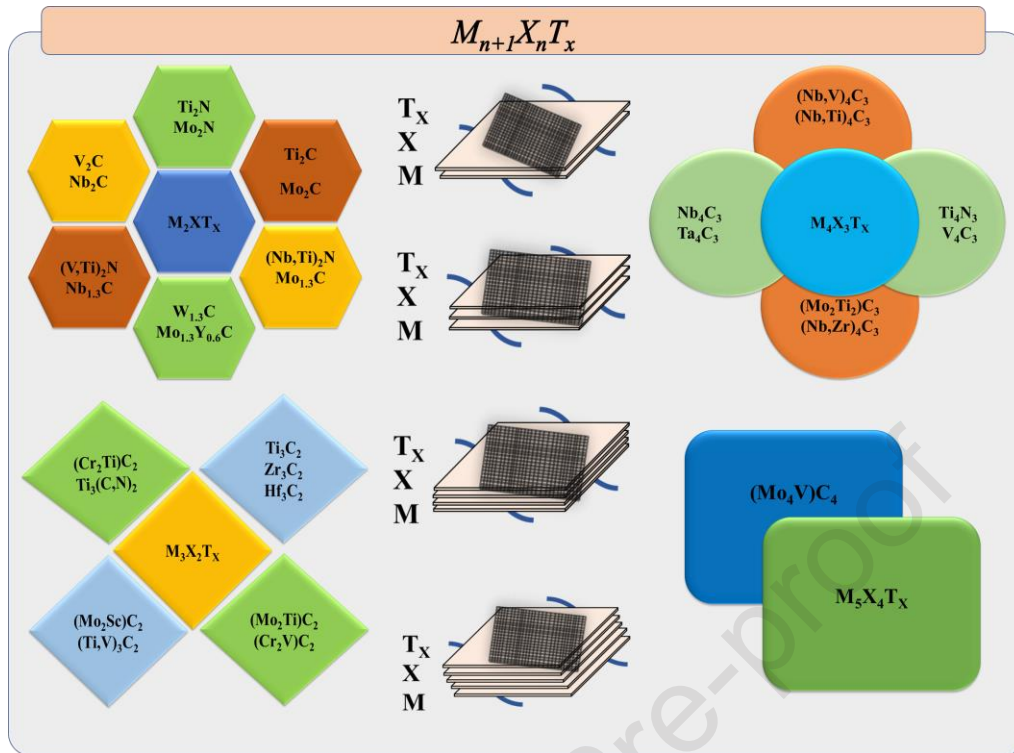
310 This review comprehensively discusses the MXene-based various kinds of intelligent  
311 biosensors with on-site and point-of-care modules and their journey toward lab-on-a-chip  
312 and hospital-on-chip biosensors. This review highlights the state-of-the-art MXene  
313 fabrication, advancements in its physicochemical attributes, diversified 5<sup>th</sup> generation  
314 biosensing modules and applications, and intelligent prospects to design HOC strategies.  
315 Besides, it discusses the challenges related to the practical development and  
316 commercialization of MXene-based on-site biosensor modules and their possible alternate  
317 solutions with innovative intelligent prospects.

### 318 **3. Engineering MXenes and its hybrids to architect future-generation biosensors**

319 Since the extraction of monolayer graphene sheets from monolithic graphite in 2004, two-  
320 dimensional (2D) materials have gained much attention. The two-dimensional substances  
321 are usually thin atomic mono-layers of 5-10 nm thickness or a few numbers of thin layers  
322 coupled by van-der Waals (vdW) interactions (Dwivedi et al., 2021). Due to its linear  
323 electronic dispersion, graphene and its distinct forms, such as reduced graphene oxide  
324 (rGO), graphene nanoplatelets (GNPs) and graphene oxide (GO), have been the most  
325 thoroughly investigated 2D materials to date, with substantial progress toward  
326 commercialization (Wu et al., 2022; H. Zhang et al., 2022). However, in 2D materials, where  
327 vdW forces may segregate an atomically thin layer from bulk material, they are only the tip  
328 of the iceberg. In recent years, novel vdW 2D nanostructured future-generation materials,  
329 such as MXenes, have emerged, with similar physicochemical behavior to graphene and its  
330 derivatives and the added benefits of hydrophilic nature, high stability, accessible to  
331 functionalized, increased flake size, improved yield, and better machine processability  
332 (Chakraborty et al., 2018; Ho et al., 2021; Naguib et al., 2021). These 2D materials have  
333 diverse surface compositions, adjustable interlayer spacing, and physicochemical properties  
334 that may be optimized, making them ideal alternatives for developing advanced future-  
335 generation sensors. Most investigations have been dedicated to designing their structure  
336 and optimizing their characteristics by regulating the interaction factors, modifying  
337 interlayer spacing, exploring stoichiometry, and tuning and functionalizing the surface.

338 2D MXenes, ever since their inception in 2011, has attracted extensive research  
339 interest across all 2D materials (Huang et al., 2020; Jiang et al., 2020; Naguib et al., 2021).  
340 MXenes are a newly developed family of 2D layered transitional metallic  
341 nitrides/carbides/carbonitrides elucidated by  $M_{n+1}X_nT_x$ , where 'n' signifies layers, number  
342 bonded together through vdW forces, 'M' denotes initial transitional metals (e.g., Ti, Mo, Sc  
343 and V). 'X' stands for nitrogen/carbon/carbonitrides, and 'T' refers to the surface terminals  
344 groups, i.e., oxygen (-O), chlorine (-Cl), fluorine (-F) and hydroxyl (-OH) (Naguib et al., 2021).  
345 The 'M' atoms in the double transitional metal MXene can be found in either an arranged or  
346 randomized phase of solid solution, with an ordered arrangement being far more  
347 energetically stable (Jiang et al., 2020; Naguib et al., 2021). MXenes family is continuously  
348 growing due to the development of a myriad of synthetic MXenes together with varied

349 stoichiometry, including  $Ti_3C_2T_x$ ,  $Ti_3CNT_x$ , and  $(Ti_{0.5}Nb_{0.5})_2CT_x$ , as shown in **Figure 6**.



350

351 **Figure 6.** Expanding family of MXenes classified based on numbers of layers, stoichiometry,  
 352 and surface functionalities, displaying all MXene classes grouped by layer count.

353 Similarly, the number of etching strategies, such as 3D 'MAX' ( $M_{n+1}AX_n$ , where A is  
 354 13/14 group element) (Jiang et al., 2020; Naguib et al., 2021), 'non-MAX'[14], i.e.,  
 355  $(MC)_n[Al(A)]_mC_{(m-1)}$ , where m is 3,4, and A is Si or Ge and 'modified-MAX' with 'i-max phase,'  
 356 i.e.,  $(M^{1/2/3}M^{2/1/3})_2AX$  have been utilised to develop MXenes (Chaudhary et al., 2022c). A  
 357 Multi-layered MXene is produced after discarding the layers of 'A/A-C' from its original  
 358 precursor's form (Jiang et al., 2020; Naguib et al., 2021). Therefore, with the applications of  
 359 modern computational methodologies based on a detailed electronic structure and phonon  
 360 analyses, a verified, more detailed image of the potential of eliminating the middle layer  
 361 (A/A-C) out of the precursor to produce MXene was assessed theoretically (Jiang et al.,  
 362 2020). For example, to envision the exfoliating and etching prospects of 82 MAX precursors,  
 363 the static-exfoliation energies were predicted using force constants (Khazaei et al., 2013).  
 364 The findings demonstrated that projected average force constants for 'A' atoms within  
 365 precursors were in linear relation with the exfoliation perspective, revealing that eliminating  
 366 'A' layers may form MXene.



367 To extract and develop the MXene layer from its MAX phase precursors, chemical  
368 methods comprising two primary phases, namely selective etching and delamination, were  
369 applied in the experimental investigation (Huang et al., 2020; Naguib et al., 2021). In  
370 contrast, numerous etching techniques segregate the middle layers of 'A/A-C/Al-A-C' from  
371 the precursor for producing the MXene sheet (Naguib et al., 2021). These approaches tend  
372 to etch MXene layers, encompassing fluorine-carrying etchants (e.g. HF, LiF and HCl mixture,  
373 fluorine-incorporated liquefied salt, and fluoride salts), non-fluorinated etching, such as  
374 electrochemistry and alkaline rich hydrothermal etching process, and non-aqueous liquid  
375 phased etching method employing Lewis acidic salts (Jiang et al., 2020; Naguib et al., 2021).  
376 To illustrate this, Naguib et al. (Naguib et al., 2011) disclosed the initial production of  
377  $Ti_3C_2T_x$ -based MXene from its respective  $Ti_3AlC_2$  MAX precursor through selective HF etching  
378 of 'Al'. Molecular dynamic ab-initio-based computing simulations show that the structural  
379 bonding of Ti-Al degrades significantly when the radicals F/H from the adsorbed HF are  
380 decomposed over Ti atoms, resulting in surface functionalities and the formation of  $Ti_3C_2T_x$ .  
381 Following this, ample etching techniques have been devised to construct distinct MXenes, as  
382 illustrated in **Table 1**.

383 A selective etching process is usually a kinetically controlled process in which the  
384 emergence of surface functionalities onto the MXene surface is governed by the precise  
385 etching method and reaction environment. Fluorine-based etchants, for example, lead to  
386 surface terminations of -F, -OH and -O. While etching process without fluorine eliminates  
387 fluorine surface functions from MXenes (Khaledialidusti et al., 2020; Q. Li et al., 2021).  
388 Mono-layered MXene sheets could be produced successfully through a suitable  
389 delamination approach that may depend on the type of surface functions occurring within  
390 multi-layer MXene. To illustrate, the emergence of oxygen-based functional groups leads to  
391 highly critical interlayer bonding. While the active hydroxide (-OH) groups are more likely to  
392 deform the MXene layers (Wei et al., 2021). Ion intercalation may readily delaminate  
393 several layer MXenes, extending the interlayer gap of multilayer MXenes. The intercalation  
394 process incorporates intercalation compounds, i.e., DMSO and TBAOH, metal cations, and  
395 secondary nanofillers, such as macromolecules (Wei et al., 2021). In this section, the  
396 strategies evolved to produce diversified MXenes utilizing selective etching have been  
397 reviewed comprehensively (Jiang et al., 2020; Naguib et al., 2021; Wei et al., 2021). A

398 rigorous description of MXene manufacturing utilizing multiple precursors and etching  
 399 techniques is presented in **Table 1**.

400 **Table 1.** A comprehensive summary of diversified MXene's fabrication strategies resulting in  
 401 different surface terminations using a top-down strategy comprised of selective etching  
 402 from different precursors (Chakraborty et al., 2018; Chaudhary et al., 2022c; Ho et al., 2021;  
 403 Jiang et al., 2020; Naguib et al., 2021; Wei et al., 2021)

MAX Phases	Etched MXene	Etchant Used	Etchant Strategy	Surface Termination Group
Ti <sub>3</sub> AlC <sub>2</sub> , V <sub>2</sub> AlC, Nb <sub>2</sub> AlC, Nb <sub>4</sub> AlC <sub>3</sub> , Ta <sub>4</sub> AlC <sub>3</sub> , (Ti,Nb) <sub>2</sub> AlC, Mo <sub>2</sub> Ti <sub>2</sub> AlC <sub>3</sub> , Mo <sub>2</sub> Ga <sub>2</sub> C <sub>2</sub> T <sub>x</sub> , Hf <sub>3</sub> (AlSi) <sub>4</sub> C <sub>6</sub> , Zr <sub>3</sub> Al <sub>3</sub> C <sub>5</sub> (Mo <sub>2/3</sub> Sc <sub>1/3</sub> ) <sub>2</sub> AlC	Ti <sub>3</sub> C <sub>2</sub> T <sub>x</sub> , V <sub>2</sub> CT <sub>x</sub> , Nb <sub>2</sub> CT <sub>x</sub> , Nb <sub>4</sub> C <sub>3</sub> T <sub>x</sub> , Ta <sub>4</sub> C <sub>3</sub> T <sub>x</sub> , (Ti,Nb) <sub>2</sub> CT <sub>x</sub> , Mo <sub>2</sub> Ti <sub>2</sub> C <sub>3</sub> T <sub>x</sub> , Mo <sub>2</sub> C, Hf <sub>3</sub> C <sub>2</sub> T <sub>x</sub> , Zr <sub>3</sub> C <sub>2</sub> T <sub>x</sub> , Mo <sub>1.33</sub> CT <sub>x</sub>	HF	HF etching	-O, -OH, -F
Ti <sub>2</sub> AlC, Ti <sub>3</sub> AlC <sub>2</sub> , (Nb,Zr) <sub>4</sub> AlC <sub>3</sub> , V <sub>2</sub> AlC, Ti <sub>3</sub> AlCN	Ti <sub>2</sub> CT <sub>x</sub> , Ti <sub>3</sub> C <sub>2</sub> T <sub>x</sub> , (Nb,Zr) <sub>4</sub> C <sub>3</sub> T <sub>x</sub> , V <sub>2</sub> CT <sub>x</sub> , Ti <sub>3</sub> CNT <sub>x</sub>	LiF/KF/NaF/ FeF <sub>3</sub> / NH <sub>4</sub> F + HCl, NaHF <sub>2</sub> /KHF <sub>2</sub> /NH <sub>4</sub> HF <sub>2</sub> ; LiF/KF/NaF/ FeF <sub>3</sub> / NH <sub>4</sub> F + HCl; NH <sub>4</sub> F+C <sub>5</sub> H <sub>14</sub> Cl H <sub>2</sub> C <sub>2</sub> O <sub>4</sub> ; Ionic liquid (EMIMBF <sub>4</sub> /BMIMPF <sub>6</sub> ), LiF +HCl, NaF + HCl, LiF + HCl	In situ HF formation etching	-O, -OH, -F -O, -F (ionic liquid)
Ti <sub>3</sub> AlC <sub>2</sub>	Ti <sub>3</sub> C <sub>2</sub> T <sub>x</sub>	NaOH + H <sub>2</sub> SO <sub>4</sub> , NaOH, KOH	Alkali etching	-OH, -O
Ti <sub>3</sub> AlC <sub>2</sub> , V <sub>2</sub> AlC, Cr <sub>2</sub> AlC	Ti <sub>3</sub> C <sub>2</sub> T <sub>x</sub> , V <sub>2</sub> CT <sub>x</sub> , Cr <sub>2</sub> CT <sub>x</sub>	NH <sub>4</sub> Cl +TMAOH/HCl, HCl, HCl	Electrochemical Etching	-OH, -O, -Cl
Ti <sub>3</sub> SiC <sub>2</sub> ,Ti <sub>3</sub> ZnC <sub>2</sub> Ti <sub>4</sub> AlN <sub>3</sub>	Ti <sub>3</sub> C <sub>2</sub> T <sub>x</sub> Ti <sub>4</sub> N <sub>3</sub> T <sub>x</sub>	CuCl <sub>2</sub> , FeCl <sub>2</sub> /CoCl <sub>2</sub> /NiCl <sub>2</sub> /AgCl <sub>2</sub> /CdCl <sub>2</sub> KF/LiF/NaF	Molten salt etching	-O, -Cl -O, -F
Ti <sub>3</sub> AlC <sub>2</sub>	Ti <sub>3</sub> C <sub>2</sub> T <sub>x</sub>	I <sub>2</sub>	Etching	-O, -OH, -I
Mo <sub>2</sub> Ga <sub>2</sub> C	Mo <sub>2</sub> C	Ultraviolet light (100W)	UV	-O
Ti <sub>3</sub> AlC <sub>2</sub>	Ti <sub>3</sub> C <sub>2</sub> T <sub>x</sub>	LiF	Surface acoustic waves (SAWs)	-O, -OH, -F
Ti <sub>2</sub> SC	Ti <sub>2</sub> CT <sub>x</sub>	400–900 °C	Thermal reduction Strategy	-O, -OH
Ti <sub>3</sub> AlC <sub>2</sub>	Ti <sub>3</sub> C <sub>2</sub> T <sub>x</sub>	Algae	Bioreduction	-O, -OH

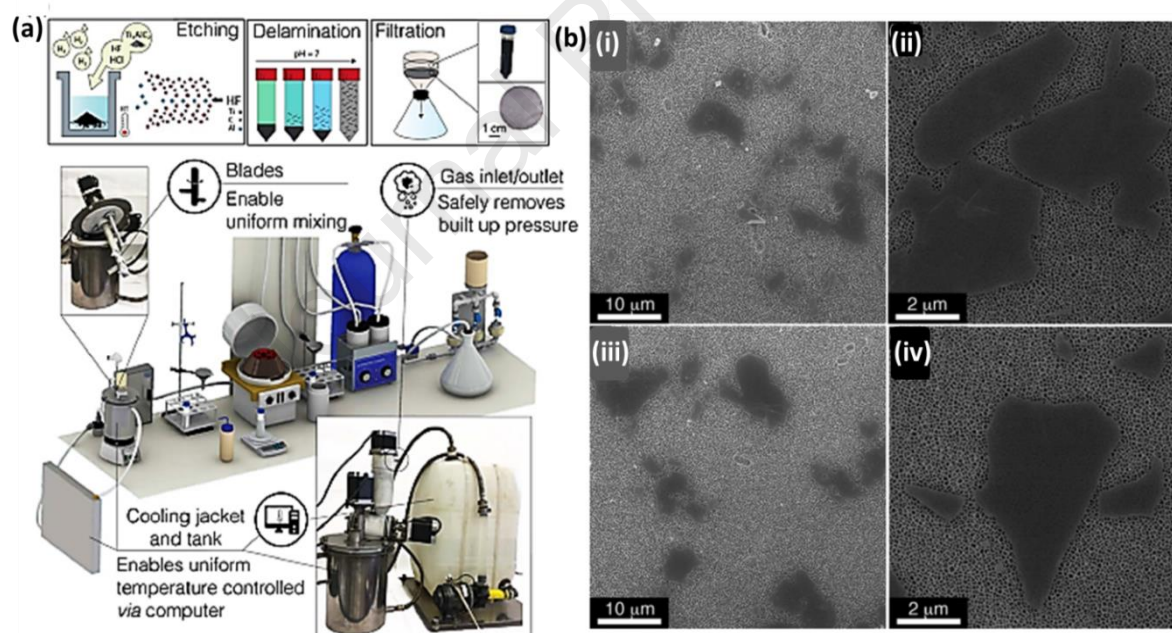
404

405 Nevertheless, the physicochemical properties and application efficacy of these  
406 mechanically stimulated MXenes get influenced due to the presence of several defects  
407 (Naguib et al., 2021). Further, harmful, and volatile HF etchant, along with other etchants,  
408 causes environmental pollutants and threatens users' safety and health. Consequently,  
409 numerous bottom-up techniques for MXene production have been explored, including  
410 atomic layer deposition, chemical vapor deposition, and plasma-enhanced pulsed laser  
411 deposition (PEPLD) (Aghamohammadi et al., 2021; Naguib et al., 2021; Wei et al., 2021).  
412 Gogotsi et al. (Gogotsi, 2015) reported the bi-layer substrate of copper, which was reduced  
413 onto molybdenum foil having a size of  $\sim 100\mu\text{m}$  to form molybdenum carbide crystal ( $-\text{Mo}_2\text{C}$ )  
414 with ultrathin size by maintaining it at  $\sim 1085^\circ\text{C}$  with a low methane content. Even though  
415 these approaches hinder secondary contamination and user-related threats, they are very  
416 complicated, costly, time-consuming, and low-yielding methods. This not only limits their  
417 commercialism but also enforces to use of top-bottom approaches based on etchants for  
418 scaling MXene production.

419 Moreover, for commercializing and carrying technology from laboratories to the  
420 appropriate marketplaces, scalable production of MXenes is vital. The stumbling blocks in  
421 scalable manufacturing of MXene are controlling reactor capacity, persistent transfer and  
422 homogenous blending of precursors, regulating thermal reactions and preserving safety  
423 considerations, and achieving optimal reaction parameters to attain required  
424 physicochemical attributes (Naguib et al., 2021; Shuck et al., 2020; Wei et al., 2021; M. Q.  
425 Zhao et al., 2019) Shuck et al. (Shuck et al., 2020) described the scalable manufacturing of  
426 MXene based on titanium carbide in a customized, large-scale chemical reactor with many  
427 necessities, such as cooling jackets, gas inlet and outlet with a screw feeding system,  
428 blender, temperature sensor and agitator for addressing the issues (**Figure 7(a)**). The HF-  
429 based selective etching throughout the processing yielded multilayer  $\text{Ti}_3\text{C}_2\text{T}_x$  MXene and  
430 mono-flake MXene. Later these materials were intercalated in a dried vacuum and water. In  
431 comparison, formation (etching utilizing traditional in-laboratory HF technique) of a large-  
432 size batch to that of the small-size batch was remarkably higher by 52%, with comparable  
433 physicochemical properties, showing the approach's effectiveness for mass manufacturing.  
434 Subsequently, the obtained MXene sheets were either several layered or few-layered after

435 intercalating using water (**Figure 7(b: i-iv)**) (Shuck et al., 2020) . It necessitated a scalable  
 436 intercalation process to achieve MXene with fewer layers or a single-layer arrangement.

437 Furthermore, Zhang et al. (S. Zhang et al., 2020) described a novel method to use an  
 438 ammonium ion to address the problems related to the adhesion and reassembly of few-  
 439 layer MXenes on a vast scale. To intercalate and delaminate the MXenes layers with a usual  
 440 processing method, a solution-form-flocculation technique and redesigned method was  
 441 implemented. This technique can scale up the production of numerable MXenes, such as  
 442  $Ti_3C_2T_x$ ,  $Nb_4C_3T_x$ ,  $V_2CT_x$ ,  $Nb_2CT_x$ , and others. On the other hand, this method has been used  
 443 merely to investigate  $M_3C_2T_x$ -MXene. This technique is yet to examine other related  
 444 configurations of MXenes or synthesized MXenes. Additionally, several concerns, such as  
 445 secondary environmental degradation and safety and health risks linked with the suggested  
 446 scale-up processing, necessitate redesigning a more sustainable MXene production process  
 447 at the commercial level.



448

449 **Figure 7.** Illustration of scalable fabrication strategy for manufacturing MXenes in (a) A large  
 450 reactor with cooling provisions, and (b) Morphological analysis based comparison between  
 451 MXenes prepared through small traditional chemical strategy and large scale reactor (Shuck  
 452 et al., 2020).

#### 453 **4. Novel characteristics of MXenes and hybrids for efficient biosensing**

454 Optimizing the material's unique physicochemical attributes is the key to obtaining  
 455 outstanding quality and fulfilling industrial material demands for the targeted application

456 (Chaudhary, 2022, 2021a; Chaudhary et al., 2022a, 2017; Chaudhary and Chavali, 2021;  
457 Chaudhary and Kaur, 2015). It implies improvements in the detection material's  
458 physicochemical traits, which may be achieved during the manufacturing phase by  
459 optimizing the reaction conditions. Similarly, MXenes display outstanding physicochemical  
460 properties, such as hydrophilicity, flexibility, high mechanical durability, adjustable band  
461 gaps, rich surface chemistries, and huge active surface area (L. Wang et al., 2021; Weng et  
462 al., 2015) This makes MXenes a highly suitable material for designing next-generation  
463 sensors exhibiting excellent selectivity and sensitivity, biocompatibility as well as simple  
464 machine processability. However, by designing and developing hybrids/nanocomposites  
465 with other substances, various challenges associated with particular 2D materials can be  
466 addressed further(Chaudhary et al., 2021a; Dhall et al., 2021; Hashtroudi et al., 2020).

467 Usually, the physicochemical properties of MXenes are strongly influenced by their  
468 stoichiometry, interlayer spacing, specific size, layer numbers, and pattern for stacking. To  
469 exemplify, during the segregation of the A/A-C layer from its respective precursors, the 'M'  
470 ions become exposed on the faces of the MXenes layer (Wei et al., 2021). In the MXene  
471 sheet, these surfaced 'M' atoms are not only unstable but also highly prone to bonding with  
472 surface functional groups, such as -F, -OH, -O, and -Cl, which emerge from the etching  
473 processes and reduces the overall surface efficiency(Naguib et al., 2021; Wei et al., 2021).  
474 As a result, it becomes critical first to understand how  $T_x$  affects the physicochemical  
475 characteristics of MXenes sheets. So that better and improved sensors can be designed.  
476 Apart from experimental validations, several computational programming based on  
477 advanced data learning techniques, such as machine learning (ML) and deep learning (DL)  
478 based on molecular dynamics (MD) or density-functional theory (DFT), have been  
479 predominantly used to analyze the changes in the physicochemical properties of MXenes in  
480 fluctuating and complex conditions.

#### 481 **4.1. Ambient and processing Stability**

482 For sensing applications, sensors must be thermally and chemically stable. The sensing  
483 material undergoes several chemical and heat treatments during machine processing for  
484 sensor manufacturing. After complete synthesis, it must perform efficiently in all  
485 operational conditions. Although MXene maintains its structural stability with saturated  
486 surface terminations, it is thermally unstable due to its stoichiometry due to the exposed

487 'M' atoms on both sides, which are unstable owing to weak interactions (Jiang et al., 2020).  
488 This enhances the nucleation growth of these exposed 'M' atoms when they react with  
489 water molecules or oxygen atoms, which then expand throughout the MXene, leading to  
490 structural defects with extended edges (Jiang et al., 2020; Zhan et al., 2020). It steadily  
491 accelerates MXene's oxidative disintegration into transition metal oxides. For example, in  
492 oxidative surroundings, such as heated temperatures,  $Ti_3C_2T_x$  is unstable and gradually  
493 transforms into  $TiO_2$  (He et al., 2021). These conversions may result in the loss of MXene's  
494 unique properties, including electrical and thermal conductance, hydrophilic nature, and  
495 increased pseudo-capacitance, adversely affecting the projected sensor performance (Iqbal  
496 et al., 2021).

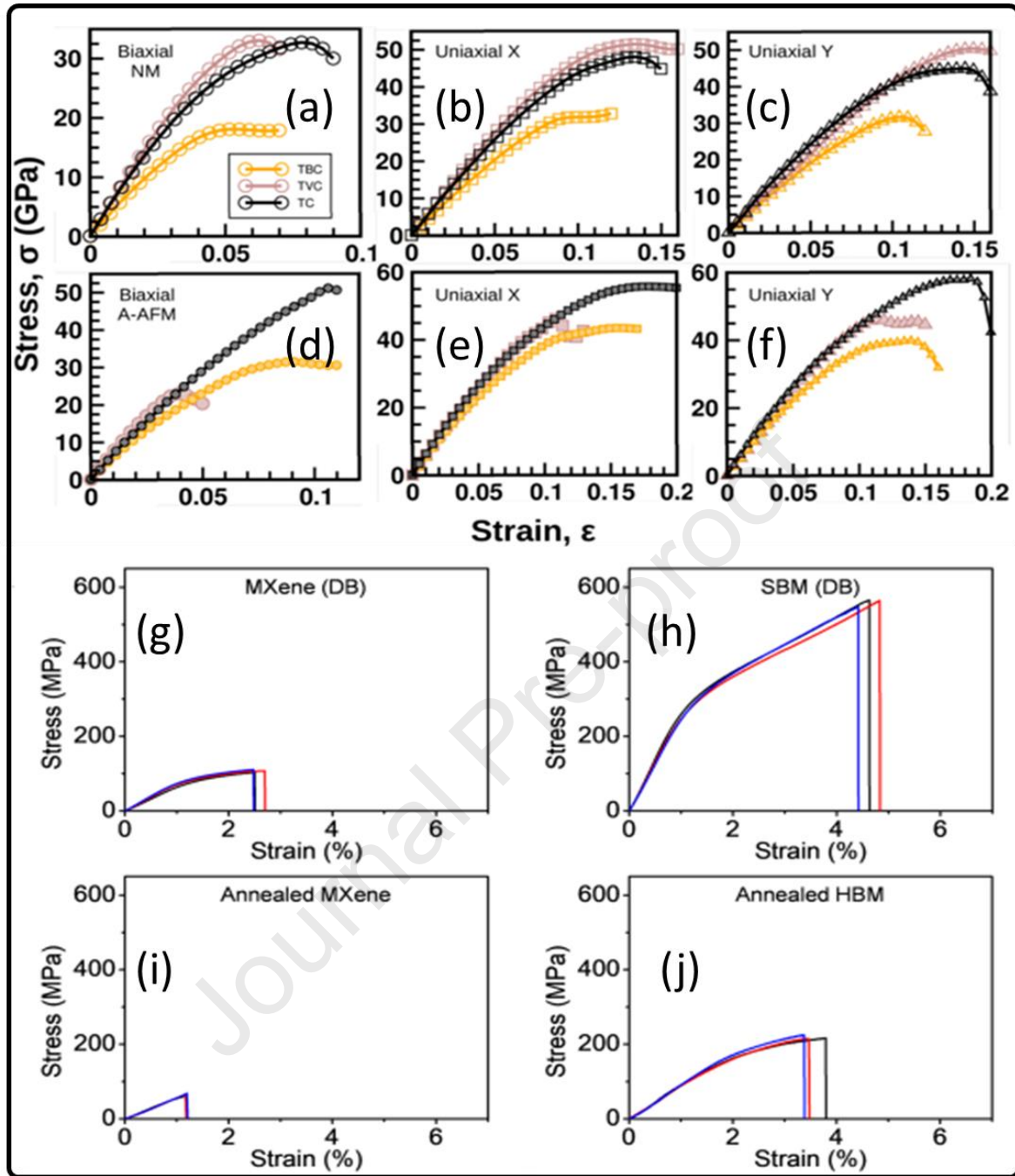
497 The production of oxidant-inhibitor MXenes employing sophisticated pre-processing  
498 and storing techniques cater to these stability limitations. These techniques consist of  
499 storage of MXene in inert conditions using gases, such as Ar for obstructing the effect of  
500 oxidation, storage at a low-temperature range to avoid nucleation propagation,  
501 Preservation of MXene in organic or inorganic dispersions, cease edge atoms through  
502 absorption of anionic salts, treat MXene with reduction gases (Chae et al., 2019; Lee et al.,  
503 2020; Natu et al., 2019; Zhang et al., 2017; X. Zhao et al., 2019). Also, designing MXene  
504 complex structures using carbon substances or macro-compounds or dispersing in ionic  
505 salted liquids have been proven strategies for an efficient antioxidant MXene (Chaudhary et  
506 al., 2021a; Du et al., 2021; Iqbal et al., 2021; Wu et al., 2017; Zhan et al., 2020). Further,  
507 treating MXene thermally at elevated temperatures (i.e., 1200°C) in an argon environment  
508 eradicates surface terminations and enhances structural patterns without impairing layered  
509 microstructure (Wei et al., 2021). Therefore, the logical design of MXene- based products  
510 should be promoted for their intended uses.

511 Moreover, surface functionalization and hybridization are two important techniques  
512 essential to modulate interlayer spacing and preventing restacking of MXene layers and  
513 ambient oxidation. For instance, the introduction of macromolecules/polymer between the  
514 MXene layers prevents their restacking, providing stability, increases surface-to-volume  
515 ratio making MXene architect more accessible to analyte/biomolecule interaction, and  
516 modifies surface terminals to provide selectivity and stability. For instance, For instance, Li  
517 et al. (X. Li et al., 2020) described that the manifestation of dendritic polyaniline

518 nanoparticles exfoliates the interlayer distance amongst the  $Ti_3C_2T_x$  nanosheets in  
519 MXene/polymer hybrids. It considerably surges the specific surface area and porosity of  
520 MXene-hybrid, prompting it as a latent candidate for analyte detection. Moreover, the core-  
521 shell type morphology of  $Ti_3C_2T_x/PAN$  contributed to its ambient stability. Furthermore,  
522 Chen et al.(Chen et al., 2020) reported the surge in surface area of DL-tartaric acid (DLTA)  
523 assembled  $Ti_3C_2T_x$ -MXene (less than  $5\text{ m}^2/\text{g}$ ) with the hybridization with polyaniline (20-23  
524  $\text{m}^2/\text{g}$ ). Besides, the hybrid was reported to be mesoporous possessing broad pore-size  
525 distributions varying from 2 to 40 nm, which expedite the rapid analyte/ion/biomolecule  
526 diffusion and is highly favorable for biosensing applications.

#### 527 4.2. Machine processability

528 Optimizing materials' flexibility and mechanical strength in terms of tribological properties  
529 to fabricate next-generation sensors is indispensable. MXenes exhibit unique tribological  
530 properties that may be improved and optimized using numerous techniques. In a bi-layer  
531  $Ti_3C_2T_x$ , for example, the young's modulus and elasticity observed were 502 GPa and  $\sim 655$   
532 N/m, respectively. This implies the improved interlayer association among surface  
533 functionalities (Borysiuk et al., 2015). Further, nanoindentation findings indicated that the  
534 elasticity of a bi-layer  $Ti_3C_2T_x$  is far more significant than other two-dimensional materials  
535 such as GO, rGO, and  $MoS_2$ . Chakraborty et al. (Chakraborty et al., 2018) reported the  
536 mechanical properties and doping effect of  $Ti_2C$  MXene. As illustrated in **Figure 8**, stress and  
537 strain relation possesses the lowest energy antiferromagnetic and non-magnetic states. It  
538 can be observed from the figure that there is a 25 to 27% decline in Young's modulus and  
539 plane stiffness of the  $Ti_2(C_{0.5}B_{0.5})$  comparable to the MXene. Moreover, titanium doping over  
540 the v sites produced the undoped stiffness of MXene. In contrast, the calculated stiffness of  
541  $Ti_2(C_{0.5}B_{0.5})$  was noted to be 4.2, 1.5, 1.86 and 3.1, which is much greater than the stiffness  
542 of graphene, h-BN,  $MoS_2$  and SiC, respectively.



543

544 **Figure 8.** Representing the stress and strain curves of the  $\text{Ti}_2\text{C}$ ,  $\text{Ti}_2(\text{C}_{0.5}\text{B}_{0.5})$  and  $(\text{Ti}, \text{V})\text{C}$   
 545 under the uniaxial and biaxial tensile strength, also showing the outcomes of the  
 546 antiferromagnetic and non-magnetic state (Chakraborty et al., 2018).

547 Flexibility in sensor architecture can further be attained by developing self-sustained  
 548 flexible thin films or using flexible materials. For example, numerous MXenes, such as  
 549  $\text{Ti}_3\text{C}_2\text{T}_x$ , display a high degree of intrinsic flexibility when transformed into a conical design  
 550 with a radius smaller than 20 nm (Naguib et al., 2011). To illustrate, self-standing  $\text{Ti}_3\text{C}_2\text{T}_x$  thin  
 551 films of approximately 3.3  $\mu\text{m}$  thickness have mechanical strength of  $\sim 22$  MPa. While



552  $Ti_3C_2T_x$  cylindrically rolled paper of  $\sim 5\mu m$  thickness showed sustainability over 4000 times its  
553 weight (Lipatov et al., 2018).

554 Moreover, there have been reports on scalable manufacturing of freestanding  
555 MXene Films with optimized flexibility utilizing distinct processes, such as sedimentation,  
556 membrane filtering, powder-coating, doctor blading, drop casting in a vacuum, and LBL  
557 assembly (Qian et al., 2022; Verma et al., 2022; J. Zhang et al., 2020; M. Q. Zhao et al.,  
558 2019). To illustrate, Lipton et al. (Lipton et al., 2020) demonstrated using an inverse-drop  
559 casting process to fabricate a scalable conductive and free-standing film of  $Ti_3C_2T_x$  on a  
560 water-insoluble plastic substrate. Interestingly, self-standing MXene thin films are free of  
561 voids, which otherwise appear during conventional manufacturing.

562 Furthermore, Wan et al. (Wan et al., 2021) have demonstrated a unique bridging-  
563 induced densification process for scalable production of MXene films. During synthesis, the  
564 layered structure of MXene was densified, and the voids were filled with a sequential  
565 mixture of covalent and hydrogen bonding molecules. Also, MXenes can be readily  
566 deposited on flexible substrate surfaces due to their outstanding dispersibility and  
567 hydrophilicity. Developing complex/hybrid MXene layers using macromolecules can also  
568 increase their flexibility (Chaudhary et al., 2021a). However, retaining the flexible nature  
569 and mechanical endurance of such complex MXenes throughout the machining process is  
570 exceptionally tedious. Still, it can be achieved through optimal precursor parameters like  
571 concentration during machine processing. Zhao et al. (L. Zhao et al., 2019) reported the  
572 flexible nature and the resilient character of  $Ti_3C_2T_x/CPAM$  HNC, which they attributed to  
573 CPAM's high affinity between the layers of  $Ti_3C_2T_x$ .

574 In contrast, Li et al. (X. Li et al., 2020) and Wang et al. (S. Wang et al., 2021a, 2021b)  
575 both groups successfully adopted the flexible PI substrate surfaces to design flexible MXene-  
576 polymer hybrid gas sensing devices. Besides this, during etching with the emergence of  
577 hydrophilic functional elements, such as -O and -F, MXenes become highly dispersible to  
578 several solvents. The most common dispersion mediums for MXene are water, cyclic  
579 propylene carbonate, dimethyl sulfoxide, dimethylformamide, and a particular  
580 concentration of about 0.3 mg m/L of non-ionized solvents like toluene and hexane, which  
581 distinguishes it apart from other carbonaceous 2D nanomaterials including graphene and  
582 graphene-based derivatives. MXene's strong dispersion ability and hydrophilic nature

583 enable their manufacturing by solution-based strategies, hybrid advances with other  
584 nanomaterials, and solution-processability to design sensing devices for numerous  
585 commercial applications.

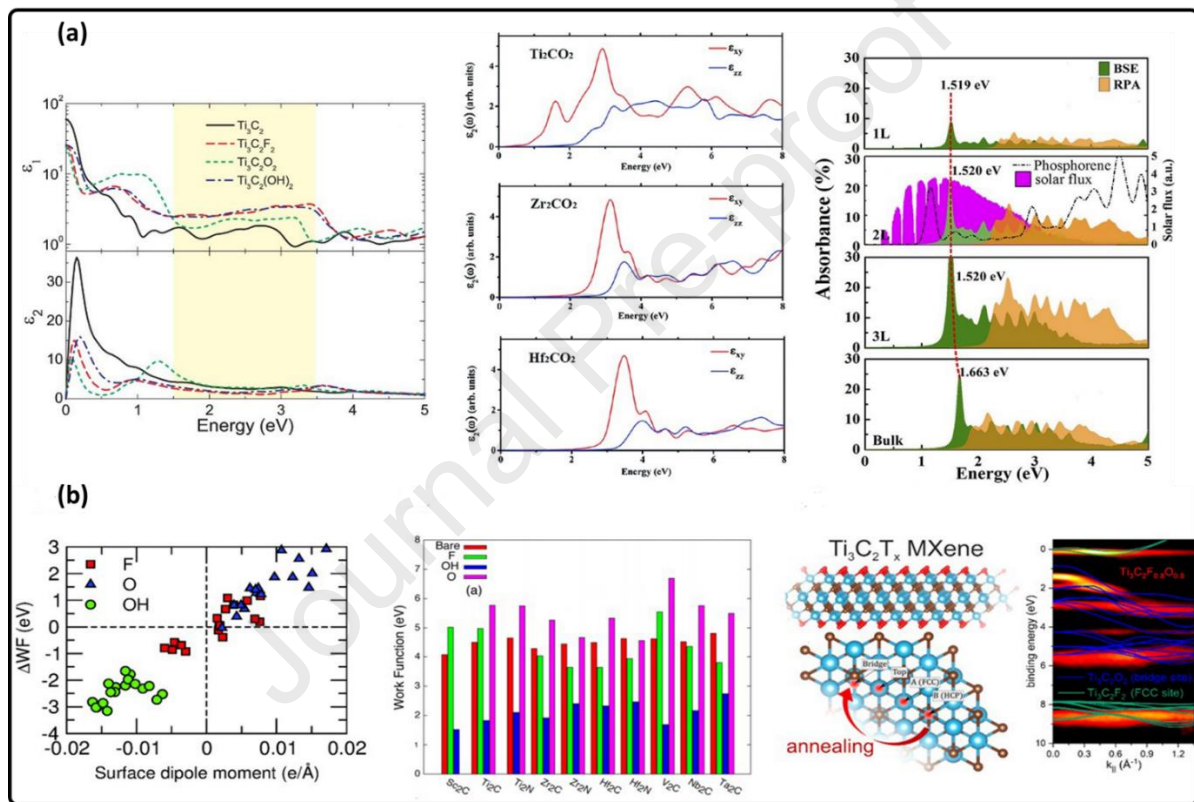
#### 586 4.3. Electronic and optical behavior

587 Electronic behavior, such as conductance and charge transfer, has become a critical  
588 underlying aspect in defining the target response of a sensing device application  
589 (Chaudhary, 2021b; Chaudhary et al., 2022a; Chaudhary and Chavali, 2021). For example, a  
590 polymer with 1D charge transfer routes detects stimulus variations more efficiently than  
591 one with 3D charge carrier transports (Chaudhary, 2022, 2021a; Chaudhary et al., 2017). It  
592 has increased the demand for pre-analyzing the electrical behavior of materials before  
593 determining their uses. Several computer simulations have revealed that the metallic  
594 behavior of MXenes, and valency and electrical conduction band are extremely close to the  
595 Fermi energy level (Jiang et al., 2020; Naguib et al., 2021). Additionally, it is proposed that  
596 surface functionalization can tailor the electrical character of MXenes to the semiconducting  
597 range (Dillon et al., 2016; Si et al., 2016; Weng et al., 2015).

598 DFT computational analysis, for example, indicated that the appearance of -OH and -  
599 F surface functionalities transform the metallic form of  $Ti_3C_2T_x$  into a semiconductor with a  
600 projected electronic band gap ranging between 0.05 eV and 0.1 eV, respectively. This  
601 curtails the electrical conductance of the material due to decreased charge transport  
602 density (Jiang et al., 2020; Xie and Kent, 2013). It has also been observed that changing the  
603 spatial arrangement of -F and -OH on MXenes leads to optical band gap modulation  
604 (Chakraborty et al., 2018; Jiang et al., 2020; Scott et al., 2022). As a result, by modifying the  
605 characteristics and geometric profile of functionalized surface groups, the electronic  
606 behavior of MXenes can be explicitly tailored for sensing applications. Also, MXenes' optical  
607 properties are intrinsically linked to their electrical character (Berdiyrov, 2016; Lashgari et  
608 al., 2014). DFT analysis revealed that most of the MXenes types, including  $Ti_{n+1}X_n$ , exhibit  
609 metallic properties because of the considerable overlap of the valence band and electrical  
610 conduction bands at the Fermi energy (Lashgari et al., 2014). Berdiyrov et al. (Berdiyrov,  
611 2016) demonstrated the reliance of essential and unreal elements of frequency-assisted  
612 dielectric functionalities on surface elemental groups for numerous pure MXenes, such as

613  $\text{Ti}_3\text{C}_2$ ,  $\text{Ti}_3\text{C}_2\text{F}_2$ ,  $\text{Ti}_3\text{C}_2\text{O}_2$ , and  $\text{Ti}_3\text{C}_2(\text{OH})_2$ . The electronic characteristics and densities of MXene  
 614 are shown in **Figure 9**.

615 Furthermore, the applicability of OH-reduced  $\text{Ti}_3\text{C}_2\text{T}_x$  with lower reflection and  
 616 absorption rate in the visible region makes it attractive for designing transparent but  
 617 wearable consumer electronic devices and photothermally targeted biosensing applications  
 618 (Lei et al., 2020). Therefore, the tailorable electrical and optical behavior of MXene makes it  
 619 a high potential material for designing the sensing devices of future-generation with  
 620 sophisticated functions and high-performance outcomes.



621

622 **Fig. 9.** Tunable electronic properties of  $\text{Ti}_2\text{CT}_x$  MXenes with diversified surface terminations  
 623 analyzed through Density Functional Theory considering density of states (Berdiyrov, 2016).

## 624 5. Engineering advanced biosensors-based on MXenes and their hybrids

625 A biosensor is an analytical device that senses biological reactions by establishing distinct  
 626 readout signals in response to interactions with biomes. It comprises two primary  
 627 components: a physical-chemical converter and a biological receptor (Ansari and Malhotra,  
 628 2022; Chaudhary et al., 2022d). Because of their greater specific area and rapid charge  
 629 transfer systems, one-dimensional (1D) nanomaterials, such as carbon nanotubes (CNTs),  
 630 metal nanowires, and macromolecule nanofibers, have lately surpassed the obstacles

631 related to typical biosensors based on bulk materials (Ansari and Malhotra, 2022; Zhou and  
632 Zhang, 2021). However, despite the remarkable biosensing performance of 1D materials,  
633 their costly production, erratic behavior in distinct device modules, and unstable in varied  
634 environments have limited their commercial possibilities.

635 MXenes, On the other hand, offer more streamlined production competencies along  
636 with the ability to maintain physicochemical as well as electrical behavior along with rich  
637 surface functionalities, clearly making them highly intriguing for designing biosensing  
638 instruments (Ansari and Malhotra, 2022; Chaudhary et al., 2022d; Khunger et al., 2021;  
639 Zhou and Zhang, 2021). There have been several findings on two-dimensional materials to  
640 form detectors or biomarkers for subjectively and quantitatively sensing metabolic  
641 abnormalities, evaluating the efficacy of various therapeutics, and assessing various  
642 environmental hazards such as infections and toxic substances. As per transducing reactions  
643 and sensing processes, a comprehensive classification of MXene-based biosensors has been  
644 discussed in this article.

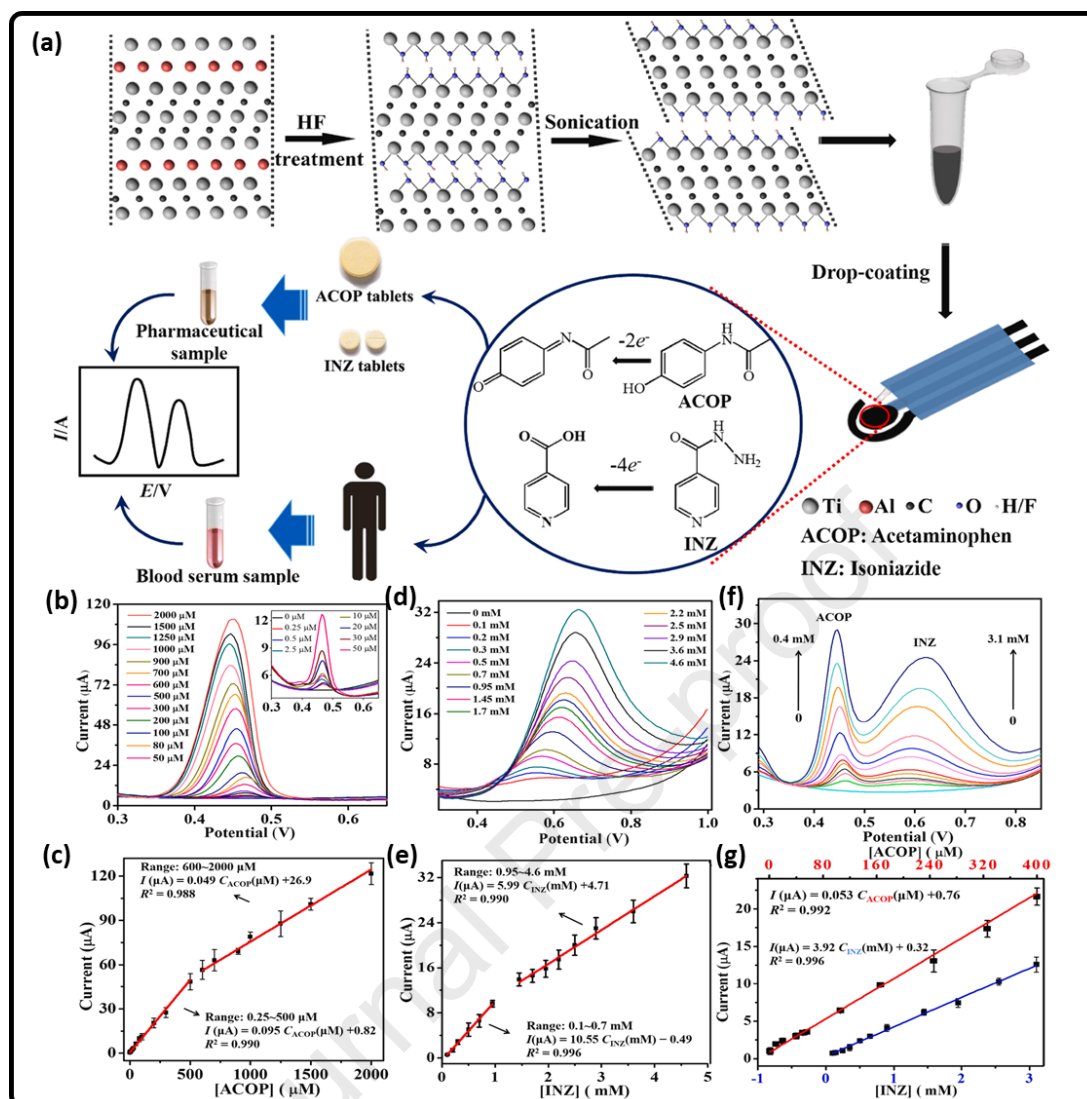
#### 645 5.1. Advancements in electrochemical and electrical biosensors based on MXenes

646 The capability to sense biomes with a biosensor needs precise, vigilant, and targeted  
647 sensing for practical viability. The biosensors, designed according to the electrochemical  
648 modules for high sensitivity and selectivity of smaller biomolecules or biomes in the solution  
649 phase, have been illustrated. MXenes, owing to rich electron-terminal surface chemistries  
650 that attract positively charged biomolecules, had been expected as attractive  
651 electrochemical biosensing receptors as well as transducers (Chaudhary et al., 2022e,  
652 2022c; Shahzad et al., 2019; Sheth et al., 2022; Wu et al., 2019; Yao et al., 2020; Y. Zhang et  
653 al., 2019). Zhang et al. (Y. Zhang et al., 2019) utilized  $Ti_3C_2T_x$  nanosheets tuned screen-  
654 printed electrode (SPE) to identify two regularly utilized medicines, namely isoniazid (INZ)  
655 and acetaminophen (ACOP), which are known to cause liver problems in human beings.  
656 Linear sensing ranges for ACOP and INZ of 0.252000 M and 0.146 M, respectively, with  
657 0.048 M and 0.064 M LODs, which were relatively higher than unmodified SPE, were  
658 observed by the detector (**Figure 10(a-g)**). It has been ascribed to the abundant vacancies  
659 on the surface of MXene owing to the occurrence of functional groups, such as -F, -O and -  
660 OH on the surface.

661 Moreover, the observed high-performance of modified MXene/SPE electrode in INZ  
662 and ACOP detection to three attributes, including mechanical robustness and faster charge  
663 transport networks of MXene, accordion-like layered structure of MXene favoring more  
664 binding sites and facilitating charge carrier charge transport, and negatively charge surface  
665 of MXene due to its surface terminals favoring the aggregation of positively charged  
666 analytes.

667 In general, for biosensing applications, 2D materials can be easily functionalized with  
668 the polymer chain via non-covalent  $\pi$ - $\pi$  bond interaction (Chaudhary et al., 2022c, 2021b,  
669 2021a; Gund et al., 2019). As a result, different antibodies can be coupled to these short-  
670 chain polymers in order to immobilize bacterial and targeted viral antigens with greater  
671 specificity for sensing evaluation. Moreover, the sensitivity progress of these 2D materials  
672 dramatically depends on the VdW types  $\pi$ - $\pi$  bond interaction along with the chain  
673 polymers. Similarly, being non-covalently bonded, the functionalization mechanism needs  
674 the specific species of chemical groups in the chain reaction to induce lower signal-to-noise  
675 ratios whenever the bonding phenomena is weak or deficient. Therefore, utilizing the  
676 MXene because of the various functional groups (-F, -H, -OH) and excellent conductive  
677 nature, it can easily form a covalent bond with other materials, especially polymers. Hence,  
678 a large number of bioanalytes can be detected by modulating the surface terminals of  
679 MXenes (Chaudhary et al., 2022c; Ho et al., 2021; Noh et al., 2022).

680 Moreover, the interaction between various functional groups and analytes is specific  
681 and can be further optimized through hybridization. Therefore, it leads to selective  
682 detection of bioanalytes by tuning the surface terminals of MXenes as per targeted  
683 diagnosis/detection. Besides, the high conductivity of MXene provides better and faster  
684 charge carrier transport in hybrid-system based biosensing layers constituting a strong  
685 detection signal and resulting in high-performance diagnosis.



686

687 **Figure 10.** (a) Schematic illustration of Ti<sub>3</sub>C<sub>2</sub>T<sub>x</sub> MXene processing and electrocatalytic  
 688 oxidation mechanism with monitoring of ACOP and INZ by Ti<sub>3</sub>C<sub>2</sub>T<sub>x</sub>-MXene/SPE and their  
 689 Differential pulse voltammograms recorded for different concentration levels of ACOP (b) in  
 690 INZ (c) in H<sub>2</sub>SO<sub>4</sub> (0.1 M), and explored the dependence of peak currents with concentrations  
 691 of ACOP, (d) of INZ (e) from 3 corresponding assessments, (f) GCE- Ti<sub>3</sub>C<sub>2</sub>T<sub>x</sub> -MXene in H<sub>2</sub>SO<sub>4</sub>  
 692 (0.1 M) with variable INZ and ACOP concentrations, (g) Recorded dependence of the peak  
 693 current over the ACOP concentration (red line) and INZ concentration (blue line) while  
 694 recording three corresponding assessments (Y. Zhang et al., 2019).

695 MXene ECL biosensors have also been widely used in sensing a range of bio-  
 696 substances, such as antigens, carcinoembryonic, and dopamine. For example, Wu et al. (Wu  
 697 et al., 2019) used linear sensing ranged (50 – 100 × 10<sup>-6</sup> m with a LOD of 10.3 × 10<sup>-9</sup> m)  
 698 Ti<sub>3</sub>C<sub>2</sub>T<sub>x</sub> based electrochemical biosensor to detect carbendazim (CBZ). They have also  
 699 observed the exceptional selectivity efficacy of the designed sensor primarily because  
 700 introducing other interfering analytes did not affect its sensing ability to carbendazim. In  
 701 addition, the surface functionalities of MXene with oxygen and fluorine terminals resulting

702 in superior catalytic/electrocatalytic activities were ascribed to its high performance in  
703 detecting CBZ.

704 Similarly, Shahzad et al. (Shahzad et al., 2019) described a Nafion coated-  $Ti_3C_2T_x$  -  
705 advanced-GCE for sensing dopamine, having a sensing range of 0.01510 mM and a LOD of 3  
706 nM. The electrostatic association between positive-charged dopamine atoms and oppositely  
707 charged  $Ti_3C_2T_x$  /Nafion was accredited to the improved dopamine sensing. It is also notable  
708 that secondary chemical additives in 2D layered materials can increase biosensors' targeting  
709 and sensitivity abilities. A superoxide ion, for instance, emerged during the antigen-antibody  
710 interaction and was identified through an electrochemical biosensing device based on  
711 MXene-Au-Pt nanoparticles (Yao et al., 2020). The biosensor depicted an excellent linear  
712 sensing range ( $0.4 - 9.5 \times 10^{-6}$  M and a LOD  $0.2 \times 10^{-6}$  M) and selectivity owing to the  
713 secondary additives (Au and Pt NPS) of the MXene probe stimulated catalytic interactions  
714 throughout the detection phenomena. Additionally, the sensor's commercial viability was  
715 elucidated by employing in-vitro evaluations of zymosan feeding to the cells of Hep-G2. As a  
716 result, the designed sensor can sense a minimal concentration of the superoxide formed  
717 due to the inclusion of Hep-G2 in 5L of zymosan. These outcomes provided a green and  
718 efficient way to construct the outperforming MXene paper-based next-generation flexible  
719 biosensor by regulating growth mechanism and surface functionalities.

720 Several reports have described electrochemical biosensors based on secondary  
721 additive MXenes to detect numerous biomolecules, such as piroxicam, ascorbic acid, uric  
722 acid and ACOP (Chaudhary et al., 2022d; Khunger et al., 2021). In biological processes,  
723 enzymes act as catalysts and react with specific ligands. Therefore, to enhance the  
724 selectivity and sensing range of biosensors, ample ligand-enzyme interactions are carried  
725 out. As a result, electrochemical biosensing approaches rely on the sensing material's  
726 indirect response with the byproducts of the enzyme-analyte active engagement rather  
727 than directly reacting with the analytic substance (Kim et al., 2015; M. Li et al., 2019; Lin et  
728 al., 2020; Neampet et al., 2019; Rasheed et al., 2019; Wang et al., 2019) For instance,  
729 MXene/CNT/Prussian blue (PB) nanocomposite was used to design ECL biosensors to  
730 monitor glucose and lactate (Lei et al., 2019; Novoselov et al., 2004). Firstly, the sensor was  
731 tuned using oxidase enzymes of lactate and glucose that produced hydrogen peroxide and  
732 ionized the PB while interacting with each other. These generated ions begin reacting with

733 the MXene probe, causing a redox reaction that increases the electrochemical sensing  
734 ability. The developed sensor exhibited a linear sensing range of  $10 \times 10^{-6}$  M to  $1.5 \times 10^{-3}$  M  
735 with  $0.33 \times 10^{-6}$  M LOD for glucose and a range of  $0 - 22 \times 10^{-3}$  M with LOD  $0.67 \times 10^{-6}$  M for  
736 detecting lactate. In a similar finding, Neampet et al. (Neampet et al., 2019) described the  
737 sensible detection of lactate using MXene/Pt-NP/PAN-based composite. The biosensor was  
738 gently tuned with lactate oxidase enzyme showing  $5 \times 10^{-6}$  M of LOD.

739 Moving further, surface chemistries and modifications help stabilize 2D  
740 nanomaterials for superior biosensing performance. For example, a hybrid Pd@Ti<sub>3</sub>C<sub>2</sub>T<sub>x</sub>  
741 nanocomposite sensor demonstrated electrochemical detection of L-Cys (Rasheed et al.,  
742 2019). The hybrid sensor also maintained a sensing range of approximately 0.5 - 10  $\mu$ M and  
743 0.14  $\mu$ M of LOD linearly for L-Cys. Identically, a biosensor synthesized hybrid  
744 MXene/graphite Ti<sub>3</sub>C<sub>2</sub>T<sub>x</sub> nanocomposite monitored adrenaline electrochemically, having 9.5  
745 nM of LOD. All the precursors of MXene-hybrids contributed to the enhanced detection of  
746 L-Cys. For instance, Ti<sub>3</sub>C<sub>2</sub>T<sub>x</sub> exhibited reducing action at the electrode surface and acts as an  
747 active conductive matrix for charge transport, while Pd NPs enhanced the ambient stability  
748 of MXene and the electrocatalytic activity of hybrid towards L-Cys monitoring.

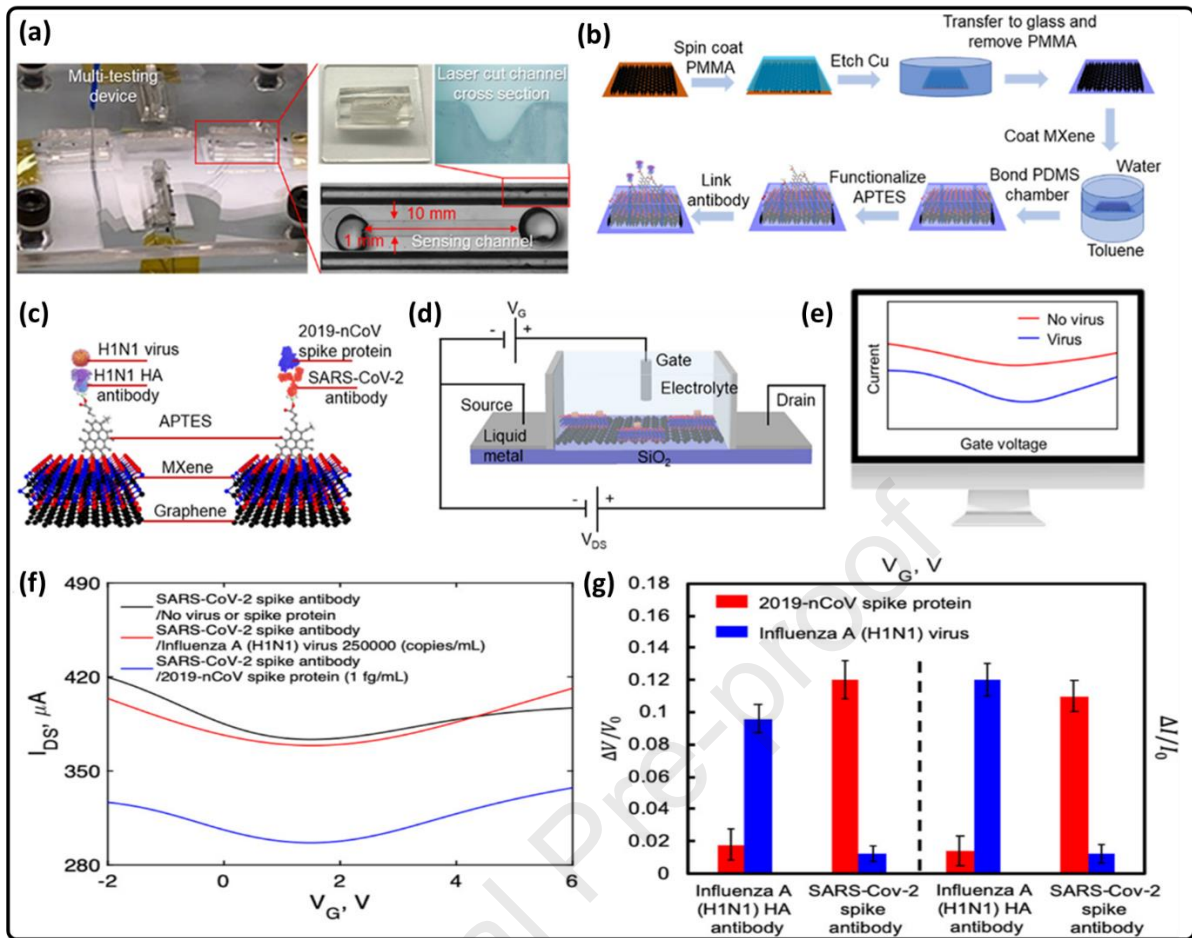
749 In addition, Li et al. (M. Li et al., 2019) demonstrated the detection of non-enzymatic  
750 glucose with a linear sensing range of 0.002 - 4.096 mM with the application of a Ti<sub>3</sub>C<sub>2</sub>T<sub>x</sub>  
751 MXene/double layered hydroxides (LDHs) sensor. This sensing mechanism is primarily due  
752 to the glucose oxidation onto Ni-Co-LDH in an alkaline solution via substantial reduction of  
753 Co (III) to Co (II) and Ni (III) to Ni (II). The abundance of functional groups on MXene's  
754 surface makes them the most suitable carriers to immobilize the active analytes, further  
755 enhancing electrochemical biosensing efficacy. For example, Ti<sub>3</sub>C<sub>2</sub>T<sub>x</sub> hybrid nanosheets  
756 immobilized tetrahedral DNA structures were used to monitor mycotoxin using a gliotoxin  
757 aptamer with a sensing range between 5 pM to 10 pM and LOD of 5 pM (Wang et al., 2019).  
758 Also, Liu et al. (J. Liu et al., 2019) manufactured a novel electrochemical biosensor with dual  
759 functionality to immobilize the urease enzyme on MXenes surface chemistries by  
760 glutaraldehyde to detect both the urea and creatinine in humans. The biosensor exhibited a  
761 linear sensing range of  $0-3 \times 10^{-3}$  M with a LOD of nearly  $0.02 \times 10^{-3}$  and  $10 - 400 \times 10^{-6}$  M  
762 with a LOD of  $1.2 \times 10^{-6}$  M for creatinine.



763 In addition to this, numerous sensors based on MXene-enzyme immobilization have  
764 been developed to monitor a wide range of analytes, namely pesticides, metabolic by-  
765 products, micronutrients, as well as parameters based on 2D material for sensing MUC<sub>1</sub>,  
766 miRNA, and gliotoxin electrochemically (Ansari and Malhotra, 2022; Khunger et al., 2021; Lei  
767 et al., 2019; Novoselov et al., 2004). For instance, Zhao et al. (Zhao et al., 2022) developed a  
768 unique process of detecting microRNA-21 (miR-21) without a label. MXene-MoS<sub>2</sub>  
769 heterostructure also exhibited an enhanced catalytic hairpin assembly (CHA) signal strategy.  
770 The synergistic effect of MXene-MoS<sub>2</sub> and CHA demonstrated high detection performance  
771 to miR-21 by providing a hybrid with excellent conductivity, accelerating the electron  
772 transfer rate during the detection phenomenon. The sensor showed a low LOD of 26 fM and  
773 a wide sensing range of 100 fM to 100 nM.

774 Interestingly, biosensors with MXenes have appeared as potential devices for  
775 monitoring harmful viruses, particularly SARS coronavirus-2 (Y. Li et al., 2021; Unal et al.,  
776 2021). Li et al. (Y. Li et al., 2021) developed a Ti<sub>2</sub>C MXene incorporating graphene hybrid  
777 field-effect transistor (FET) detector for monitoring severe viruses, such as SARS-COV-2 and  
778 influenza viruses, as depicted in Figure 8. The biosensor was able to detect viruses with a  
779 sensing range of 25 -250000 copies/mL<sup>-1</sup> for H<sub>1</sub>N<sub>1</sub>, and 1-10 pgmL<sup>-1</sup> and LOD of 125  
780 copies/mL<sup>-1</sup> for recombinant spike protein 2019-nCoV and H<sub>1</sub>N<sub>1</sub> virus, respectively, and 1  
781 FGmL<sup>-1</sup> for recombinant 2019-to in the range of 50 ms. Apart from this, DNA-based  
782 MXene's-based Ti<sub>3</sub>C<sub>2</sub>T<sub>x</sub> chemical resistive biosensor is capable of sensing rapidly and  
783 selectively the SARS-CoV-2 nucleocapsid genes. The produced sensor had a substantial LOD  
784 of 105 copies/mL in sensing saliva while considerable selectivity against SARS-CoV-I and  
785 MERS (**Figure 11**).

786 The exceptional sensing performance was ascribed to the diversified surface-  
787 terminating terminals of Ti<sub>3</sub>C<sub>2</sub>T<sub>x</sub> offering large number of binding sites for (3-aminopropyl)  
788 triethoxysilane (APTES) to hold target viruses. Moreover, the antigen-antibody sensing  
789 mechanism was explained in term of surface charge compensation during the binding event  
790 leading to variation in drain-source current–voltage response, which is recorded as sensing  
791 outcomes.



792

793 **Figure 11.** (a) FET sensor based on Graphene-MXene hybrid (optical image) (b) Illustration of  
 794 hybridisation of graphene-MXene utilising VSTM-deposition strategy. (c) Illustration of the  
 795 related antigen-antibody-based monitoring process. Schematic illustration of (d) used FET  
 796 circuit, (e) Changes in drain-source characteristics due to interaction with viruses, and (f)  
 797 FET characteristics of SARS-CoV-2 spike antibody-immobilized biosensor. (g) Normalised  
 798 drain-source and gate-voltage characteristic variation with STDs in overt binding  
 799 assessment. (Y. Li et al., 2021)

## 800 5.2. Advancements in the MXene-based photo- and calorimetric-type biosensors

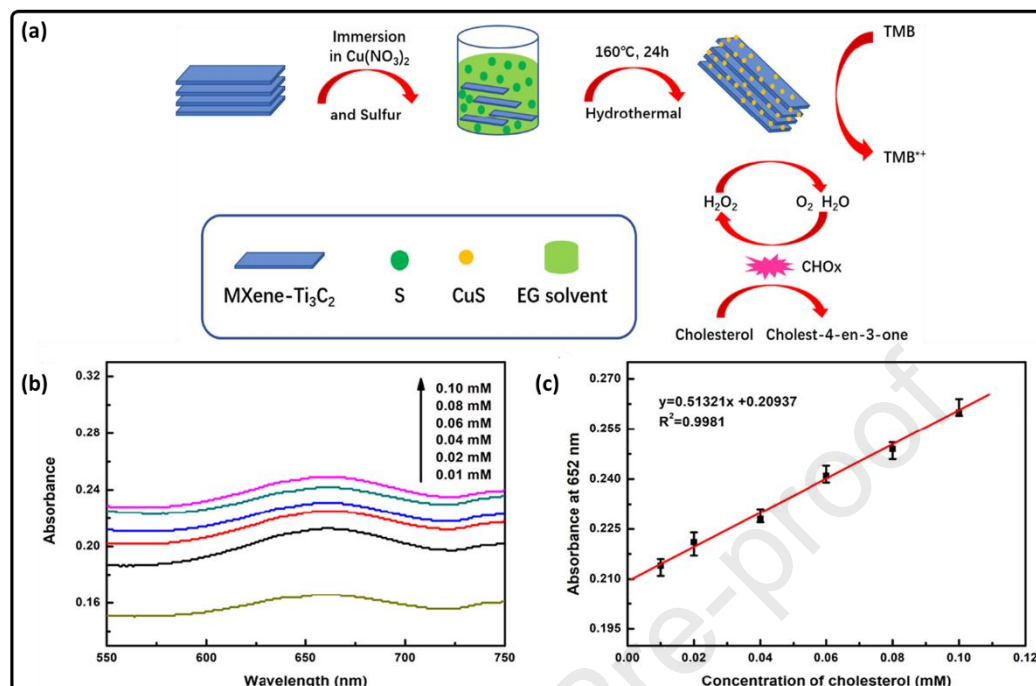
801 Due to surface and quantum confinement effects, MXenes display strong  
 802 photoluminescence. This attribute can measure biomolecules and execute cell imaging (Bai  
 803 et al., 2022; Chen et al., 2018; Guan et al., 2019; Y. Li et al., 2019; Liu et al., 2020; M. Liu et  
 804 al., 2019; Mannoor et al., 2012; Xue et al., 2017; Xun et al., 2021) This can primarily be  
 805 ascribed to the discrete energy levels present in the quantum dots based on different two-  
 806 dimensional materials, wherein excitations can mainly undergo radiative decay. Xue et al.  
 807 (Xue et al., 2017) performed multicolor RAW264.7 cells imaging using a hydrothermally  
 808 produced biocompatible QDs sensor based on Mxene having rich N-surface chemistries. As  
 809 the vast majority of QDs occurred in the cytoplasm and were substantially lesser in levels at

810 the nucleus, the prospect of QDs causing genetic modification was extremely low. Several  
811 reports have been signifying using QDs based on Mxene to perform cellular imaging of the  
812 NIH 3T3 fibroblast cells and macrophage human cells.

813 Chen et al. (Chen et al., 2018) described a biosensor with dual function based on  
814  $Ti_3C_2T_x$  QDs/Tris(bipyridine) ruthenium (II) chloride ( $[Ru(DPP)_3]Cl_2$ ) nanocomposite to  
815 detect intercellular pH as well as to capture cellular imaging, in perspective to use as a  
816 viable biosensing system to fabricate fluorescent embedded wearable sensors. It was  
817 entirely based on the pH-reliant PL response of MXene-QD incorporating  $[Ru(DPP)_3]Cl_2$   
818 nanocomposite. The  $[Ru(DPP)_3]Cl_2$  had been unresponsive to pH at 615 nm, whereas QDs  
819 have been extremely sensitive at 460 nm. Also, the correlation between PL and pH has been  
820 linear ranging between 5 to 9. Thus, it is evident that MXenes QDs can simultaneously  
821 perform two tasks, namely monitoring the pH and cell imaging. Furthermore, Liu et al. (Liu  
822 et al., 2020) developed a radiometric sensor based on glutathione (GSH) and MXene-QD  
823 nanocomposite, which assisted in detecting UA with the naked eye. The inclusion of UA in  
824 the detecting mechanism, which also contains urate oxidase (uricase), o-phenylenediamine  
825 (OPD), and horseradish peroxidase (HRP), results in the production of hydrogen peroxide to  
826 oxidise OPDs. The peak for UV absorption of 425 nm for oxidized OPDs, and the peak for PL  
827 of 430 nm for the composite (GSH/MXene-QD) over-lapses, suggesting the transition of  
828 fluorescent resonance frequency takes place from GSH/ MXENE-QD toward oxidized OPDs  
829 under the influence of UA. For UA, the sensor depicted a low LOD ( $125 \times 10^{-9}$  M). Since the  
830 oxidized OPDs are yellow, the biosensor can also work as a calorimetric form. When the  
831 level of UA in the GSH-MXene QD solution is raised in daylight and exposed to UV light, the  
832 color transforms to yellow from transparent, revealing its calorimetric effectiveness.

833 Ample calorimetric biosensors based on MXene have been discussed in this study for  
834 detecting glucose/dextrose, glutathione (an antioxidant), carcinoembryonic antigens in  
835 body fluids, and cholesterol. Li et al. (Y. Li et al., 2019) synthesized a calorimetric sensor  
836 from MXene/CuS nanocomposite with a peroxides-type reaction to monitor cholesterol, as  
837 illustrated in **Figure 12(a)**. when cholesterol oxidase reacts chemically with the cholesterol,  
838 it produces hydrogen peroxide. In addition, it causes CUS NPs to combine over the surface  
839 of MXene to form blue colored  $TMB^+$  ions. As a result, the color of the solution progressively

840 turns from transparent to blue as the content of cholesterol increases. Still, simultaneously  
 841 the sensor showed a lower LOD of  $1.9 \times 10^{-6}$  M in **Figure 12(b)**.



842 **Figure 12.** (a) Preparation scheme of the fabricated MXene and CuS nanocomposites. (b)  
 843 UV-Visible spectra comparison of MXene/CuS and TMB having the pH of 3.5 Hac-NaAC  
 844 buffer at 37 °C (Y. Li et al., 2019)  
 845

846 Similarly, GSH was also measured through a calorimetric detector  
 847 fabricated using MXene/NiFe nanoflake composite (H. Li et al., 2020). This has been  
 848 observed that with increasing GSH contents, the color of the mixture changed from blue to  
 849 transparent white due to the elimination of TMB ions. Also, the designed sensor behaved  
 850 linearly with a detection range of  $0.9 - 30 \times 10^{-6}$  M and LOD of  $84 \times 10^{-9}$  M.

### 851 5.3. Advancements in electrochemiluminescence-type MXene-biosensors

852 Biosensors that operate in the electrochemiluminescence (ECL) state have widespread use  
 853 in medical diagnostics. It is primarily due to three main reasons. Firstly, they are capable of  
 854 reducing background noises. Secondly, they provide a wide detection range and finally, they  
 855 possess high sensitivity. ECL-based sensors operate on an electro-generated  
 856 chemiluminescence signal that experiences an exergonic chemical reaction to activate  
 857 luminophores that emit light upon returning to initial operating conditions. ECL is an ideal  
 858 approach for detecting biomaterials that govern intercellular communication, such as  
 859 exosomes. It is a potential non-invasive diagnostic tool for detecting and tracking  
 860 pathogens, including malignant tumor cells. For example, Zhang et al. (H. Zhang et al., 2019)

861 described an exosome-based biosensor derived from a breast tumor cell line (MCF-7).  
862 Exosomes were initially grown on Au NP/poly(N-isopropyl acrylamide) and (AuNP/PNIPAM)-  
863 modified GCE, combining an aptamer with an amino-based functional batch. The  
864 nanoprobe based on MXene have been synthesized after MXene's electrostatic surface  
865 modification with different aptamer and PEI. The research findings indicated that the  
866 luminol solution's PL intensity was 5-fold higher for manufactured nanoprobe than the pure  
867 GCE, which supports MXene-based aptamer nanoelectrodes for exosome sensors. It had  
868 linear detection sensitivity of 500 to 5000000 particles/ $\mu\text{L}$  and LOD of about 125  
869 particles/ $\mu\text{L}$ . In this study, MXenes nanosheets serve a dual function of catalyzing the ECL  
870 process of luminol and providing a larger surface area for loading a mass of Apt2, facilitating  
871 the exosomes capture.

872 Also, Fang et al. (Fang et al., 2020) described MXene/tris(4,4'-dicarboxyl-2,2'-  
873 bipyridine) ruthenium (II) ion ( $\text{Ru}(\text{dcbpy})_3^{2+}$ ) (an organic dye)/black phosphorus-based  
874 exosome QD sensor having LOD of about 37 particles/ $\mu\text{L}$ . Similarly, Wang et al. (L. Wang et  
875 al., 2022) detected DNA phosphorylated with polynucleotide kinase (PNK) using a Ru-  
876  $\text{Ti}_3\text{C}_2\text{T}_x$ -AuNPs ECL sensor having 0.002 to 10  $\text{U mL}^{-1}$  of linear sensing range and 0.0002  $\text{U mL}^{-1}$   
877 LOD. The improvement in sensing action was ascribed to the MXene providing  
878 magnification efforts and anchoring locations for auxiliary hybrid nano-devices in the ECL  
879 sensor. Furthermore, Fang et al. (Fang et al., 2018) in another study utilized  
880 MXene/ $\text{Ru}(\text{dcbpy})_3$  to improve GCE to distinguish individual nucleotide variations in urine  
881 samples. It is expected to result in a genetic mutation based on severe illnesses in humans.  
882 The detection process is sensitive to the concentration level of an individual-nucleotide  
883 difference, which, when bonded to MXene, causes a reaction with  $\text{Ru}(\text{dcbpy})_3$ . The ECL  
884 sensor possessed 3-fold high sensing action for mismatched individual nucleotides  
885 compared to completely matched individual nucleotides, with  $1 \times 10^{-9}$  M LOD. In contrast to  
886 ECL modules, QDs based on MXene have been observed as biosensors in the  
887 photoelectrochemical module.

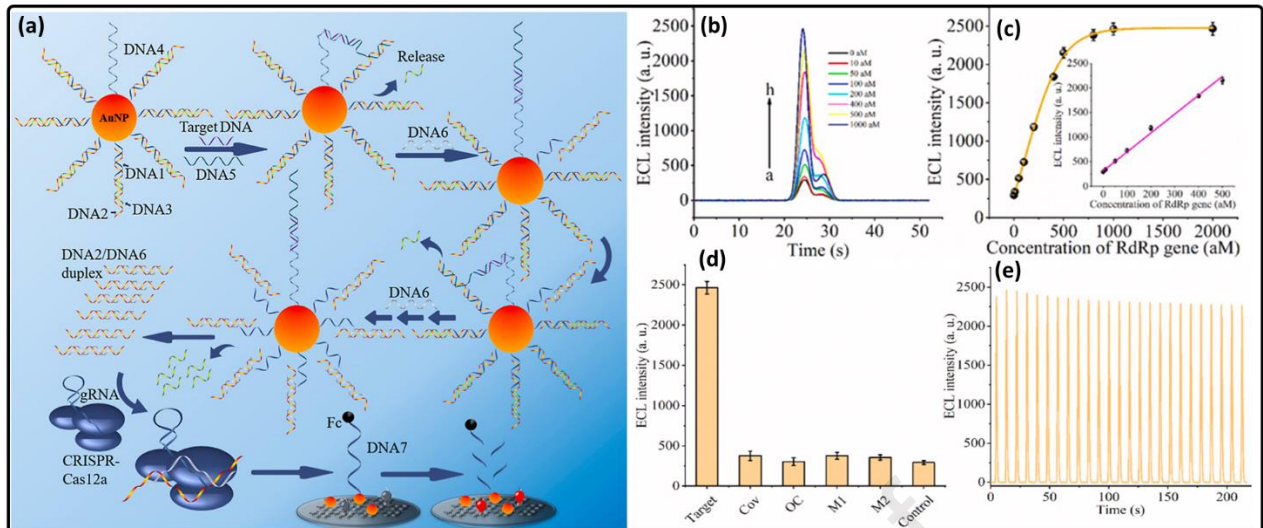
888 To illustrate, Chen et al. (Chen et al., 2018) employed MXene based QD sensor to  
889 detect glutathione photoelectrochemically having a LOD of nearly  $9 \times 10^{-9}$  M. Likewise, a 2D  
890  $\text{Ti}_2\text{C}$  MXene-based PEC biosensor with superior efficiency was fabricated for selectivity and  
891 detection of sCD146. The exceptional physicochemical properties of 2D  $\text{Ti}_2\text{C}$  MXene

892 decreased the re-joining of photogenerated holes or electrons and enhanced the sensing  
893 behavior of the biosensor. At optimal values, the sensor displayed a linear detection range  
894 (LDR) of (0.1–1000 pg/mL) with LOD (18 fg/mL) (Jiang et al., 2022).

895 Remarkably, Zhang et al. (K. Zhang et al., 2022) explored an ECL-based biosensor to  
896 detect the SARS-CoV-2 RdRp genes by integrating two different strategies, namely 3D-DNA  
897 walker and CRISPR-Cas12a trans-cleavage operation with PEI-Ru@Ti<sub>3</sub>C<sub>2</sub>@AuNPs  
898 nanocomposite (**Figure 13(a)-(c)**). As a result, the sensor showed 12.8 aM of LOD for  
899 detecting the SARS-CoV-2 RdRp gene. Furthermore, due to the active CRISPR-Cas2a, which  
900 separates individual-stranded DNA, the sensor's sensitivity improves significantly, causing  
901 one end of the DNA to disassociate from the detector surface. Contrary, Yao et al. (Yao et  
902 al., 2021) used an Au@Ti<sub>3</sub>C<sub>2</sub>@PEI-Ru(dcbpy)<sub>3</sub><sup>2+</sup> based hybrid nanocomposite ECL sensor to  
903 detect the SARS-CoV-2 RNA-dependent RNA polymerase (RdRp) gene with 1 fM-100 pM of  
904 linear detection range and 0.21 fM of LOD. The luminescent attributes of AuNPs linked with  
905 Ru(dcbpy)<sub>3</sub><sup>2+</sup>-DNA fixed on MXene surface contribute to superior sensitivity of the ECL  
906 biosensor. Further, the interconnectivity of PEI with Ru(dcbpy)<sub>3</sub><sup>2+</sup> through an amide bond  
907 improved the luminous efficacy of the hybrid. Moreover, the amplification method using a  
908 unipedal DNA walker improved the detection efficiency of ECL biosensor. It was further  
909 activated using SARS-CoV-2 RdRp, which leads to the excision of HP DNAs bound to model  
910 DNA-AgNCs. The combination of these two strategies leads to high-performance of ECL  
911 biosensors in detecting SARS-CoV-2 RdRp gene.

912 Further, to screen severe COVID-19 patients, Mi et al. (Mi et al., 2021) explored the  
913 use of a tetrahedral DNA/aptamer cardiac troponin-I biosensor based on an in-situ  
914 hybridised chain reaction on an Au/Ti<sub>3</sub>C<sub>2</sub>-MXene substrate. The sensor depicted a LOD as  
915 0.04 fM and a sensing range of 0.1fM – 1 pM towards cTnl. The designed sensor  
916 demonstrates an innovative method of screening COVID-19 patients in portable cabin  
917 healthcare facilities. Since installing Electrocardiogram apparatus at every required site and  
918 at home is complicated, the biomarker assays such as of cTnl in peripheral blood is more  
919 cost-effective and prompt way. Moreover, such miniature biosensors have the potential to  
920 contribute towards designing HOC module biosensors.

921



922  
923

924 **Figure 13.** (a) Schematic depiction of the 3D-DNA walker-CRISPR Cas 12a-based ECL  
925 biosensor for sensing SARS-CoV-2 RdRp genes. (b) Time-dependent ECL spectra for different  
926 SARS-CoV-2 RdRp gene's concentration of 0 aM to 1000 aM, and association of SARS-CoV-2  
927 RdRp gene's concentration with ECL observations. (With inset: Dependence of the ECL  
928 intensity over the concentration of SARS-CoV-2 RdRp gene. (c) Selectivity studies of ECL  
929 biosensor (K. Zhang et al., 2022)

## 930 6. Progressing towards hospital-on-chip strategies: Intelligent and sustainable approach

931 The energy-saving, compact, affordable, transportable, simple design, wearable, highly  
932 flexible, skin-embedded, transparent, multipurpose, ultralight, excellent biocompatibility  
933 and fast sensing systems have transformed the sensor's world dynamically, culminating on  
934 the internet of nano-things (IoNT). Such monitoring means can be linked to Bluetooth  
935 devices, internet networks and each other, allowing for a meaningful, intelligent assessment  
936 of various environmental stimuli. The robustness of these sensors is outstanding, and they  
937 can endure intense pressure and environmental variations easily. Due to the modest size of  
938 core elements, sensors in IoT may be positioned at every conceivable stimulation location,  
939 allowing for more efficient, reliable and accurate data collection and monitoring compared  
940 with conventional IoT systems. IoT-based next-phase sensors can wirelessly sense stimuli  
941 and transmit signals directly to the recording and analyzing devices. IoT sensors have great  
942 potential to transform existing public management methods consuming less time, labor,  
943 and vital resources (Chaudhary et al., 2022e, 2022c; Kim et al., 2015; Lin et al., 2020;  
944 Mannoor et al., 2012; Neampet et al., 2019; Qian et al., 2022; Scott et al., 2022; Shahzad et  
945 al., 2019; Sheth et al., 2022; Verma et al., 2022; Wu et al., 2019; Yao et al., 2020). For  
946 example, associating IoT sensing devices to COVID-19 diagnostics enables the production of

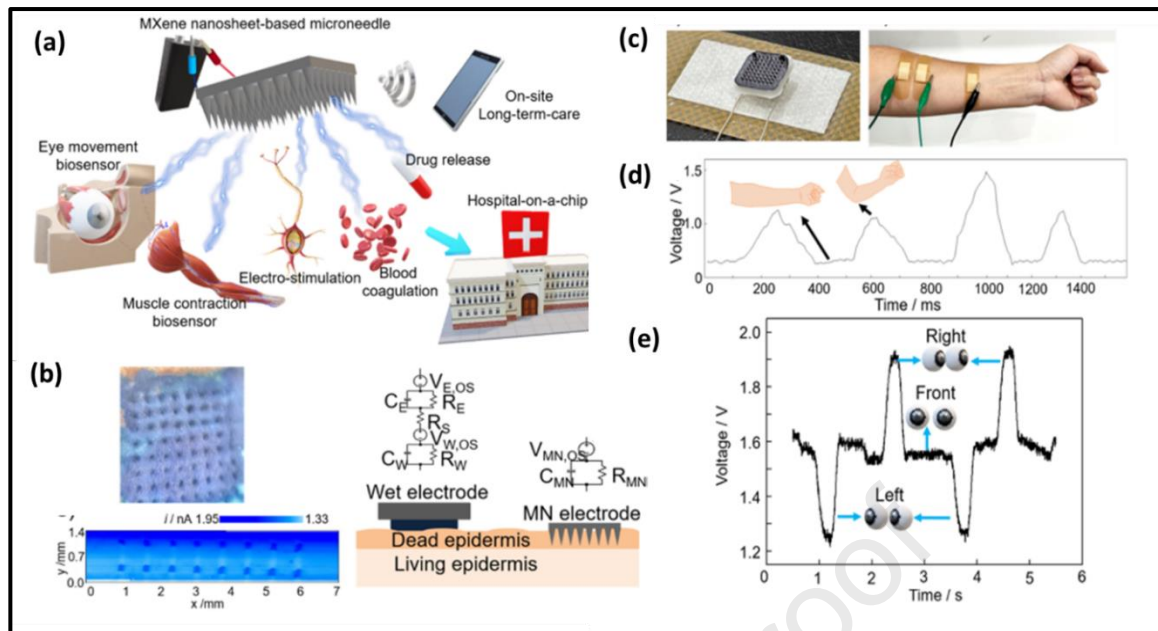
947 a hospital-on-chip system that can identify SARS-CoV-2, even in the most remote areas  
948 connected to modern healthcare centers.

949 Guanhua et al. (Xun et al., 2021) reported the fabrication of the most accessible and  
950 most scalable testing system for COVID-19 detection, which includes the rapid, entirely  
951 accurate and sensitive assay likely to battery-based portable powdered devices. Similarly,  
952 various relatable samples have been collected from the human body to diagnose several  
953 infectious diseases which deadly viruses and pathogens can cause. But all tears, saliva and  
954 body sweat can be collected in a non-inverse way. In contrast, saliva contains the variation  
955 of biomarkers naturally created from external substances, microorganisms, and salivary  
956 glands. Therefore, to identify and protect from all these point-of-care and lab-in-a-mouth  
957 based sensors are also utilized to monitor health, infection, and pathogens status. Mannoor  
958 et al. (Mannoor et al., 2012) produced saliva-based graphene wearable sensors, which help  
959 to detect the H-pylori results from the body to diagnose stomach and liver diseases. In these  
960 sensors, they applied the printing method to combine the single layer graphene with soluble  
961 water-based silk fibroin films and fixed it on tooth enamel. Whereas, through this method,  
962 electrode patterns are designed on silk-based graphene films. Later this sensor is moved  
963 onto the tooth's surface related to the root canal and other activities.

964 Kim et al. (Kim et al., 2015) also reported that wearable sensors for detecting  
965 salivary uric acid, together with integrated and portable wireless devices, are utilized for the  
966 concentration of salivary uric acid. Lin et al. (Lin et al., 2020) reported the soluble PVP  
967 microneedle therapeutic system encumbered with the Nb<sub>2</sub>C-based MXene NS for  
968 photothermal ablation and implantation of superficial tumors in the 2<sup>nd</sup> NIR biological  
969 windows. According to the report, it was noticed that at 70 °C, tumor temperature  
970 increased under the irradiation source of 1064 nm, which further possesses enough  
971 bearable conditions for the photonics-based tumor ablation. The same group in another  
972 study reported the Nb<sub>2</sub>C MXene by utilizing the 1<sup>st</sup> and 2<sup>nd</sup> NIR biological window for the  
973 photothermal tumor detection, in which the sample yields the conversion efficiency of 36.4  
974 and 45.65 % for both NIR-I and NIR-II windows, respectively. Later, Yang et al. (Yang et al.,  
975 2021) successfully developed a hospital-on-chip device using an MXene nanosheet-based  
976 multipurpose microneedle, as shown in **Figure 14((a)-(e))**.

977





978  
979

980 **Figure 14.** Hospital-on-chip module: (a) Illustration using multifunctional MXene-based  
 981 microneedles. (b) Schematic depiction of the bioimpedance model of the traditional  
 982 microneedle and wet electrode module on the epidermis and optical micrographs of  
 983 microneedle penetrated the skin. (c) Optical micrograph of the MXene-microneedle over  
 984 bandage and wearable biosensor based on MXene over the arm. (d) Sensitivity of biosensor  
 985 by voltage produced by bending the elbow. (e) Sensitivity of biosensors by voltage produced  
 986 by the movement of the human eye (Yang et al., 2021).

987 The biosensor built with a single chip has enhanced human diagnostics and remedial  
 988 therapeutics like a micro-hospital. Through puncturing the dead skin, MXene-microneedles  
 989 aid in medication delivery. Additionally, it can identify even a minor potential disparity  
 990 inside the body brought on by arm muscle and eye movements. Furthermore, the biosensor  
 991 is multifunctional, much like a hospital unit. Thus, incorporating IoT sensors has enormous  
 992 potential for building e-healthcare facilities that are intelligent, adaptable, and  
 993 interoperation. Biosensor connected with IoT using MXene is uniquely addressed and  
 994 identifiable by the internet worldwide and at any time to detect, monitor, store, evaluate,  
 995 and reply to the signal. Also, they can send information immediately to any location in the  
 996 world that is linked to the internet, designed to simplify setup, process, and administration  
 997 tasks. These intelligent sensors based on IoT can be used in intelligent alarms on little  
 998 modifications in specific stimuli and to prevent and manage serious global issues. IoT  
 999 sensors, for example, can be developed utilizing thermally stable MXenes to observe  
 1000 volcanoes erupting, reducing enormous resource and human life loss. Moreover, using the  
 1001 idea of nano-triboelectric attributes of MXenes or their interface with several more

1002 triboelectric resources, they can function on a self-sustaining model that does not require  
1003 an external power source.

1004 Computational and analytical technologies, including AI, DI, ML and data analytics,  
1005 are progressing rapidly with applications that extend beyond information technology (IT) to  
1006 materials and sensor design. They offer incredible potential as an enhanced forecasting and  
1007 accurate sensing operating tool. Before enduring experimental analyses, technologies such  
1008 as AI and ML are used to forecast the performance, limitations theoretically, and alternative  
1009 remedies related to the functioning of the particular sensor, resulting in time, expenditure,  
1010 materials, contamination, and human resources savings. For example, while designing  
1011 breath analyzing sensors, AI and ML can operate together to gather different information  
1012 from human exhaled breath and evaluate large datasets of digitized biomarkers using the DL  
1013 method to develop prognostic evaluations of physiological details and facts. As a result, it  
1014 can improve the assessment of effective medications, specific drug responses, and the  
1015 accurate drug dose for each patient. Likewise, previous stimulus responses can enhance  
1016 sensing device performance. A distinctive aspect is that relevant data can be accessed and  
1017 measured with an intelligent computing device or cellular mobile device. However,  
1018 implementing AI within future sensors can segregate operational data from the massive  
1019 data obtained through regular monitoring of particular stimuli. Therefore, researchers need  
1020 fast progress of more advanced algorithms for pre-processing and elucidating the practical  
1021 information to produce huge-data-based estimations, such as early diagnostics of chronic  
1022 ailments or early recognition of leakage, particularly gases, which can benefit humanity to a  
1023 great extent.

1024 **Table 2.** Summary of classes of various biosensor strategies for detection of various  
1025 biomolecules and pathogens

Type of Biosensor	Probing method	MXene Species	Target	Linear Detection Range	LOD	Ref.
Electrochemical	Screen-Printed electrode	Ti <sub>3</sub> C <sub>2</sub> T <sub>x</sub>	Isoniazid and acetaminophen drugs	0.048 μM and 0.1-4.6 μM	0.064 μM	(Y. Zhang et al., 2019)
Electrochemical		Ti <sub>3</sub> C <sub>2</sub> T <sub>x</sub>	Carbendazim (CBZ)	50-100×10 <sup>-6</sup> m	10.3×10 <sup>-9</sup> m	(Wu et al., 2019)

Electrochemical		Nafion coated- Ti <sub>3</sub> C <sub>2</sub> T <sub>x</sub> - modified-GCE	Dopamine	0.015–10 mM	3nM	(Shahza d et al., 2019)
Electrochemical	MXene based	MXene-Au-Pt	Superoxide molecule	0.4–9.5 × 10 <sup>-6</sup> M	0.2 × 10 <sup>-6</sup> M	(Yao et al., 2020)
Electrochemical	MXene based	MXene/CNT/P russian blue (PB) composite	Glucose	10 × 10 <sup>-6</sup> M to 1.5 × 10 <sup>-3</sup> M	0.33× 10 <sup>-6</sup> M	(Lei et al., 2019)
			Lactate	0–22 × 10 <sup>-3</sup> M	0.67 × 10 <sup>-6</sup> M	
Electrochemical		MXene/Pt- NP/PAN composite	Lactate		5 × 10 <sup>-6</sup> M	(Neam pet et al., 2019)
Electrochemical		Pd@Ti <sub>3</sub> C <sub>2</sub> T <sub>x</sub> hybrid nanocomposit e	L-Cys	0.5-10μM	0.14 μM	(Rashe ed et al., 2019)
Electrochemical		Ti <sub>3</sub> C <sub>2</sub> T <sub>x</sub> MXene/graphi te nanocomposit e	Adrenaline		9.5nM	No ref.
Electrochemical		Ti <sub>3</sub> C <sub>2</sub> T <sub>x</sub> MXene/layere d double hydroxides (LDHs) composite	Glucose	0.002- 4.096mM		(M. Li et al., 2019)
Electrochemical		Ti <sub>3</sub> C <sub>2</sub> T <sub>x</sub> nanosheets	Mycotoxin	5 pM-10 pM	5 pM	(Wang et al., 2019)
Electrochemical	capture hairpin probe (H1)	Ti <sub>3</sub> AlC <sub>2</sub> MAX powder	microRNA- 21 (miR-21)	m 100 fM to 100 nM	26 fM	(Zhao et al., 2022)

<b>Electrochemical</b>	anionic redox	AuNPs/MXene @PAMAM, using 2D $Ti_3C_2T_x$	Human cardiac troponin T (cTnT)	0.1–1000 ng/mL	0.069 ng/mL	(X. Liu et al., 2022)
<b>Dual-function Electrochemical</b>		Urease enzyme immobilised MXene	Creatinine	$10-400 \times 10^{-6}$ M	$1.2 \times 10^{-6}$ M	(J. Liu et al., 2019)
			Urea	$0-3 \times 10^{-3}$ M	$0.02 \times 10^{-3}$ M	
<b>Dual-target Electrochemical</b>	Dual-type Au microgap electrode	Aptamer/MXene ( $Ti_3C_2$ ) nanosheet	Tumor necrosis factor $\alpha$ (TNF- $\alpha$ )	1 pg/mL to 10 ng/mL	0.25 pg/mL	(Noh et al., 2022)
			interferon gamma (IFN- $\gamma$ )		0.26 pg/mL	
<b>Field-Effect Transistor (FET)</b>		$Ti_2C$ MXene-graphene	SARS-CoV-2	25-250,000 copies/mL <sup>-1</sup>	125copies/mL <sup>-1</sup>	(Y. Li et al., 2021)
			2019-nCoV	1-10 pgmL <sup>-1</sup>	1FG mL <sup>-1</sup>	
<b>Ratio-metric (Colorimetric)</b>		Glutathione (GSH)–MXene QD composite	UA		$125 \times 10^{-9}$ M	(Liu et al., 2020)
<b>Colorimetric</b>		MXene/CuS nanocomposite	cholesterol		$1.9 \times 10^{-6}$ M	(Y. Li et al., 2019)
<b>Colorimetric</b>		MXene/NiFe nanoflake composite	GSH	$0.9-30 \times 10^{-6}$ M	$84 \times 10^{-9}$ M	(H. Li et al., 2020)
<b>Colorimetric/fluorometric</b>		N, P- $Ti_3C_2$ MXene quantum dots	Recognition of NO <sub>2</sub>	1.5 to 80 $\mu$ M	0.71 $\mu$ M	(Bai et al., 2022)
<b>Colorimetric</b>		Au/Pt/ $Ti_3C_2Cl_2$ nanoflakes	Hydrogen peroxide (H <sub>2</sub> O <sub>2</sub> )	50–10000 $\mu$ M	10.24 $\mu$ M	(Xi et al., 2022)

			Glutathione (GSH)	0.1–20 $\mu\text{M}$	0.07 $\mu\text{M}$	
<b>ECL</b>	MXene-aptamer nanoprobe	MXene adsorbed exosome-cultured AuNP/PNIPAM/GCE	Breast cancer cell (MCF-7)	500–5000000 particles per $\mu\text{L}$	~125 particles per $\mu\text{L}$	(H. Zhang et al., 2019)
<b>ECL</b>		MXene/tris(4,4'-dicarboxyl-2,2'-bipyridine) ruthenium (II) ion ( $\text{Ru}(\text{dcbpy})_3^{2+}$ ) (an organic dye)/black phosphorus QD			37 particles per $\mu\text{L}$	(Fang et al., 2020)
<b>ECL</b>		MXene/ $\text{Ru}(\text{dcbpy})_3$ modified GCE	Single nucleotide mismatch in human urine	3fold superior ECL sensing response than whole matched nucleotides	$1 \times 10^{-9} \text{ M}$	(Fang et al., 2018)
<b>Photoelectrochemical</b>		MXene QD	Glutathione		$9 \times 10^{-9} \text{ M}$	NO
<b>Photoelectrochemical</b>		2D $\text{Ti}_2\text{C}$	soluble CD146 (sCD146)	0.1–1000 pg/mL	18 fg/mL	(Jiang et al., 2022)
<b>Photoelectrochemical</b>	MB sensitized MXene@ITO photoelectrodes	Label-free $\text{Ti}_3\text{C}_2$ MXene	Phosphorus	0.5–200 $\mu\text{M}$	0.21 $\mu\text{M}$	(Chang et al., 2022)
<b>Photoelectrochemical / Electrochemical dual mode</b>		$\text{Bi}_2\text{S}_3/\text{Ti}_3\text{C}_2\text{TX}$ MXene nanocomposites	chlorogenic acid (CGA)	0.0282 $\mu\text{M}$ to 2824 $\mu\text{M}$ (PEC sensor)	2.4 nM	(Qiu et al., 2022)
				0.1412 $\mu\text{M}$ to 22.59 $\mu\text{M}$ (EC sensor)	43.1 nM	

ECL		PEI-Ru@Ti <sub>3</sub> C <sub>2</sub> @Au NPs composite	SARS-CoV-2 RdRp gene		12.8 aM	(K. Zhang et al., 2022)
ECL		Au@Ti <sub>3</sub> C <sub>2</sub> @PEI-Ru(dcbpy) <sub>3</sub> <sup>2+</sup> hybrid nanocomposite	RNA-dependent RNA polymerase (RdRp) gene of SARS-CoV-2	1fM-100pM	0.21 FM	(Yao et al., 2021)
ECL	tetrahedral DNA/aptamers cardiac troponin-I	Au/Ti <sub>3</sub> C <sub>2</sub> -MXene	Screening COVID-19	0.1 fM-1 pM to cTnl	0.04 FM	(Mi et al., 2021)
ECL		Ru-Ti <sub>3</sub> C <sub>2</sub> T <sub>x</sub> -AuNPs	DNA phosphorylated with polynucleotide kinase (PNK)	0.002 to 10 U mL144	0.0002 U mL144	(L. Wang et al., 2022)
ECL		2D Ti <sub>3</sub> C <sub>2</sub> and CDS: W nanocrystals	MicroRNA-141	0.6 pM to 4000 pM	0.26 pM	(Du et al., 2022)

## 1026 7. Challenges, potential solutions, and prospects

1027 Most viable, efficient, widespread, and sensitive methodologies for designing various  
 1028 sensors depend on the availability of inorganic nanomaterials, mainly metal oxides. Using  
 1029 inorganic elements, on the other hand, introduces obstacles in a particular family of  
 1030 sensors. For example, metal oxide-based chemical detectors need high-temperature  
 1031 processes, which raise their cost, energy usage, and lifetime. However, the environmental  
 1032 contamination caused by the incorporation of hazardous compounds, sulphur poisoning,  
 1033 poor biocompatibility, limited flexibility, toxicity, and restricted sensitivity is significant  
 1034 downsides of these sensors. It reduces the feasibility of metal oxides for machine processing  
 1035 and easy integration into wearable future-generation sensing devices.

1036 The emergence of MXenes and other 2D nanomaterials, like carbon nanotubes, have  
 1037 transformed the world of sensors dynamically, which will benefit humanity eventually. To  
 1038 demonstrate, wearable biosensors embedded with transparent skins for non-invaded and

1039 rapid monitoring of human well-being via exhaled breath are technological breakthroughs.  
1040 Additionally, sensing, and scavenging virus-laden aerosols and other air pollutants could be  
1041 a potential strategy for combating infectious illnesses and achieving a sustainable  
1042 environment. Particularly in this period of the COVID-19 pandemic, MXenes can aid in  
1043 designing diagnostics and therapeutics. Sensors using MXenes can achieve remarkable and  
1044 tunable physicochemical properties, such as large specific area, hydrophilicity, adjustable  
1045 electronic as well as optical bands, improved dispersibility, enhanced surface terminal  
1046 functionalities, more flexibility and optimal porosity.

1047         Nonetheless, despite the enormous diversity of MXene stoichiometry, phases, and  
1048 architecture, many researchers have focused on analyzing the sensing outcome of  $Ti_3C_2T_x$ . It  
1049 increases a significant gap among theoretical anticipations, in-laboratory technology,  
1050 applicability, and commercial usability. Machine processing, DL, and ab-initio computations  
1051 are practical tools for researchers investigating exact stoichiometry, interactions, and  
1052 architecture of MXenes with next-generation sensing insights. For example, simulation was  
1053 initially used to predict the prospects of MXenes for sensing purposes. However,  
1054 simultaneous computation and experimental analysis of MXene-based biosensors are  
1055 required for long-term fast development.

1056         Further, for the mass production of MXenes-based sensors, scalable but low-  
1057 temperature fabrication of MXenes has become a key benefit. Furthermore, the effective  
1058 production of MXene free-standing films has depicted their practical incorporation in  
1059 flexible, wearable, and lightweight mobile sensors. Sensor designing methodologies that are  
1060 diverse, scalable, environmentally sustainable, affordable, repeatable, and power-saving are  
1061 critical to merging technology for producing MXene-based sensors for future generations.

1062         Although MXenes have demonstrated significant potential in designing  
1063 physicochemical biosensors with outcomes equivalent to or higher than previously  
1064 developed sensing materials, they still face several fundamental obstacles in terms of  
1065 commercial opportunities. However, other solutions, such as strategically designed  
1066 exclusive protocols, have been proposed to resolve these limitations. Consequently,  
1067 MXenes-based biosensors are significantly concerned with establishing secure techniques,  
1068 energy savers, machine-processing, affordable and increased productivity.

### 1069 **7.1. Improvements in fabrication**

1070 The present MXene developing processes are influenced by severe corrosive chemical  
1071 reactions, which negatively impact the ecosystem. Even the more improved, advanced and  
1072 highly developed in-situ chemical synthesizing techniques contaminate the ecology to some  
1073 degree. To exemplify, fluorinated chemical manufacturing procedures produce far more  
1074 fluorine compounds on the surface of MXene, which can be harmful to gas and VOC sensing  
1075 action. It prompted the exploration of alternate manufacturing technologies, such as  
1076 chemical vapour deposition (CVD) or salt-templating methods. However, the applicability of  
1077 salt-template techniques is limited since the structure of MXenes depends on the crystalline  
1078 structure and crystal geometries of specific precursors.

1079 On the other hand, CVD has been a more feasible synthesising process to  
1080 manufacture a few layers MXene, such as  $M_2X$ -MXene. However, synthesising higher order  
1081 MXene using CVD is challenging due to their metamorphism structure and multifarious  
1082 stoichiometry. Also, CVD, MBE and other mechanical alternative techniques produce a  
1083 limited yield of terminated 2D materials. Another stumbling block is the practical storage  
1084 and post-processing of MXene, as they are unstable in humid and oxygen-rich conditions.  
1085 Even though there are other methods for storing and post-processing them, they are still  
1086 more complicated, expensive, laborious, and time-consuming. Therefore, more improved,  
1087 and advanced synthesis processes can be developed to achieve a high yield of MXenes with  
1088 suitable surface characteristics for focused sensing applications.

### 1089 **7.2. Improvements through hybridization**

1090 Considering the issues associated with cutting-edge MXene-based sensor technology, the  
1091 most favourable approach is to design secondary nanomaterials hybrids. For instance,  
1092 macromolecules can provide significant flexibility in fabricating wearable sensing devices.  
1093 However, scalable fabrication of such hybrids demands optimal precursor concentration.  
1094 This is highly challenging to achieve—this limits their commercial viability. For example, the  
1095 flexibility achieved by incorporating macromolecules occurs at the expense of MXenes'  
1096 electrical conductivity.

1097 Further, during hybrid machine processing, the interaction between MXene's  
1098 mechanical strength and the flexibility of macromolecules arises. Also, if the concentration



1099 of a precursor is higher than a specific limit, it would deplete the quality of another. At the  
1100 same time, a greater concentration of one precursor can degrade the effectiveness of  
1101 another. For instance, adding polymers in MXene layers raises the interlayer spacing,  
1102 causing a specific strain that disrupts MXene's conducting network. By contrast, the  
1103 increased MXenes concentration causes the metal conductivity to lose its semiconducting  
1104 properties.

1105 Consequently, a simultaneous balance must occur between the precursor  
1106 concentration rate, processing, and operational conditions. It includes diverse tribological  
1107 analyses to evaluate the concentration of a threshold precursor in the hybrid with predicted  
1108 attributes. These findings indicate the trade-offs between the concentration of the  
1109 precursor and the processing elements of hybrids.

### 1110 **7.3. Improvements in sensing characteristics**

1111 Sensors based on non-oxide materials undergo atmospheric oxidation and degradation due  
1112 to humidification. Thereby, the lifespan of the non-oxide-based sensor declines  
1113 substantially. Besides this, MXenes are also susceptible to surface oxidation and  
1114 deterioration, particularly when stored at ambient temperature conditions. Consequently, it  
1115 degrades the sensor's efficacy and reduces its operating life. Hence, this hindrance must be  
1116 handled before developing a sensor for a specific application. Several distinct approaches  
1117 have been proposed to increase surface stability, such as using secondary  
1118 nanomaterials/coatings. However, reproducing the sensor's reproducibility and  
1119 repeatability over time remains challenging.

1120 Furthermore, unadulterated MXenes are highly sensitive to numerous stimuli, such  
1121 as toxic gases, fumes, humidity, and biomes, culminating in an identical deceitful response.  
1122 In contrast, it aids in the development of multipurpose sensors capable of sensing distinct  
1123 stimuli at the same time. In contrast, it increases cross-sensitivity in sensors which is  
1124 undesirable for their design as it might result in inaccurate stimuli identification and  
1125 quantification. For example, monitoring biomarkers in human breath through non-invasive  
1126 biosensors is strongly interfered by the moisture in exhaled breath produced by biological  
1127 metabolism. Subsequently, a sensor must have a high anti-interference potential for  
1128 unwanted stimuli to ensure its durability and precision. It can be attained by categorising  
1129 the detected signals per their character and origin using the most suitable electronically

1130 integrated circuits and systems based on artificial intelligence (AI). Numerous advanced  
1131 techniques, including AI, artificial neural networks (ANN), pattern recognition, and data  
1132 evaluating tools, are critical in developing favourable intelligent modules that can address  
1133 the cross-sensitivity bottleneck.

1134 Next-generation wearable biosensors coupled to the body need constant data  
1135 processing, which is critical for monitoring environmental stimuli modifications. MXenes can  
1136 promptly respond to stimuli changes and return to their original form between a few  
1137 seconds and hundreds of seconds. However, they exhibit a deliberative reaction and  
1138 response to various stimuli, restricting their realistic prospects. This is owing to the strong  
1139 binding forces of sophisticated 2D surfaces in the direction of particular analytes or  
1140 biomarkers. Furthermore, it causes the sensor to take a prolonged time to reform to its  
1141 initial position, extending the restoration time to hundreds of seconds from a few. Still, the  
1142 short response and recovery time, particularly in milliseconds, of revolutionary sensors is  
1143 not only indispensable but also highly required. All these challenges can be resolved by  
1144 investigating various sensory device architects, such as using interdigitated probes rather  
1145 than conventional parallel conducting electrodes, hybrid/nanocomposite secondary  
1146 materials, surface alterations, and incorporating rapid data collecting techniques.

#### 1147 **7.4. Exploring theoretical predictions**

1148 Although rapid progress and significant simulative projections of MXenes with distinct  
1149 stoichiometry, architectures, and phases, relatively few have been validated experimentally  
1150 for sensing functions, indicating a huge gap between theoretical sensing calculations and  
1151 their actual implementations. So far, for instance, a small number of 2D material phases  
1152 have been developed experimentally and on a couple of substrates. In contrast, researchers  
1153 have focused far less on nitride based MXenes than MXenes based on carbide. Despite the  
1154 tremendous possibilities of these microstructure and phase modifications, as well as  
1155 stoichiometric and layer-based alterations in MXenes, relatively few have been tuned for  
1156 sensing applications. Moreover, researchers have done little research on hybrid  
1157 nanocomposites, although ample materials are available. Therefore, it is noticeable that  
1158 MXenes have been immensely unexplored unconfirmed possibilities based on  
1159 morphological and chemical composition that may be used to accomplish progressive and  
1160 innovative sensing needs. To illustrate this point, selectivity to sense nitro-oxide can be

1161 attained through optimal hydrogenation and in MXenes through careful transitional metal  
1162 selection. Hence, by selecting the most suitable chemical and structural compositions,  
1163 scalable production, and superior machine processing, the difference between the  
1164 theoretical evaluations, experimental technologies, applied analysis, and viable  
1165 advancement of MXenes may be bridged.

#### 1166 **7.5. Cutting-edge Sustainable Prospects of MXenes**

1167 Distinct biosensors, which may be functioning physically, chemically, and biologically, are  
1168 revolutionising nearly every industry that requires real-time assessments, rationalized  
1169 decision-making methods, and intelligent workability, thanks to the integration with  
1170 techniques like AI and IoT. Moreover, the world is becoming increasingly intelligent and  
1171 sophisticated based on smart communities, astute farming, innovative technology, and  
1172 intelligent medical services. Over the next ten or more years, 150 billion network-based  
1173 monitoring sensors coupled with IoTs are expected to be implemented globally. The  
1174 sustainable development of sensing devices relies on several factors that depend on the  
1175 particular component. These factors include energy efficiency, eco-friendliness, recyclability,  
1176 greener manufacturing, biocompatibility, and biodegradability. For example, substrates,  
1177 electrical circuitry components, such as PCB boards and cables, probes, and detecting  
1178 materials should be ecological and user-friendly. Also, they must be fabricated using  
1179 greener methods, such as bioinspired/biodiverse substances, or the outcome must be  
1180 environmentally beneficial. For example, Verma et al. (Abdolhosseinzadeh et al., 2020)  
1181 developed an unadulterated MXene-based  $Ti_3C_2T_x$  liquid ink for large-scale printing  
1182 applications, with possible applications in 3D and 4D printed sensing device manufacturing.

1183 Interestingly, the ink was produced using the "treasure from trash" concept, which  
1184 included making ink from unetched chemical precursors and several layer MXenes residues  
1185 generally rejected after delamination—producing ink by reprocessing the refused substance  
1186 into worthy material for screen printing. It reveals that the unused recyclable MXene can be  
1187 used for substrate printing for workable and scalable production of next-generation  
1188 wearable intelligent sensors. Furthermore, applying such large-scale sensors must not  
1189 generate solid waste issues. These materials must be reusable or biodegradable, and they  
1190 must be conveniently discarded after their intended usage. For instance, Geravand et al.

1191 (Abbasi Geravand et al., 2021) developed a novel biodegradable nano-filtration membrane  
1192 using a hybrid nanocomposite fabricated from polycaprolactone (PLC) and  $Ti_3C_2(OH)_2$   
1193 hydrophilic MXene sheets for the treatment of dyed aqueous solutions. Also, Zhang et al.  
1194 (W. Zhang et al., 2022) revealed an intriguing biodegradable multipurpose pressure sensor  
1195 developed using cross-attached collagen fibres (CCFs) with MXene aerogel exhibiting a great  
1196 sensitivity response of  $61.99 \text{ kPa}^{-1}$  within a short time of 0.30s, speedy recovery within few  
1197 milliseconds of 0.15s, high thermal steadiness, and small LDL(0.4 kPa).

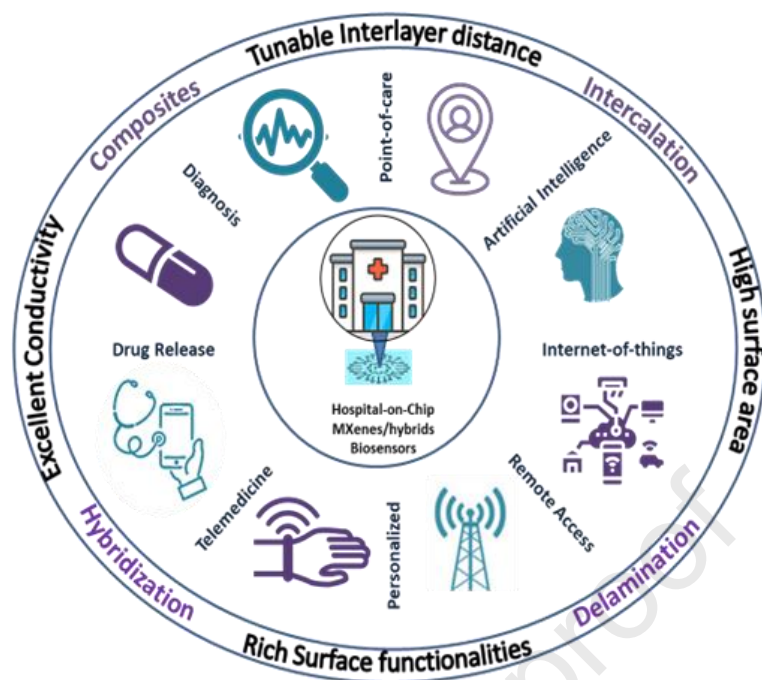
1198           Moreover, immersing the aerogel in an alkaline medium destroys it in forty days. The  
1199 degradation rate is attributed to using whole natural fibres in aerosol production. Energy  
1200 sustainability has been accomplished in sensing devices through self-operating aspects or  
1201 ambient temperature functioning. It is clear from the earlier discussions that MXene-based  
1202 sensors can sense stimuli at ambient temperature, preserving energy for dynamic  
1203 performance. Furthermore, the incorporation of triboelectric nanogenerators in MXenes  
1204 has already initiated the transformation of wearable electronic devices with sensor  
1205 integration (Lei et al., 2020; S. Li et al., 2020; Tan et al., 2020; Xin et al., 2020). In addition to  
1206 this, based on the application area, the complete unit of smart sensing sets can be operated  
1207 on green energy resources, such as triboelectricity, wind power energy, hydrothermal  
1208 energy, tidal wave energy, and sun-powered energy. For instance, farming based on  
1209 intelligent sensors can be powered by sustainable solar energy via rapidly recharging solar  
1210 panels. Depending on the application, motion detectors deployed in submarines or ship  
1211 bottom decks can be designed to work on ocean-based sustainable energy. MXenes are  
1212 employed in developing the future generation of nanogenerator-based triboelectric  
1213 generators that can be coupled with MXene sensing devices to provide autonomous  
1214 operation. For example, an intelligent wristwatch linked with a particular oxygen detector  
1215 can be powered by the back-and-forth motion of the hand using triboelectric principles.  
1216 Thus, sensors based on MXene have great potential to assist in achieving various sustainable  
1217 development goals (SDGs).

## 1218 **8. Conclusive outlook and viewpoint**

1219 This article discusses the rise of the paradigm of intelligent biosensors, generally focusing on  
1220 the lab-on-a-chip module progressing towards the hospital-on-chip model. These biosensor

1221 modules possess diversified applications such as clinical devices, hospital needs, and  
1222 personalized healthcare monitoring, especially in the COVID-19 scenarios, to protect human  
1223 lives. The practical applications of these biosensors are usually demanded in the medical  
1224 world, which is tranquil in its beginning by utilizing various kinds of nanomaterials, such as  
1225 2D materials, transition metals dichalcogenides, and organic and inorganic materials.  
1226 Among all, MXene-based biosensors are the most up-and-coming class owing to their  
1227 remarkable properties and applications, which are necessary for devising future generation  
1228 biosensors with intelligent and on-site modules.

1229           Additionally, the advantages of MXene-based intelligent biosensors depicts mobility,  
1230 compactness, wearability, smartness, intelligence, innovative 3D and 4D printable features,  
1231 multifunctionality, point-of-action, single-chip function, remote monitoring, self-driven,  
1232 selectivity with the inclusion of IoTs, AI, ML, cloud computing, and 5G technologies are all  
1233 5<sup>th</sup> generation aspects (**Figure 15**). These innovative prospects and potential alternatives can  
1234 only be realized through the collaborative endeavors of material scholars, designers, data  
1235 analysts, informatics, environmental activists, health care workers, legislators, and  
1236 industries to commercialize MXenes as advanced sensing materials. Therefore, MXenes are  
1237 expected to increase and develop in all real-world areas to construct future-generation  
1238 smart and intelligent sensors with sustainable and scalable characteristics. In addition, these  
1239 kinds of integrated intelligent biosensors are welcoming the ways toward the electronic,  
1240 portable, and cost-effective hospital-on-a-chip based diagnosis platforms that could be  
1241 easily applicable both inside and outside the hospitals, houses, clinics and other medical  
1242 premises, especially in remote areas.



1243

1244 **Figure 15.** Prospects of MXenes based 5<sup>th</sup> generation biosensor with the integration of  
 1245 modern-age technologies

1246 However, there are still some restrictions in this research in which the integration of  
 1247 all the applied arts in only a single frame and their connection with the worldwide  
 1248 applications should be overwhelmed. Nevertheless, these hospital-on-chip module-based  
 1249 biosensors are the future of modern-age wearable, portable, compact, energy-efficient, and  
 1250 cost-effective healthcare devices to reach even the world's remotest area. Furthermore, it  
 1251 will help attain the sustainable development goals of human healthcare and well-being by  
 1252 accessing every individual with healthcare facilities. Hence, hospital-in-chip biosensors  
 1253 possess the potential to transform the current healthcare system into a miniature solution  
 1254 to control future mortalities and severities due to fatal and infectious diseases.

1255

### 1256 **Acknowledgements**

1257 All authors acknowledge their respective institutions/universities for overall support. VC  
 1258 also acknowledges GOING GLOBAL PARTNERSHIPS EXPLORATORY GRANT (UNIQUE  
 1259 APPLICATION ID: 877799913) awarded by BRITISH COUNCIL of project entitled "ENHANCING  
 1260 COMMERCIAL ACUMEN AND ORGANISATIONAL CAPABILITY IN BUISNESS (ECOBUSS)".MK

1261 acknowledges Sunway University's International Research Network Grant Scheme (STR-  
1262 IRNGS-SET-GAMRG-01-2022) for this work.

### 1263 **Conflict of Interests**

1264 All authors declare no conflict of interest associated with this article.

### 1265 **References**

1266 Abbasi Geravand, M.H., Saljoughi, E., Mousavi, S.M., Kiani, S., 2021. Biodegradable  
1267 polycaprolactone/MXene nanocomposite nanofiltration membranes for the treatment  
1268 of dye solutions. *J. Taiwan Inst. Chem. Eng.* 128, 124–139.

1269 <https://doi.org/10.1016/j.jtice.2021.08.048>

1270 Abdolhosseinzadeh, S., Schneider, R., Verma, A., Heier, J., Nüesch, F., Zhang, C.J., 2020.

1271 Turning Trash into Treasure: Additive Free MXene Sediment Inks for Screen-Printed  
1272 Micro-Supercapacitors. *Adv. Mater.* 32, e2000716.

1273 <https://doi.org/10.1002/adma.202000716>

1274 Aghamohammadi, H., Amousa, N., Eslami-Farsani, R., 2021. Recent advances in developing  
1275 the MXene/polymer nanocomposites with multiple properties: A review study. *Synth.*

1276 *Met.* 273, 116695. <https://doi.org/10.1016/j.synthmet.2020.116695>

1277 Ahmed, B., Ghazaly, A. El, Rosen, J., 2020. i-MXenes for Energy Storage and Catalysis. *Adv.*

1278 *Funct. Mater.* 30, 2000894. <https://doi.org/10.1002/adfm.202000894>

1279 Ansari, A.A., Malhotra, B.D., 2022. Current progress in organic–inorganic hetero-nano-

1280 interfaces based electrochemical biosensors for healthcare monitoring. *Coord. Chem.*

1281 *Rev.* 452, 214282. <https://doi.org/10.1016/j.ccr.2021.214282>

1282 Bai, Y., He, Y., Wang, M., Song, G., 2022. Microwave-assisted synthesis of nitrogen,

1283 phosphorus-doped Ti<sub>3</sub>C<sub>2</sub> MXene quantum dots for colorimetric/fluorometric dual-

1284 modal nitrite assay with a portable smartphone platform. *Sensors Actuators B Chem.*

1285 357, 131410. <https://doi.org/10.1016/j.snb.2022.131410>

1286 Berdiyrov, G.R., 2016. Optical properties of functionalized Ti<sub>3</sub>C<sub>2</sub>T<sub>2</sub> (T = F, O, OH)

1287 MXene: First-principles calculations. *AIP Adv.* 6, 055105.

1288 <https://doi.org/10.1063/1.4948799>

- 1289 Beshar, K.M., Subah, Z., Ali, M.Z., 2021. IoT Sensor Initiated Healthcare Data Security. IEEE  
1290 Sens. J. 21, 11977–11982. <https://doi.org/10.1109/JSEN.2020.3013634>
- 1291 Borysiuk, V.N., Mochalin, V.N., Gogotsi, Y., 2015. Molecular dynamic study of the  
1292 mechanical properties of two-dimensional titanium carbides  $Ti_{n+1}C_n$  (MXenes).  
1293 Nanotechnology 26, 265705. <https://doi.org/10.1088/0957-4484/26/26/265705>
- 1294 Chae, Y., Kim, S.J., Cho, S.-Y., Choi, J., Maleski, K., Lee, B.-J., Jung, H.-T., Gogotsi, Y., Lee, Y.,  
1295 Ahn, C.W., 2019. An investigation into the factors governing the oxidation of two-  
1296 dimensional  $Ti_3C_2$  MXene. Nanoscale 11, 8387–8393.  
1297 <https://doi.org/10.1039/C9NR00084D>
- 1298 Chakraborty, P., Das, T., Nafday, D., Saha-Dasgupta, T., 2018. Manipulating the mechanical  
1299 properties of  $Ti_2C$  MXene: Effect of substitutional doping. p. 040008.  
1300 <https://doi.org/10.1063/1.5050748>
- 1301 Chang, J., Yu, L., Li, H., Li, F., 2022. Dye sensitized  $Ti_3C_2$  MXene-based highly sensitive  
1302 homogeneous photoelectrochemical sensing of phosphate through decomposition of  
1303 methylene blue-encapsulated zeolitic imidazolate framework-90. Sensors Actuators B  
1304 Chem. 352, 131021. <https://doi.org/10.1016/j.snb.2021.131021>
- 1305 Chaudhary, V., 2022. Charge Carrier Dynamics of Electrochemically Synthesized Poly (Aniline  
1306 Co-Pyrrole) Nanospheres Based Sulfur Dioxide Chemiresistor. Polym. Technol. Mater.  
1307 61, 107–115. <https://doi.org/10.1080/25740881.2021.1959932>
- 1308 Chaudhary, V., 2021a. One-dimensional variable range charge carrier hopping in  
1309 polyaniline–tungsten oxide nanocomposite-based hydrazine chemiresistor. Appl. Phys.  
1310 A 127, 536. <https://doi.org/10.1007/s00339-021-04690-8>
- 1311 Chaudhary, V., 2021b. High performance X-band electromagnetic shields based on methyl-  
1312 orange assisted polyaniline-silver core-shell nanocomposites. Polym. Technol. Mater.  
1313 60, 1–10. <https://doi.org/10.1080/25740881.2021.1912095>
- 1314 Chaudhary, V., Ashraf, N., Khalid, M., Walvekar, R., Yang, Y., Kaushik, A., Mishra, Y.K., 2022a.  
1315 Emergence of MXene–Polymer Hybrid Nanocomposites as High-Performance Next-  
1316 Generation Chemiresistors for Efficient Air Quality Monitoring. Adv. Funct. Mater.  
1317 2112913. <https://doi.org/10.1002/adfm.202112913>



- 1318 Chaudhary, V., Bhadola, P., Kaushik, A., Khalid, M., Furukawa, H., Khosla, A., 2022b.  
1319 Assessing temporal correlation in environmental risk factors to design efficient area-  
1320 specific COVID-19 regulations: Delhi based case study. *Sci. Rep.* 12, 12949.  
1321 <https://doi.org/10.1038/s41598-022-16781-4>
- 1322 Chaudhary, V., Chavali, M., 2021. Novel methyl-orange assisted core-shell polyaniline-silver  
1323 nanosheets for highly sensitive ammonia chemiresistors. *J. Appl. Polym. Sci.* 138,  
1324 51288. <https://doi.org/10.1002/app.51288>
- 1325 Chaudhary, V., Gautam, A., Mishra, Y.K., Kaushik, A., 2021a. Emerging MXene–Polymer  
1326 Hybrid Nanocomposites for High-Performance Ammonia Sensing and Monitoring.  
1327 *Nanomaterials* 11, 2496. <https://doi.org/10.3390/nano11102496>
- 1328 Chaudhary, V., Kaur, A., 2015. Enhanced room temperature sulfur dioxide sensing behaviour  
1329 of in situ polymerized polyaniline–tungsten oxide nanocomposite possessing  
1330 honeycomb morphology. *RSC Adv.* 5, 73535–73544.  
1331 <https://doi.org/10.1039/C5RA08275G>
- 1332 Chaudhary, V., Kaushik, A., Furukawa, H., Khosla, A., 2022c. Review—Towards 5th  
1333 Generation AI and IoT Driven Sustainable Intelligent Sensors Based on 2D MXenes and  
1334 Borophene. *ECS Sensors Plus* 1, 013601. <https://doi.org/10.1149/2754-2726/ac5ac6>
- 1335 Chaudhary, V., Mostafavi, E., Kaushik, A., 2022d. De-coding Ag as an efficient antimicrobial  
1336 nano-system for controlling cellular/biological functions. *Matter* 5, 1995–1998.  
1337 <https://doi.org/10.1016/j.matt.2022.06.024>
- 1338 Chaudhary, V., Royal, A., Chavali, M., Yadav, S.K., 2021b. Advancements in research and  
1339 development to combat COVID-19 using nanotechnology. *Nanotechnol. Environ. Eng.*  
1340 6, 8. <https://doi.org/10.1007/s41204-021-00102-7>
- 1341 Chaudhary, V., Sharma, A., Bhadola, P., Kaushik, A., 2022e. Advancements in MXenes. pp.  
1342 301–324. [https://doi.org/10.1007/978-3-031-05006-0\\_12](https://doi.org/10.1007/978-3-031-05006-0_12)
- 1343 Chaudhary, V., Singh, H., Kaur, A., 2017. Effect of charge carrier transport on sulfur dioxide  
1344 monitoring performance of highly porous polyaniline nanofibres. *Polym. Int.* 66, 699–  
1345 704. <https://doi.org/10.1002/pi.5311>

- 1346 Chen, X., Sun, X., Xu, W., Pan, G., Zhou, D., Zhu, J., Wang, H., Bai, X., Dong, B., Song, H., 2018.  
1347 Ratiometric photoluminescence sensing based on Ti<sub>3</sub>C<sub>2</sub> MXene quantum dots as an  
1348 intracellular pH sensor. *Nanoscale* 10, 1111–1118.  
1349 <https://doi.org/10.1039/C7NR06958H>
- 1350 Chen, Z., Wang, Yikun, Han, J., Wang, T., Leng, Y., Wang, Yanmin, Li, T., Han, Y., 2020.  
1351 Preparation of Polyaniline onto dl -Tartaric Acid Assembled MXene Surface as an  
1352 Electrode Material for Supercapacitors. *ACS Appl. Energy Mater.* 3, 9326–9336.  
1353 <https://doi.org/10.1021/acsaem.0c01662>
- 1354 Choi, J.R., 2020. Development of Point-of-Care Biosensors for COVID-19. *Front. Chem.* 8.  
1355 <https://doi.org/10.3389/fchem.2020.00517>
- 1356 Clark, L.C., Lyons, C., 2006. ELECTRODE SYSTEMS FOR CONTINUOUS MONITORING IN  
1357 CARDIOVASCULAR SURGERY. *Ann. N. Y. Acad. Sci.* 102, 29–45.  
1358 <https://doi.org/10.1111/j.1749-6632.1962.tb13623.x>
- 1359 Dhall, S., Mehta, B.R., Tyagi, A.K., Sood, K., 2021. A review on environmental gas sensors:  
1360 Materials and technologies. *Sensors Int.* 2, 100116.  
1361 <https://doi.org/10.1016/j.sintl.2021.100116>
- 1362 Dillon, A.D., Ghidui, M.J., Krick, A.L., Griggs, J., May, S.J., Gogotsi, Y., Barsoum, M.W.,  
1363 Fafarman, A.T., 2016. Highly Conductive Optical Quality Solution-Processed Films of 2D  
1364 Titanium Carbide. *Adv. Funct. Mater.* 26, 4162–4168.  
1365 <https://doi.org/10.1002/adfm.201600357>
- 1366 Du, C.-F., Zhao, X., Wang, Z., Yu, H., Ye, Q., 2021. Recent Advanced on the MXene–Organic  
1367 Hybrids: Design, Synthesis, and Their Applications. *Nanomaterials* 11, 166.  
1368 <https://doi.org/10.3390/nano11010166>
- 1369 Du, J.-F., Chen, J.-S., Liu, X.-P., Mao, C.-J., Jin, B.-K., 2022. Coupled electrochemiluminescent  
1370 and resonance energy transfer determination of microRNA-141 using functionalized  
1371 Mxene composite. *Microchim. Acta* 189, 264. [https://doi.org/10.1007/s00604-022-](https://doi.org/10.1007/s00604-022-05359-6)  
1372 [05359-6](https://doi.org/10.1007/s00604-022-05359-6)
- 1373 Dwivedi, N., Dhand, C., Kumar, P., Srivastava, A.K., 2021. Emergent 2D materials for  
1374 combating infectious diseases: the potential of MXenes and MXene–graphene

- 1375 composites to fight against pandemics. *Mater. Adv.* 2, 2892–2905.  
1376 <https://doi.org/10.1039/D1MA00003A>
- 1377 Fang, D., Zhao, D., Zhang, S., Huang, Y., Dai, H., Lin, Y., 2020. Black phosphorus quantum  
1378 dots functionalized MXenes as the enhanced dual-mode probe for exosomes sensing.  
1379 *Sensors Actuators B Chem.* 305, 127544. <https://doi.org/10.1016/j.snb.2019.127544>
- 1380 Fang, Y., Yang, X., Chen, T., Xu, G., Liu, M., Liu, J., Xu, Y., 2018. Two-dimensional titanium  
1381 carbide (MXene)-based solid-state electrochemiluminescent sensor for label-free  
1382 single-nucleotide mismatch discrimination in human urine. *Sensors Actuators B Chem.*  
1383 263, 400–407. <https://doi.org/10.1016/j.snb.2018.02.102>
- 1384 Gogotsi, Y., 2015. Chemical vapour deposition: Transition metal carbides go 2D. *Nat. Mater.*  
1385 <https://doi.org/10.1038/nmat4386>
- 1386 Gorton, L., Lindgren, A., Larsson, T., Munteanu, F.D., Ruzgas, T., Gazaryan, I., 1999. Direct  
1387 electron transfer between heme-containing enzymes and electrodes as basis for third  
1388 generation biosensors. *Anal. Chim. Acta* 400, 91–108. [https://doi.org/10.1016/S0003-2670\(99\)00610-8](https://doi.org/10.1016/S0003-2670(99)00610-8)
- 1390 Guan, Q., Ma, J., Yang, W., Zhang, R., Zhang, X., Dong, X., Fan, Y., Cai, L., Cao, Y., Zhang, Y., Li,  
1391 N., Xu, Q., 2019. Highly fluorescent Ti<sub>3</sub>C<sub>2</sub> MXene quantum dots for macrophage  
1392 labeling and Cu<sup>2+</sup> ion sensing. *Nanoscale* 11, 14123–14133.  
1393 <https://doi.org/10.1039/C9NR04421C>
- 1394 Gund, G.S., Park, J.H., Harpalsinh, R., Kota, M., Shin, J.H., Kim, T. il, Gogotsi, Y., Park, H.S.,  
1395 2019. MXene/Polymer Hybrid Materials for Flexible AC-Filtering Electrochemical  
1396 Capacitors. *Joule* 3, 164–176. <https://doi.org/10.1016/j.joule.2018.10.017>
- 1397 Hashtroudi, H., Mackinnon, I.D.R., Shafiei, M., 2020. Emerging 2D hybrid nanomaterials:  
1398 towards enhanced sensitive and selective conductometric gas sensors at room  
1399 temperature. *J. Mater. Chem. C* 8, 13108–13126. <https://doi.org/10.1039/D0TC01968B>
- 1400 He, J., Wu, P., Chen, L., Li, Hongping, Hua, M., Lu, L., Wei, Y., Chao, Y., Zhou, S., Zhu, W., Li,  
1401 Huaming, 2021. Dynamically-generated TiO<sub>2</sub> active site on MXene Ti<sub>3</sub>C<sub>2</sub>: Boosting  
1402 reactive desulfurization. *Chem. Eng. J.* 416, 129022.  
1403 <https://doi.org/10.1016/j.cej.2021.129022>

- 1404 Ho, D.H., Choi, Y.Y., Jo, S.B., Myoung, J., Cho, J.H., 2021. Sensing with MXenes: Progress and  
1405 Prospects. *Adv. Mater.* 33, 2005846. <https://doi.org/10.1002/adma.202005846>
- 1406 Huang, W., Hu, L., Tang, Y., Xie, Z., Zhang, H., 2020. Recent Advances in Functional 2D  
1407 MXene-Based Nanostructures for Next-Generation Devices. *Adv. Funct. Mater.* 30,  
1408 2005223. <https://doi.org/10.1002/adfm.202005223>
- 1409 Iqbal, A., Hong, J., Ko, T.Y., Koo, C.M., 2021. Improving oxidation stability of 2D MXenes:  
1410 synthesis, storage media, and conditions. *Nano Converg.* 8, 9.  
1411 <https://doi.org/10.1186/s40580-021-00259-6>
- 1412 Jiang, G., Yang, R., Liu, J., Liu, H., Liu, L., Wu, Y., A., Y., 2022. Two-dimensional Ti<sub>2</sub>C MXene-  
1413 induced photocurrent polarity switching photoelectrochemical biosensing platform for  
1414 ultrasensitive and selective detection of soluble CD146. *Sensors Actuators B Chem.*  
1415 350, 130859. <https://doi.org/10.1016/j.snb.2021.130859>
- 1416 Jiang, X., Kuklin, A. V., Baev, A., Ge, Y., Ågren, H., Zhang, H., Prasad, P.N., 2020. Two-  
1417 dimensional MXenes: From morphological to optical, electric, and magnetic properties  
1418 and applications. *Phys. Rep.* 848, 1–58. <https://doi.org/10.1016/j.physrep.2019.12.006>
- 1419 Jin, X., Liu, C., Xu, T., Su, L., Zhang, X., 2020. Artificial intelligence biosensors: Challenges and  
1420 prospects. *Biosens. Bioelectron.* 165, 112412.  
1421 <https://doi.org/10.1016/j.bios.2020.112412>
- 1422 Kaushik, A., Jayant, R.D., Nair, M., 2018. Nanomedicine for neuroHIV/AIDS management.  
1423 *Nanomedicine* 13, 669–673. <https://doi.org/10.2217/nnm-2018-0005>
- 1424 Kaushik, A., Kumar, R., Arya, S.K., Nair, M., Malhotra, B.D., Bhansali, S., 2015. Organic–  
1425 Inorganic Hybrid Nanocomposite-Based Gas Sensors for Environmental Monitoring.  
1426 *Chem. Rev.* 115, 4571–4606. <https://doi.org/10.1021/cr400659h>
- 1427 Kaushik, A.K., Dhau, J.S., Gohel, H., Mishra, Y.K., Kateb, B., Kim, N.-Y., Goswami, D.Y., 2020.  
1428 Electrochemical SARS-CoV-2 Sensing at Point-of-Care and Artificial Intelligence for  
1429 Intelligent COVID-19 Management. *ACS Appl. Bio Mater.* 3, 7306–7325.  
1430 <https://doi.org/10.1021/acsabm.0c01004>
- 1431 Khaledialidusti, R., Mishra, A.K., Barnoush, A., 2020. Atomic defects in monolayer ordered

- 1432 double transition metal carbide ( $\text{Mo}_2\text{TiC}_2\text{T}_x$ ) MXene and  $\text{CO}_2$  adsorption. *J. Mater.*  
1433 *Chem. C* 8, 4771–4779. <https://doi.org/10.1039/C9TC06046D>
- 1434 Khazaei, M., Arai, M., Sasaki, T., Chung, C.-Y., Venkataramanan, N.S., Estili, M., Sakka, Y.,  
1435 Kawazoe, Y., 2013. Novel Electronic and Magnetic Properties of Two-Dimensional  
1436 Transition Metal Carbides and Nitrides. *Adv. Funct. Mater.* 23, 2185–2192.  
1437 <https://doi.org/10.1002/adfm.201202502>
- 1438 Khunger, A., Kaur, N., Mishra, Y.K., Ram Chaudhary, G., Kaushik, A., 2021. Perspective and  
1439 prospects of 2D MXenes for smart biosensing. *Mater. Lett.* 304, 130656.  
1440 <https://doi.org/10.1016/j.matlet.2021.130656>
- 1441 Kim, D.W., Lee, J.H., Kim, J.K., Jeong, U., 2020. Material aspects of triboelectric energy  
1442 generation and sensors. *NPG Asia Mater.* 12, 6. [https://doi.org/10.1038/s41427-019-](https://doi.org/10.1038/s41427-019-0176-0)  
1443 [0176-0](https://doi.org/10.1038/s41427-019-0176-0)
- 1444 Kim, J., Campbell, A.S., de Ávila, B.E.-F., Wang, J., 2019. Wearable biosensors for healthcare  
1445 monitoring. *Nat. Biotechnol.* 37, 389–406. <https://doi.org/10.1038/s41587-019-0045-y>
- 1446 Kim, J., Imani, S., de Araujo, W.R., Warchall, J., Valdés-Ramírez, G., Paixão, T.R.L.C., Mercier,  
1447 P.P., Wang, J., 2015. Wearable salivary uric acid mouthguard biosensor with integrated  
1448 wireless electronics. *Biosens. Bioelectron.* 74, 1061–1068.  
1449 <https://doi.org/10.1016/j.bios.2015.07.039>
- 1450 Kukhtin, A.C., Sebastian, T., Golova, J., Perov, A., Knickerbocker, C., Linger, Y., Bueno, A., Qu,  
1451 P., Villanueva, M., Holmberg, R.C., Chandler, D.P., Cooney, C.G., 2019. Lab-on-a-Film  
1452 disposable for genotyping multidrug-resistant *Mycobacterium tuberculosis* from  
1453 sputum extracts. *Lab Chip* 19, 1217–1225. <https://doi.org/10.1039/C8LC01404C>
- 1454 Lashgari, H., Abolhassani, M.R., Boochani, A., Elahi, S.M., Khodadadi, J., 2014. Electronic and  
1455 optical properties of 2D graphene-like compounds titanium carbides and nitrides: DFT  
1456 calculations. *Solid State Commun.* 195, 61–69.  
1457 <https://doi.org/10.1016/j.ssc.2014.06.008>
- 1458 Lee, Y., Kim, S.J., Kim, Y.-J., Lim, Y., Chae, Y., Lee, B.-J., Kim, Y.-T., Han, H., Gogotsi, Y., Ahn,  
1459 C.W., 2020. Oxidation-resistant titanium carbide MXene films. *J. Mater. Chem. A* 8,  
1460 573–581. <https://doi.org/10.1039/C9TA07036B>

- 1461 Lei, D., Liu, N., Su, T., Wang, L., Su, J., Zhang, Z., Gao, Y., 2020. Research progress of MXenes-  
1462 based wearable pressure sensors. *APL Mater.* 8, 110702.  
1463 <https://doi.org/10.1063/5.0026984>
- 1464 Lei, Y., Zhao, W., Zhang, Y., Jiang, Q., He, J., Baeumner, A.J., Wolfbeis, O.S., Wang, Z.L.,  
1465 Salama, K.N., Alshareef, H.N., 2019. A MXene-Based Wearable Biosensor System for  
1466 High-Performance In Vitro Perspiration Analysis. *Small* 15, 1901190.  
1467 <https://doi.org/10.1002/sml.201901190>
- 1468 Li, H., Wen, Y., Zhu, X., Wang, J., Zhang, L., Sun, B., 2020. Novel Heterostructure of a  
1469 MXene@NiFe-LDH Nanohybrid with Superior Peroxidase-Like Activity for Sensitive  
1470 Colorimetric Detection of Glutathione. *ACS Sustain. Chem. Eng.* 8, 520–526.  
1471 <https://doi.org/10.1021/acssuschemeng.9b05987>
- 1472 Li, M., Fang, L., Zhou, H., Wu, F., Lu, Y., Luo, H., Zhang, Y., Hu, B., 2019. Three-dimensional  
1473 porous MXene/NiCo-LDH composite for high performance non-enzymatic glucose  
1474 sensor. *Appl. Surf. Sci.* 495, 143554. <https://doi.org/10.1016/j.apsusc.2019.143554>
- 1475 Li, Q., Li, X., Zhou, P., Chen, R., Xiao, R., Pang, Y., 2022. Split aptamer regulated  
1476 CRISPR/Cas12a biosensor for 17 $\beta$ -estradiol through a gap-enhanced Raman tags based  
1477 lateral flow strategy. *Biosens. Bioelectron.* 215, 114548.  
1478 <https://doi.org/10.1016/j.bios.2022.114548>
- 1479 Li, Q., Li, Y., Zeng, W., 2021. Preparation and Application of 2D MXene-Based Gas Sensors: A  
1480 Review. *Chemosensors* 9, 225. <https://doi.org/10.3390/chemosensors9080225>
- 1481 Li, S., Zhang, Yong, Wang, Y., Xia, K., Yin, Z., Wang, Huimin, Zhang, M., Liang, X., Lu, H., Zhu,  
1482 M., Wang, Haomin, Shen, X., Zhang, Yingying, 2020. Physical sensors for skin-inspired  
1483 electronics. *InfoMat* 2, 184–211. <https://doi.org/10.1002/inf2.12060>
- 1484 Li, X., Xu, J., Jiang, Y., He, Z., Liu, B., Xie, H., Li, H., Li, Z., Wang, Y., Tai, H., 2020. Toward  
1485 agricultural ammonia volatilization monitoring: A flexible polyaniline/Ti3C2T hybrid  
1486 sensitive films based gas sensor. *Sensors Actuators B Chem.* 316, 128144.  
1487 <https://doi.org/10.1016/j.snb.2020.128144>
- 1488 Li, Y., Kang, Z., Kong, L., Shi, H., Zhang, Y., Cui, M., Yang, D.-P., 2019. MXene-Ti3C2/CuS  
1489 nanocomposites: Enhanced peroxidase-like activity and sensitive colorimetric

- 1490 cholesterol detection. *Mater. Sci. Eng. C* 104, 110000.  
1491 <https://doi.org/10.1016/j.msec.2019.110000>
- 1492 Li, Y., Peng, Z., Holl, N.J., Hassan, M.R., Pappas, J.M., Wei, C., Izadi, O.H., Wang, Y., Dong, X.,  
1493 Wang, C., Huang, Y.-W., Kim, D., Wu, C., 2021. MXene–Graphene Field-Effect Transistor  
1494 Sensing of Influenza Virus and SARS-CoV-2. *ACS Omega* 6, 6643–6653.  
1495 <https://doi.org/10.1021/acsomega.0c05421>
- 1496 Lin, S., Lin, H., Yang, M., Ge, M., Chen, Y., Zhu, Y., 2020. A two-dimensional MXene  
1497 potentiates a therapeutic microneedle patch for photonic implantable medicine in the  
1498 second NIR biowindow. *Nanoscale* 12, 10265–10276.  
1499 <https://doi.org/10.1039/D0NR01444C>
- 1500 Lipatov, A., Lu, H., Alhabeab, M., Anasori, B., Gruverman, A., Gogotsi, Y., Sinitskii, A., 2018.  
1501 Elastic properties of 2D Ti<sub>3</sub>C<sub>2</sub>T<sub>x</sub> MXene monolayers and bilayers. *Sci. Adv.* 4.  
1502 <https://doi.org/10.1126/sciadv.aat0491>
- 1503 Lipton, J., Röhr, J.A., Dang, V., Goad, A., Maleski, K., Lavini, F., Han, M., Tsai, E.H.R., Weng,  
1504 G.-M., Kong, J., Riedo, E., Gogotsi, Y., Taylor, A.D., 2020. Scalable, Highly Conductive,  
1505 and Micropatternable MXene Films for Enhanced Electromagnetic Interference  
1506 Shielding. *Matter* 3, 546–557. <https://doi.org/10.1016/j.matt.2020.05.023>
- 1507 Liu, J., Jiang, X., Zhang, R., Zhang, Y., Wu, L., Lu, W., Li, J., Li, Y., Zhang, H., 2019. MXene-  
1508 Enabled Electrochemical Microfluidic Biosensor: Applications toward Multicomponent  
1509 Continuous Monitoring in Whole Blood. *Adv. Funct. Mater.* 29, 1807326.  
1510 <https://doi.org/10.1002/adfm.201807326>
- 1511 Liu, M., He, Y., Zhou, J., Ge, Y., Zhou, J., Song, G., 2020. A "naked-eye" colorimetric and  
1512 ratiometric fluorescence probe for uric acid based on Ti<sub>3</sub>C<sub>2</sub> MXene quantum dots.  
1513 *Anal. Chim. Acta* 1103, 134–142. <https://doi.org/10.1016/j.aca.2019.12.069>
- 1514 Liu, M., Zhou, J., He, Y., Cai, Z., Ge, Y., Zhou, J., Song, G., 2019. ε-Poly-L-lysine-protected  
1515 Ti<sub>3</sub>C<sub>2</sub> MXene quantum dots with high quantum yield for fluorometric determination of  
1516 cytochrome c and trypsin. *Microchim. Acta* 186, 770. [https://doi.org/10.1007/s00604-](https://doi.org/10.1007/s00604-019-3945-0)  
1517 [019-3945-0](https://doi.org/10.1007/s00604-019-3945-0)
- 1518 Liu, S.-J., Ma, K., Liu, L.-S., Wang, K., Zhang, Y.-A., Bi, Z.-R., Chen, Y.-X., Chen, K.-Z., Wang, C.-

- 1519 X., Qiao, S.-L., 2022. Point-of-care non-invasive enzyme-cleavable nanosensors for  
1520 acute transplant rejection detection. *Biosens. Bioelectron.* 215, 114568.  
1521 <https://doi.org/10.1016/j.bios.2022.114568>
- 1522 Liu, X., Qiu, Y., Jiang, D., Li, F., Gan, Y., Zhu, Y., Pan, Y., Wan, H., Wang, P., 2022. Covalently  
1523 grafting first-generation PAMAM dendrimers onto MXenes with self-adsorbed AuNPs  
1524 for use as a functional nanoplatform for highly sensitive electrochemical biosensing of  
1525 cTnT. *Microsystems Nanoeng.* 8, 35. <https://doi.org/10.1038/s41378-022-00352-8>
- 1526 Mani, V., Chikkaveeraiah, B. V., Patel, V., Gutkind, J.S., Rusling, J.F., 2009. Ultrasensitive  
1527 Immunosensor for Cancer Biomarker Proteins Using Gold Nanoparticle Film Electrodes  
1528 and Multienzyme-Particle Amplification. *ACS Nano* 3, 585–594.  
1529 <https://doi.org/10.1021/nn800863w>
- 1530 Mannoor, M.S., Tao, H., Clayton, J.D., Sengupta, A., Kaplan, D.L., Naik, R.R., Verma, N.,  
1531 Omenetto, F.G., McAlpine, M.C., 2012. Graphene-based wireless bacteria detection on  
1532 tooth enamel. *Nat. Commun.* 3, 763. <https://doi.org/10.1038/ncomms1767>
- 1533 Mi, X., Li, H., Tan, R., Feng, B., Tu, Y., 2021. The TDs/aptamer cTnI biosensors based on HCR  
1534 and Au/Ti3C2-MXene amplification for screening serious patient in COVID-19  
1535 pandemic. *Biosens. Bioelectron.* 192, 113482.  
1536 <https://doi.org/10.1016/j.bios.2021.113482>
- 1537 Naguib, M., Barsoum, M.W., Gogotsi, Y., 2021. Ten Years of Progress in the Synthesis and  
1538 Development of MXenes. *Adv. Mater.* 33, 2103393.  
1539 <https://doi.org/10.1002/adma.202103393>
- 1540 Naguib, M., Kurtoglu, M., Presser, V., Lu, J., Niu, J., Heon, M., Hultman, L., Gogotsi, Y.,  
1541 Barsoum, M.W., 2011. Two-Dimensional Nanocrystals Produced by Exfoliation of  
1542 Ti3AlC2. *Adv. Mater.* 23, 4248–4253. <https://doi.org/10.1002/adma.201102306>
- 1543 Natu, V., Hart, J.L., Sokol, M., Chiang, H., Taheri, M.L., Barsoum, M.W., 2019. Edge Capping  
1544 of 2D-MXene Sheets with Polyanionic Salts To Mitigate Oxidation in Aqueous Colloidal  
1545 Suspensions. *Angew. Chemie Int. Ed.* 58, 12655–12660.  
1546 <https://doi.org/10.1002/anie.201906138>
- 1547 Nayak, S., Patgiri, R., Member, S., 2020. 6G Communication Technology: A Vision on



- 1548 Intelligent Healthcare. *IEEE Internet Things J.*
- 1549 Neampet, S., Ruecha, N., Qin, J., Wonsawat, W., Chailapakul, O., Rodthongkum, N., 2019. A  
1550 nanocomposite prepared from platinum particles, polyaniline and a Ti<sub>3</sub>C<sub>2</sub> MXene for  
1551 amperometric sensing of hydrogen peroxide and lactate. *Microchim. Acta* 186, 752.  
1552 <https://doi.org/10.1007/s00604-019-3845-3>
- 1553 Nguyen, D.C., Ding, M., Pathirana, P.N., Seneviratne, A., Li, J., Niyato, D., Dobre, O., Poor,  
1554 H.V., 2022. 6G Internet of Things: A Comprehensive Survey. *IEEE Internet Things J.* 9.  
1555 <https://doi.org/10.1109/JIOT.2021.3103320>
- 1556 Noh, S., Lee, H., Kim, J., Jang, H., An, J., Park, C., Lee, M.-H., Lee, T., 2022. Rapid  
1557 electrochemical dual-target biosensor composed of an Aptamer/MXene hybrid on Au  
1558 microgap electrodes for cytokines detection. *Biosens. Bioelectron.* 207, 114159.  
1559 <https://doi.org/10.1016/j.bios.2022.114159>
- 1560 Novoselov, K.S., Geim, A.K., Morozov, S. V., Jiang, D., Zhang, Y., Dubonos, S. V., Grigorieva, I.  
1561 V., Firsov, A.A., 2004. Electric Field Effect in Atomically Thin Carbon Films. *Science* (80-  
1562 ). 306, 666–669. <https://doi.org/10.1126/science.1102896>
- 1563 Pan, H., Dong, Y., Gong, L., Zhai, J., Song, C., Ge, Z., Su, Y., Zhu, D., Chao, J., Su, S., Wang, L.,  
1564 Wan, Y., Fan, C., 2022. Sensing gastric cancer exosomes with MoS<sub>2</sub>-based SERS  
1565 aptasensor. *Biosens. Bioelectron.* 215, 114553.  
1566 <https://doi.org/10.1016/j.bios.2022.114553>
- 1567 Patel, S., Nanda, R., Sahoo, S., Mohapatra, E., 2016. Biosensors in Health Care: The  
1568 Milestones Achieved in Their Development towards Lab-on-Chip-Analysis. *Biochem.*  
1569 *Res. Int.* 2016, 1–12. <https://doi.org/10.1155/2016/3130469>
- 1570 Pathania, D., Kumar, S., Thakur, P., Chaudhary, V., Kaushik, A., Varma, R.S., Furukawa, H.,  
1571 Sharma, M., Khosla, A., 2022. Essential oil-mediated biocompatible magnesium  
1572 nanoparticles with enhanced antibacterial, antifungal, and photocatalytic efficacies.  
1573 *Sci. Rep.* 12, 11431. <https://doi.org/10.1038/s41598-022-14984-3>
- 1574 Qian, S., Cui, Y., Cai, Z., Li, L., 2022. Applications of smartphone-based colorimetric  
1575 biosensors. *Biosens. Bioelectron.* X 11, 100173.  
1576 <https://doi.org/10.1016/j.biosx.2022.100173>

- 1577 Qiu, Z., Fan, D., Xue, X., Guo, S., Lin, Y., Chen, Y., Tang, D., 2022. Molecularly Imprinted  
1578 Polymer Functionalized Bi<sub>2</sub>S<sub>3</sub>/Ti<sub>3</sub>C<sub>2</sub>T<sub>x</sub> MXene Nanocomposites for  
1579 Photoelectrochemical/Electrochemical Dual-Mode Sensing of Chlorogenic Acid.  
1580 *Chemosensors* 10, 252. <https://doi.org/10.3390/chemosensors10070252>
- 1581 Rasheed, P.A., Pandey, R.P., Jabbar, K.A., Ponraj, J., Mahmoud, K.A., 2019. Sensitive  
1582 electrochemical detection of <sc>|</sc> -cysteine based on a highly stable Pd@Ti<sub>3</sub>C  
1583 <sub>2</sub>T<sub>x</sub> (MXene) nanocomposite modified glassy carbon electrode. *Anal. Methods* 11,  
1584 3851–3856. <https://doi.org/10.1039/C9AY00912D>
- 1585 Scheller, F.W., Schubert, F., Neumann, B., Pfeiffer, D., Hintsche, R., Dransfeld, I.,  
1586 Wollenberger, U., Renneberg, R., Warsinke, A., Johansson, G., Skoog, M., Yang, X.,  
1587 Bogdanovskaya, V., Bückmann, A., Zaitsev, S.Y., 1991. Second generation biosensors.  
1588 *Biosens. Bioelectron.* 6, 245–253. [https://doi.org/10.1016/0956-5663\(91\)80010-U](https://doi.org/10.1016/0956-5663(91)80010-U)
- 1589 Scott, A., Pandey, R., Saxena, S., Osman, E., Li, Y., Soleymani, L., 2022. A Smartphone  
1590 Operated Electrochemical Reader and Actuator that Streamlines the Operation of  
1591 Electrochemical Biosensors. *ECS Sensors Plus* 1, 014601. [https://doi.org/10.1149/2754-](https://doi.org/10.1149/2754-2726/AC5FB3)  
1592 [2726/AC5FB3](https://doi.org/10.1149/2754-2726/AC5FB3)
- 1593 Seitz, W.R., 1984. Chemical Sensors Based on Fiber Optics. *Anal. Chem.* 56, 16A-34A.  
1594 <https://doi.org/10.1021/ac00265a711>
- 1595 Shahzad, F., Iqbal, A., Zaidi, S.A., Hwang, S.-W., Koo, C.M., 2019. Nafion-stabilized two-  
1596 dimensional transition metal carbide (Ti<sub>3</sub>C<sub>2</sub>T<sub>x</sub> MXene) as a high-performance  
1597 electrochemical sensor for neurotransmitter. *J. Ind. Eng. Chem.* 79, 338–344.  
1598 <https://doi.org/10.1016/j.jiec.2019.03.061>
- 1599 Sheth, Y., Dharaskar, S., Chaudhary, V., Khalid, M., Walvekar, R., 2022. Prospects of titanium  
1600 carbide-based MXene in heavy metal ion and radionuclide adsorption for wastewater  
1601 remediation: A review. *Chemosphere* 293, 133563.  
1602 <https://doi.org/10.1016/j.chemosphere.2022.133563>
- 1603 Shuck, C.E., Sarycheva, A., Anayee, M., Levitt, A., Zhu, Y., Uzun, S., Balitskiy, V., Zahorodna,  
1604 V., Gogotsi, O., Gogotsi, Y., 2020. Scalable Synthesis of Ti<sub>3</sub>C<sub>2</sub>T<sub>x</sub> MXene. *Adv. Eng.*  
1605 *Mater.* 22, 1901241. <https://doi.org/10.1002/adem.201901241>

- 1606 Si, C., Jin, K.-H., Zhou, J., Sun, Z., Liu, F., 2016. Large-Gap Quantum Spin Hall State in  
1607 MXenes: d -Band Topological Order in a Triangular Lattice. *Nano Lett.* 16, 6584–6591.  
1608 <https://doi.org/10.1021/acs.nanolett.6b03118>
- 1609 Singh, K.R., Nayak, V., Singh, J., Singh, R.P., 2021. Nano-enabled wearable sensors for the  
1610 Internet of Things (IoT). *Mater. Lett.* 304, 130614.  
1611 <https://doi.org/10.1016/j.matlet.2021.130614>
- 1612 Solanki, P.R., Kaushik, A., Agrawal, V. V., Malhotra, B.D., 2011. Nanostructured metal oxide-  
1613 based biosensors. *NPG Asia Mater.* 3, 17–24.  
1614 <https://doi.org/10.1038/asiamat.2010.137>
- 1615 Tan, P., Zou, Y., Fan, Y., Li, Z., 2020. Self-powered wearable electronics. *Wearable Technol.*  
1616 1, e5. <https://doi.org/10.1017/wtc.2020.3>
- 1617 Tiwari, S., Atluri, V., Kaushik, A., Yndart, A., Nair, M., 2019. Alzheimer’s disease:  
1618 pathogenesis, diagnostics, and therapeutics. *Int. J. Nanomedicine Volume 14*, 5541–  
1619 5554. <https://doi.org/10.2147/IJN.S200490>
- 1620 Unal, M.A., Bayrakdar, F., Fusco, L., Besbinar, O., Shuck, C.E., Yalcin, S., Erken, M.T., Ozkul,  
1621 A., Gurcan, C., Panatli, O., Summak, G.Y., Gokce, C., Orecchioni, M., Gazzi, A., Vitale, F.,  
1622 Somers, J., Demir, E., Yildiz, S.S., Nazir, H., Grivel, J.-C., Bedognetti, D., Crisanti, A.,  
1623 Akcali, K.C., Gogotsi, Y., Delogu, L.G., Yilmazer, A., 2021. 2D MXenes with antiviral and  
1624 immunomodulatory properties: A pilot study against SARS-CoV-2. *Nano Today* 38,  
1625 101136. <https://doi.org/10.1016/j.nantod.2021.101136>
- 1626 Verma, D., Singh, K.R., Yadav, A.K., Nayak, V., Singh, J., Solanki, P.R., Singh, R.P., 2022.  
1627 Internet of things (IoT) in nano-integrated wearable biosensor devices for healthcare  
1628 applications. *Biosens. Bioelectron. X* 11, 100153.  
1629 <https://doi.org/10.1016/j.biosx.2022.100153>
- 1630 Verma, N., Bhardwaj, A., 2015. Biosensor Technology for Pesticides—A review. *Appl.*  
1631 *Biochem. Biotechnol.* 175, 3093–3119. <https://doi.org/10.1007/s12010-015-1489-2>
- 1632 Wan, S., Li, X., Chen, Y., Liu, N., Du, Y., Dou, S., Jiang, L., Cheng, Q., 2021. High-strength  
1633 scalable MXene films through bridging-induced densification. *Science (80-. )*. 374, 96–  
1634 99. <https://doi.org/10.1126/science.abg2026>

- 1635 Wang, H., Li, H., Huang, Y., Xiong, M., Wang, F., Li, C., 2019. A label-free electrochemical  
1636 biosensor for highly sensitive detection of gliotoxin based on DNA  
1637 nanostructure/MXene nanocomplexes. *Biosens. Bioelectron.* 142, 111531.  
1638 <https://doi.org/10.1016/j.bios.2019.111531>
- 1639 Wang, L., Zhang, H., Zhuang, T., Liu, J., Sojic, N., Wang, Z., 2022. Sensitive  
1640 electrochemiluminescence biosensing of polynucleotide kinase using the versatility of  
1641 two-dimensional Ti3C2TX MXene nanomaterials. *Anal. Chim. Acta* 1191, 339346.  
1642 <https://doi.org/10.1016/j.aca.2021.339346>
- 1643 Wang, L., Zhang, M., Yang, B., Tan, J., Ding, X., Li, W., 2021. Recent Advances in  
1644 Multidimensional (1D, 2D, and 3D) Composite Sensors Derived from MXene: Synthesis,  
1645 Structure, Application, and Perspective. *Small Methods* 5, 2100409.  
1646 <https://doi.org/10.1002/smtd.202100409>
- 1647 Wang, S., Jiang, Y., Liu, B., Duan, Z., Pan, H., Yuan, Z., Xie, G., Wang, J., Fang, Z., Tai, H.,  
1648 2021a. Ultrathin Nb2CT nanosheets-supported polyaniline nanocomposite: Enabling  
1649 ultrasensitive NH3 detection. *Sensors Actuators B Chem.* 343, 130069.  
1650 <https://doi.org/10.1016/j.snb.2021.130069>
- 1651 Wang, S., Liu, B., Duan, Z., Zhao, Q., Zhang, Y., Xie, G., Jiang, Y., Li, S., Tai, H., 2021b. PANI  
1652 nanofibers-supported Nb2CTx nanosheets-enabled selective NH3 detection driven by  
1653 TENG at room temperature. *Sensors Actuators B Chem.* 327, 128923.  
1654 <https://doi.org/10.1016/j.snb.2020.128923>
- 1655 Wang, Y., Huo, T., Du, Y., Qian, M., Lin, C., Nie, H., Li, W., Hao, T., Zhang, X., Lin, N., Huang,  
1656 R., 2022. Sensitive CTC analysis and dual-mode MRI/FL diagnosis based on a magnetic  
1657 core-shell aptasensor. *Biosens. Bioelectron.* 215, 114530.  
1658 <https://doi.org/10.1016/j.bios.2022.114530>
- 1659 Wei, Y., Zhang, P., Soomro, R.A., Zhu, Q., Xu, B., 2021. Advances in the Synthesis of 2D  
1660 MXenes. *Adv. Mater.* 33, 2103148. <https://doi.org/10.1002/adma.202103148>
- 1661 Weng, H., Ranjbar, A., Liang, Y., Song, Z., Khazaei, M., Yunoki, S., Arai, M., Kawazoe, Y., Fang,  
1662 Z., Dai, X., 2015. Large-gap two-dimensional topological insulator in oxygen  
1663 functionalized MXene. *Phys. Rev. B* 92, 075436.

- 1664 <https://doi.org/10.1103/PhysRevB.92.075436>
- 1665 Wu, C., Zhang, X., Wang, R., Chen, L.J., Nie, M., Zhang, Z., Huang, X., Han, L., 2022. Low-  
1666 dimensional material based wearable sensors. *Nanotechnology* 33, 072001.  
1667 <https://doi.org/10.1088/1361-6528/ac33d1>
- 1668 Wu, D., Wu, M., Yang, J., Zhang, H., Xie, K., Lin, C.-T., Yu, A., Yu, J., Fu, L., 2019. Delaminated  
1669 Ti<sub>3</sub>C<sub>2</sub>T<sub>x</sub> (MXene) for electrochemical carbendazim sensing. *Mater. Lett.* 236, 412–415.  
1670 <https://doi.org/10.1016/j.matlet.2018.10.150>
- 1671 Wu, X., Wang, Z., Yu, M., Xiu, L., Qiu, J., 2017. Stabilizing the MXenes by Carbon Nanoplatting  
1672 for Developing Hierarchical Nanohybrids with Efficient Lithium Storage and Hydrogen  
1673 Evolution Capability. *Adv. Mater.* 29, 1607017.  
1674 <https://doi.org/10.1002/adma.201607017>
- 1675 Xi, X., Wang, J., Wang, Y., Xiong, H., Chen, M., Wu, Z., Zhang, X., Wang, S., Wen, W., 2022.  
1676 Preparation of Au/Pt/Ti<sub>3</sub>C<sub>2</sub>Cl<sub>2</sub> nanoflakes with self-reducing method for colorimetric  
1677 detection of glutathione and intracellular sensing of hydrogen peroxide. *Carbon* N. Y.  
1678 <https://doi.org/10.1016/j.carbon.2022.06.068>
- 1679 Xie, Y., Kent, P.R.C., 2013. Hybrid Density Functional Study of Structural and Electronic  
1680 Properties of Functionalized  $\text{Ti}_{n+1}\text{X}_n$  (X= C, N) monolayers. *Phys. Rev. B* 87,  
1681 235441. <https://doi.org/10.1103/PhysRevB.87.235441>
- 1682 Xin, M., Li, J., Ma, Z., Pan, L., Shi, Y., 2020. MXenes and Their Applications in Wearable  
1683 Sensors. *Front. Chem.* 8. <https://doi.org/10.3389/fchem.2020.00297>
- 1684 Xue, Q., Zhang, H., Zhu, M., Pei, Z., Li, H., Wang, Z., Huang, Yang, Huang, Yan, Deng, Q.,  
1685 Zhou, J., Du, S., Huang, Q., Zhi, C., 2017. Photoluminescent Ti<sub>3</sub>C<sub>2</sub> MXene Quantum  
1686 Dots for Multicolor Cellular Imaging. *Adv. Mater.* 29, 1604847.  
1687 <https://doi.org/10.1002/adma.201604847>
- 1688 Xun, G., Lane, S.T., Petrov, V.A., Pepa, B.E., Zhao, H., 2021. A rapid, accurate, scalable, and  
1689 portable testing system for COVID-19 diagnosis. *Nat. Commun.* 12, 2905.  
1690 <https://doi.org/10.1038/s41467-021-23185-x>
- 1691 Yang, Y.-C., Lin, Y.-T., Yu, J., Chang, H.-T., Lu, T.-Y., Huang, T.-Y., Preet, A., Hsu, Y.-J., Wang, L.,

- 1692 Lin, T.-E., 2021. MXene Nanosheet-Based Microneedles for Monitoring Muscle  
1693 Contraction and Electrostimulation Treatment. *ACS Appl. Nano Mater.* 4, 7917–7924.  
1694 <https://doi.org/10.1021/acsnm.1c01237>
- 1695 Yao, B., Zhang, J., Fan, Z., Ding, Y., Zhou, B., Yang, R., Zhao, J., Zhang, K., 2021. Rational  
1696 Engineering of the DNA Walker Amplification Strategy by Using a Au@Ti<sub>3</sub>C<sub>2</sub>@PEI-  
1697 Ru(dcbpy)<sub>3</sub><sup>2+</sup> Nanocomposite Biosensor for Detection of the SARS-CoV-2 RdRp Gene.  
1698 *ACS Appl. Mater. Interfaces* 13, 19816–19824. <https://doi.org/10.1021/acсами.1c04453>
- 1699 Yao, Y., Lan, L., Liu, X., Ying, Y., Ping, J., 2020. Spontaneous growth and regulation of noble  
1700 metal nanoparticles on flexible biomimetic MXene paper for bioelectronics. *Biosens.*  
1701 *Bioelectron.* 148, 111799. <https://doi.org/10.1016/j.bios.2019.111799>
- 1702 Zha, X.-H., Zhou, J., Eklund, P., Bai, X., Du, S., Huang, Q., 2019. Non-MAX Phase Precursors  
1703 for MXenes, in: *2D Metal Carbides and Nitrides (MXenes)*. Springer International  
1704 Publishing, Cham, pp. 53–68. [https://doi.org/10.1007/978-3-030-19026-2\\_4](https://doi.org/10.1007/978-3-030-19026-2_4)
- 1705 Zhan, X., Si, C., Zhou, J., Sun, Z., 2020. MXene and MXene-based composites: synthesis,  
1706 properties and environment-related applications. *Nanoscale Horizons* 5, 235–258.  
1707 <https://doi.org/10.1039/C9NH00571D>
- 1708 Zhang, C.J., Pinilla, S., McEvoy, N., Cullen, C.P., Anasori, B., Long, E., Park, S.-H., Seral-Ascaso,  
1709 A., Shmeliov, A., Krishnan, D., Morant, C., Liu, X., Duesberg, G.S., Gogotsi, Y., Nicolosi,  
1710 V., 2017. Oxidation Stability of Colloidal Two-Dimensional Titanium Carbides (MXenes).  
1711 *Chem. Mater.* 29, 4848–4856. <https://doi.org/10.1021/acs.chemmater.7b00745>
- 1712 Zhang, H., He, R., Niu, Y., Han, F., Li, J., Zhang, X., Xu, F., 2022. Graphene-enabled wearable  
1713 sensors for healthcare monitoring. *Biosens. Bioelectron.* 197, 113777.  
1714 <https://doi.org/10.1016/j.bios.2021.113777>
- 1715 Zhang, H., Wang, Z., Zhang, Q., Wang, F., Liu, Y., 2019. Ti<sub>3</sub>C<sub>2</sub> MXenes nanosheets catalyzed  
1716 highly efficient electrogenerated chemiluminescence biosensor for the detection of  
1717 exosomes. *Biosens. Bioelectron.* 124–125, 184–190.  
1718 <https://doi.org/10.1016/j.bios.2018.10.016>
- 1719 Zhang, J., Kong, N., Uzun, S., Levitt, A., Seyedin, S., Lynch, P.A., Qin, S., Han, M., Yang, W.,  
1720 Liu, J., Wang, X., Gogotsi, Y., Razal, J.M., 2020. Scalable Manufacturing of Free-

- 1721 Standing, Strong Ti<sub>3</sub>C<sub>2</sub>T<sub>x</sub> MXene Films with Outstanding Conductivity. *Adv. Mater.*  
1722 32, 2001093. <https://doi.org/10.1002/adma.202001093>
- 1723 Zhang, K., Fan, Z., Huang, Y., Ding, Y., Xie, M., 2022. A strategy combining 3D-DNA Walker  
1724 and CRISPR-Cas12a trans-cleavage activity applied to MXene based  
1725 electrochemiluminescent sensor for SARS-CoV-2 RdRp gene detection. *Talanta* 236,  
1726 122868. <https://doi.org/10.1016/j.talanta.2021.122868>
- 1727 Zhang, S., Huang, P., Wang, J., Zhuang, Z., Zhang, Z., Han, W.-Q., 2020. Fast and Universal  
1728 Solution-Phase Flocculation Strategy for Scalable Synthesis of Various Few-Layered  
1729 MXene Powders. *J. Phys. Chem. Lett.* 11, 1247–1254.  
1730 <https://doi.org/10.1021/acs.jpcllett.9b03682>
- 1731 ZHANG, W., LI, G., 2004. Third-Generation Biosensors Based on the Direct Electron Transfer  
1732 of Proteins. *Anal. Sci.* 20, 603–609. <https://doi.org/10.2116/analsci.20.603>
- 1733 Zhang, W., Pan, Z., Ma, J., Wei, L., Chen, Z., Wang, J., 2022. Degradable Cross-Linked  
1734 Collagen Fiber/MXene Composite Aerogels as a High-Performing Sensitive Pressure  
1735 Sensor. *ACS Sustain. Chem. Eng.* 10, 1408–1418.  
1736 <https://doi.org/10.1021/acssuschemeng.1c05757>
- 1737 Zhang, Y., Jiang, X., Zhang, J., Zhang, H., Li, Y., 2019. Simultaneous voltammetric  
1738 determination of acetaminophen and isoniazid using MXene modified screen-printed  
1739 electrode. *Biosens. Bioelectron.* 130, 315–321.  
1740 <https://doi.org/10.1016/j.bios.2019.01.043>
- 1741 Zhao, J., He, C., Wu, W., Yang, H., Dong, J., Wen, L., Hu, Z., Yang, M., Hou, C., Huo, D., 2022.  
1742 MXene-MoS<sub>2</sub> heterostructure collaborated with catalyzed hairpin assembly for label-  
1743 free electrochemical detection of microRNA-21. *Talanta* 237, 122927.  
1744 <https://doi.org/10.1016/j.talanta.2021.122927>
- 1745 Zhao, L., Wang, K., Wei, W., Wang, L., Han, W., 2019. High-performance flexible sensing  
1746 devices based on polyaniline/MXene nanocomposites. *InfoMat* 1, 407–416.  
1747 <https://doi.org/10.1002/inf2.12032>
- 1748 Zhao, M.Q., Trainor, N., Ren, C.E., Torelli, M., Anasori, B., Gogotsi, Y., 2019. Scalable  
1749 Manufacturing of Large and Flexible Sheets of MXene/Graphene Heterostructures.

- 1750 Adv. Mater. Technol. 4, 1800639. <https://doi.org/10.1002/admt.201800639>
- 1751 Zhao, X., Vashisth, A., Prehn, E., Sun, W., Shah, S.A., Habib, T., Chen, Y., Tan, Z., Lutkenhaus,  
1752 J.L., Radovic, M., Green, M.J., 2019. Antioxidants Unlock Shelf-Stable Ti<sub>3</sub>C<sub>2</sub>T (MXene)  
1753 Nanosheet Dispersions. Matter 1, 513–526.  
1754 <https://doi.org/10.1016/j.matt.2019.05.020>
- 1755 Zhou, T., Zhang, T., 2021. Recent Progress of Nanostructured Sensing Materials from 0D to  
1756 3D: Overview of Structure–Property–Application Relationship for Gas Sensors. Small  
1757 Methods 5, 2100515. <https://doi.org/10.1002/smtd.202100515>
- 1758



### **Declaration of interests**

The authors declare that they have no known competing financial interests or personal relationships that could have appeared to influence the work reported in this paper.

Journal Pre-proof